Tuning the Substrate Specificity of the Glutathione Transferase GstB from *Escherichia coli* via Site-directed Mutagenesis

by

Jennifer M. Moore

Submitted in Partial Fulfillment of the Requirements

for the Degree of

Master of Science

in the

Chemistry

Program

YOUNGSTOWN STATE UNIVERSITY

August, 2017

Tuning the Substrate Specificity of the Glutathione Transferase GstB from *Escherichia coli* via Site-directed Mutagenesis

Jennifer M. Moore

I hereby release this thesis to the public. I understand that this thesis will be made available from the OhioLINK ETD Center and the Maag Library Circulation Desk for public access. I also authorize the University or other individuals to make copies of this thesis as needed for scholarly research.

Signature:

Jennifer M. Moore, Student Date

Approvals:

Dr. Nina V. Stourman, Thesis Advisor Date

Dr. Michael Serra, Committee Member Date

Dr. Peter Norris, Committee Member Date

Dr. Salvatore A. Sanders, Dean of Graduate Studies Date

ABSTRACT

Glutathione transferases (GSTs) are detoxication enzymes that are widely distributed in nature. They fulfill their protective roles by catalyzing the conjugation of the tripeptide glutathione to both endogenous and xenobiotic electrophiles. Eukaryotic GSTs are the subject of thorough investigation, while the prokaryotic enzymes remain relatively unexplored. GstB is a glutathione transferase from *Escherichia coli* that is known to detoxify bromoacetate, a water disinfection by-product. This work has served to expand the substrate scope for GstB. Site-directed mutagenesis of the electrophile-binding site residue arginine 119 was performed, generating the alanine, glutamine, histidine, and serine enzyme variants. The activities of the mutants toward a range of electrophiles were evaluated to investigate the impact of the amino acid substitutions on substrate specificity. Initial activity screening results indicate that some mutants display rate enhancement for acrylate and iodoacetamide conjugation. Kinetic parameters with iodoacetamide suggest that certain mutants are more catalytically efficient and resistant to inhibition compared to the wild type enzyme. The finding that amino acid substitution at position 119 can modify GstB substrate specificity provides support for pollutant-targeted bioremediation strategies.

ACKNOWLEDGEMENTS

I extend tremendous gratitude to my advisor Dr. Nina V. Stourman. Working tirelessly in her roles as an educator and research advisor, she has taught me the importance of dedication. Her patience, knowledge, and talent as an educator have advanced my growth as a researcher. I am inspired by her commitment to excellence and thank her for being a role model. I thank Dr. Michael Serra for his service on my committee. I am grateful for the support and education he has provided throughout my undergraduate and graduate studies. Dr. Peter Norris first introduced me to the world of research when I entered his laboratory as a sophomore at YSU. I thank him for his research mentorship and service on my committee.

I am thankful to have worked alongside Linda Sui, who has patiently trained me in biochemical techniques and contributed to this work. Additionally, I thank Collins Aboagye for laying the foundation for the GstB project. I appreciate the friendship and support from the past and present members of the Stourman lab. The YSU Chemistry Department faculty, staff, and students have made my experience an enjoyable one. I thank them for the knowledge, support, and camaraderie they have shared with me over the years.

I thank my significant other Frank George for encouraging me to pursue my goals with confidence. Most importantly, I would not have achieved success in my scholastic endeavors without the love and upbringing I have received from my family. I thank my mother for being the embodiment of compassion and selflessness. She has taught me to approach life with both grace and grit. She was also the first to introduce me to science at a young age. Thank you, Mom.

Table of Contents

List of Figures

List of Tables

List of Abbreviations

Abs	absorbance
Acr	acrylic acid
Ala, A	alanine
Arg, R	arginine
BrAc	bromoacetic acid
2-BrBt	2-bromobutyric acid
3-BrPrOH	3-bromo-1-propanol
trans-CA	*trans*-cinnamic acid
CDNB	1-chloro-2,4-dinitrobenzene
Chloram	chloramphenicol
ClAc	chloroacetic acid
Da	Dalton
DNA	deoxyribonucleic acid
DiClAc	dichloroacetic acid
DMSO	dimethyl sulfoxide
DTNB	5,5'-dithiobis(2-nitrobenzoic acid)
DTT	dithiothreitol
ε	molar extinction coefficient
E. coli	*Escherichia coli*
EDTA	ethylenediaminetetraacetic acid
EtBrAc	ethyl bromoacetate
Fos	fosfomycin
Gln, Q	glutamine
GSH	glutathione
GST	glutathione transferase
His, H	histidine
IAc	iodoacetate
$IAcNH_2$	iodoacetamide
IPTG	isopropyl-β-D-1-thiogalactopyranoside
λ_{max}	wavelength of maximum absorbance
LB	Luria-Bertani medium
OD_{600}	optical density at 600 nm
pI	isoelectric point
rpm	revolutions per minute
SDS-PAGE	sodium dodecyl sulfate polyacrylamide gel electrophoresis
Ser, S	serine
SOB	super optimal broth
SOC	super optimal broth with catabolite represison

CHAPTER 1. INTRODUCTION

The glutathione transferases (EC 2.5.1.18) comprise a superfamily of enzymes found in representative organisms from five of the six kingdoms of life. Among many of their roles, they are key members of nature's arsenal of detoxication enzymes, affording protection from deleterious endogenous and exogenous molecules. This review will focus on the distribution and functions of glutathione and glutathione transferases in bacteria, as the level of investigation and understanding in prokaryotes pales in comparison to that already accomplished in eukaryotes. Bacterial glutathione transferases are currently being investigated to solve problems in areas such as environmental remediation, further necessitating their intensive study.

Glutathione

Properties of Glutathione

Glutathione (GSH) is an important endogenous molecule present in a vast array of organisms, including animals, plants, fungi, most aerobic bacteria, and some archea.[1] L-Glutathione is a tripeptide composed of the L-amino acids glutamate, cysteine, and glycine (Figure 1-1).[2] The peptide bond bridging glutamate and cysteine is unique in that glutamate's γ-carboxyl group contributes to the amide linkage, rather than the α-carboxyl group. This isopeptide bond renders glutathione resistant to degradation by proteases.[1] At physiological pH, the pK_a of the cysteine sulfhydryl group in glutathione is about 9, so the protonated thiol species is predominant.[3] Due to the presence of the

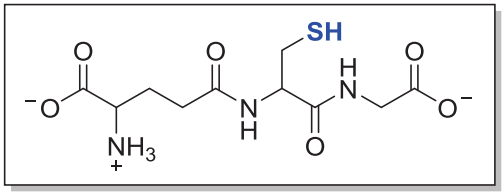

Figure 1-1: The chemical structure of L-glutathione.

sulfhydryl functionality, glutathione can easily undergo dimerization under oxidative conditions, resulting in the formation of glutathione disulfide (GSSG). The amino and carboxy termini of the tripeptide, as well as the α-carboxyl group of the glutamate residue, are ionized at physiological pH because their pK_a values are 8.75, 3.59, and 2.12, respectively.[4]

In bacteria, glutathione is mainly present in aerobic Gram-negative species, with rare occurrences in anaerobes and Gram-positive species, such as the *Enterococcus* and *Streptococcus* species.[1] Specifically, in *Escherichia coli* (*E. coli*), a Gram-negative facultative anaerobe, glutathione is present in concentrations ranging from 3.5 to 6.6 millimolar.[5] Under normal conditions, about 99.5% of glutathione in *E. coli* cells exists in the reduced monomeric state.[1]

Biosynthesis of Glutathione

Glutathione biosynthesis takes place in the cytosol, with subsequent organellar transport occurring in certain organisms. The synthesis of glutathione occurs in two steps, each facilitated by the action of a synthetase, an enzyme that ligates molecules through the use of adenosine triphosphate (ATP). The first step, the conjugation of L-glutamate and L-cysteine, is rate-determining and results in the production of γ-glutamyl-L-cysteine. This initial conjugation is catalyzed by γ-glutamylcysteine synthetase, also known as glutamate cysteine ligase (GCL).[6,7] GCL is composed of two subunits, a heavier catalytic subunit of 73 kDa (GCLC) and a smaller regulatory subunit of 28 kDa (GCLM). Feedback inhibition ensues when glutathione binds to GCLC at the glutamate binding site, but the action of GCLM can reduce the degree of inhibition by

glutathione.[7,8] Additionally, the activity of GCL is controlled by the levels of L-cysteine in the organism.[9] Expression of the GCL subunits can also dictate GCL activity and thus regulate glutathione concentration. Glutathione levels are elevated when expression of GCLC is increased, and highest when expression of both GCLC and GCLM is increased.[6] Following the action of GCL, γ-glutamyl-L-cysteine is subsequently ligated to L-glycine by glutathione synthetase, a homodimer with a subunit size of about 118 kDa. The resulting tripeptide is L-γ-glutamylcysteinylglycine.[6]

Functions of Glutathione

Detoxication of Xenobiotics

Glutathione serves a myriad of roles, most of which are defensive in nature. Glutathione can undergo spontaneous or enzyme-mediated reaction with harmful compounds to form glutathione adducts as a means of detoxication. The glutathione tranferases (GSTs) are a class of enzymes that catalyze the non-spontaneous reaction.[6] GSTs aid in enabling glutathione's interception of many deleterious alkylating agents. This prevents their reaction with nucleophilic components of important biomolecules, such as DNA and cysteine sulfhydryl groups that would otherwise result in disruption of normal cellular processes. The glutathione-toxicant adducts exhibit enhanced water solubility and attenuated reactivity, allowing for their facile excretion from the cell by ATP-powered Multidrug Resistance Proteins (MRPs).[2,10,11]

Antioxidant Function

By-products of normal cellular processes such as oxidative phosphorylation are the superoxide anion, hydrogen peroxide, and the hydroxyl radical, known collectively as reactive oxygen species (ROS). ROS are produced in large quantities under abnormal stress conditions, such as exposure to ionizing radiation. High levels of ROS can be damaging to lipids, proteins, and DNA.[12] When in close proximity to cellular membranes, highly reactive hydroxyl radicals abstract hydrogen atoms from lipids, propagating lipid peroxidation. In addition to obliterating cell membranes, highly toxic lipid peroxide products are generated that can react with cysteine, histidine, and lysine residues in proteins.[6]

Glutathione functions as an antioxidant, protecting organisms from oxidative stress. Similar to small molecules such as ascorbic acid and bilirubin, glutathione can accomplish this nonenzymatically, reducing the ROS while undergoing oxidation to form glutathione disulfide. This process occurs via the intermediary formation of thiyl radicals, as the sulfhydryl hydrogen atom is abstracted to reduce the radical species. Eventually, two thiyl radicals terminate to form the disulfide dimer.[13] Glutathione disulfide is subsequently reduced to glutathione by the NADPH-dependent enzyme glutathione reductase.[9] Selenoenzymes known as glutathione peroxidases (GPx) utilize glutathione as a co-substrate and reduce the hydroxyl radical, hydrogen peroxide, and lipid peroxides.[12,14] Some members of the glutathione transferase family of enzymes can catalyze the reduction of radical species in a selenium-independent manner.[11]

Glutathione's Interactions with Metals

Reduced glutathione is involved in the release, reduction, and transport of a variety of metals. Using the sulfhydryl moiety for coordination, glutathione can spontaneously bind arsenic, cadmium, copper, lead, mercury, silver, and zinc, forming glutathione-metal complexes. These complexes have been proposed to facilitate such processes as the transport of metals across cell membranes and ligand exchange.[13,15] Glutathione can reduce toxic chromium (VI) to chromium (III), a species better suited for cellular efflux. This reduction can be carried out both spontaneously and through the mediation of enzymes such as glutathione reductase.[13,16] Additionally, glutathione is able to retrieve copper from storage, reduce native copper (II) to copper (I), the required oxidation state for protein incorporation, and shuttle it to newly forming copper-containing proteins.[13,15]

S-Glutathionylation

S-Glutathionylation is the post-translational modification of a protein that involves the linkage of glutathione to the protein's cysteine residue(s). It is implicated as a preventative measure to protect proteins from oxidative damage. It is also thought to serve an important regulatory function with respect to the modulation of enzymatic activity and cellular signaling.[17] For example, when an organism is exposed to an external threat, such as a virus, glutathionylation affects a responsive signaling pathway by modification of interferon regulatory factor 3 (IRF3). IRF3 is normally glutathionylated, but when the organism recognizes an intruder, deglutathionylation results in the activation of transcription of interferon genes.[17,18] Additionally,

glutathionylation plays a role in the regulation of tumor necrosis factor-α-induced apoptosis. The enzyme caspase-3 is rendered inactive when glutathionylated because a crucial cysteine sulfhydryl group is oxidized. A study performed in endothelial cells found that when exposed to the enzyme glutaredoxin, caspase-3 was deglutathionylated, and necrosis factor-α-induced apoptosis ensued.[17,19] Bacterial glutathionylation mechanisms have not been as widely studied as those in eukaryotes. One example of a bacterial enzyme regulated by glutathionylation is 3'-phosphoadenylylsulfate reductase (PAPS-reductase) in *E. coli*. PAPS-reductase is inactive when its Cys239 active site residue is glutathionylated, but becomes active when glutaredoxin enzymes reduce the disulfide bond.[19,20]

Glutathione Transferases

Glutathione Transferase Discovery

The laboratories of Booth and Combes simultaneously discovered the enzymatic activity of a glutathione transferase enzyme in 1961.[21,22] Booth and co-workers partially purified the enzyme from rat liver, and found that it afforded a substantial rate enhancement for the conjugation of glutathione and 1,2-dichloro-4-nitrobenzene to yield *S*-(2-chloro-4-nitrophenyl)glutathione.[21] At nearly the same time, Combes' laboratory discovered that the presence of the soluble fraction of rat liver homogenate greatly accelerated the rate of the reaction between glutathione and sulfobromophthalein sodium, resulting in the formation of a thioether linkage via bromide displacement.[22] A glutathione transferase was not completely purified until 1974, when Habig and

colleagues purified two distinct glutathione transferases, "B and C", from rat liver to homogeneity using ion exchange chromatography and isoelectric focusing.[23]

Classification of Glutathione Transferases

It is accepted that glutathione transferases evolved to combat oxidative stress in organisms.[14] GSTs are found in both eukaryotes and prokaryotes, with more limited representation in archaea and Gram-positive bacteria.[24] An evolutionary rationale may be that these enzymes are absent in the same organisms that typically lack the ability to biosynthesize glutathione.[11] Glutathione transferases can be broadly divided into four major superfamilies: cytosolic (cytGSTs), mitochondrial, Membrane-Assisted Proteins in Eicosanoid and Glutathione Metabolism (MAPEG GSTs), and the Vicinal Oxygen Chelate Fold Superfamily (VOC GSTs).[25]

The largest superfamily of glutathione transferases is the cytosolic GSTs. Further divided into fourteen classes, this assortment of enzymes possesses great functional diversity. Each class of cytosolic GSTs is traditionally differentiated by a Greek letter, and members of the same class possess greater than 40% sequence identity.[26] This research is centered on a bacterial glutathione transferase. Therefore, only the relevant bacterial cytosolic classes will be discussed. To date, bacterial GSTs are represented by members of the beta, chi, nu, theta, and zeta classes.[11,27]

General Structure of Glutathione Transferases

Most glutathione transferases are homodimeric proteins. However, studies have shown that members of certain GST classes, for example alpha and mu, can form

heterodimers.[28] The overall fold of the GST subunit is highly conserved. Each subunit consists of an N-terminal domain and a C-terminal domain. The N-terminal domain displays a characteristic thioredoxin-like fold, consisting of four beta strands with two alpha helices on one side and one alpha helix on the other. The overall topology is β1-α1-β2-α2-β3-β4-α3. Beta strands 1 and 2 are parallel to each other, while strands 3 and 4 are antiparallel. The N-terminal domain is the location of the glutathione-binding site (G-site).[29]

The ββα motif in the N-terminal domain aids in glutathione recruitment to the active site by its recognition of glutathione's γ-glutamate residue.[30] Glutathione is then anchored to the enzyme via many non-covalent interactions, consisting of electrostatic interactions and hydrogen bonds. Of interest in beta class GSTs is an aspartate residue from the second subunit that hydrogen bonds to glutathione docked on the first subunit.[11] Once anchored to the enzyme, glutathione's cysteine sulfhydryl group experiences a significant decrease in pK_a, dropping from around 9 to a value ranging from 6.0 to 6.7. Armstrong and colleagues determined the pK_a of the sulfhydryl group of glutathione bound to isozyme 4-4 of rat liver glutathione transferase to be 6.6 via ultraviolet difference spectroscopy and solidly proved that the thiolate species was predominant in the glutathione active site.[3] The thiolate species is stabilized by hydrogen bond donation from certain amino acid residues, depending on GST class. In the beta class, a cysteine residue is responsible for hydrogen bond donation via its sulfhydryl group.[11] Hydrogen bond donation is provided by the hydroxyl group of a serine residue in members of the theta class.[30] Members of the zeta class possess a Tyr-Ser-Tyr sequence near the active

site, and it is not yet known whether serine or tyrosine participates as the hydrogen bond donor.[31]

A small loop links the N-terminal and C-terminal domains. The C-terminal domain contains only alpha helices, and the number of helices within the domain varies according to GST class. The C-terminal domain contains the hydrophobic-binding site (H-site), in which the electrophilic substrate can bind. While the G-site amino acid residues have been found to be relatively conserved, there is a high degree of variability in the H-site residues between GSTs. This variation is the basis for the different substrate specificities of GSTs.[29]

Bacterial Glutathione Transferases

Beta Class Characteristics

Members of the beta class of GSTs are found chiefly in aerobic bacteria. GSTs belonging to this class can be distinguished by several structural variations. In contrast to the majority of cytGSTs, the beta class dimer interface is not open. Instead, there is tight packing of residues. Additionally, the residues that line the interface are predominantly polar, while lipophilic residues typically populate the interface of GSTs. Beta class GSTs also contain a network of hydrogen bonds that links the final α-helix of the C-terminal domain to the beginning α-helix of the N-terminal domain.[11] Beta GSTs possess a Cys residue in the active site that is responsible for GSH thiol activation. Chemically, they are characterized by the ability to catalyze the conjugation of 1-chloro-2,4-dinitrobenzene (CDNB) and GSH. During protein purification, beta class GSTs will readily bind to a glutathione affinity matrix, allowing for relatively facile isolation.[11] Beta class GSTs can

be functionally categorized by their ability to bind certain compounds, including antibiotics, and by the variety of chemical reactions that they facilitate.

Beta class GSTs are of special interest due to their potential to actively bind antibiotics, and they have been found to utilize this binding mechanism to promote antibiotic resistance. An excellent example of a bacterial enzyme that demonstrates this ability both *in vitro* and *in vivo* is PmGSTB1-1, also known as GST-6.0, from *Proteus mirabilis*. Immunogold localization techniques determined that PmGSTB1-1 is more abundant in the periplasm, the space separating the cell wall and the cell membrane, than the cytosplasm, indicating its potential for antibiotic defense.[32] The minimum inhibitory concentrations were greatly increased for the antibiotics amikacin, ampicillin, cefotaxime, cephalothin, and nalidixic acid in a study that involved bacterial cell growth in the presence of purified PmGSTB1-1. The dissociation constants that were obtained for the drugs also suggested high affinity binding.[33] In a subsequent study, the authors concluded that PmGSTB1-1 binds rifamycin and the tetracyclines tightly after conducting inhibition studies that examined how antibiotics affected PmGSTB1-1 activity with CDNB. The IC_{50} values for PmGSTB1-1 CDNB activity were 85 μM for rifamycin, 54 μM for minocyclin, and 49 μM for tetracycline. Experiments verified that PmGSTB1-1 binds antibiotics at a site that is entirely separate from the G- and H-sites. Overexpression of PmGSTB1-1 permitted bacterial cell proliferation in the presence of 6.25 μg/mL rifamycin. Cells that did not overexpress PmGSTB1-1 were unable to grow in media supplemented with rifamycin, while no difference in growth was observed for the cell lines with the tetracycline compounds.[34] Following this work, the X-ray crystal structure

of PmGSTB1-1 was solved. A large hydrophobic cavity at the dimer interface was revealed, further supporting the antibiotic binding ability of PmGSTB1-1.[35]

Reactions Catalyzed by Bacterial GSTs

A variety of chemical reactions are catalyzed by bacterial GSTs. These GSTs belong to the beta class, "theta-like" class, or have yet to be assigned to a class. The reaction types promoted by bacterial GSTs include peroxide reduction, nucleophilic aromatic substitution (S_NAr), Michael addition, bimolecular nucleophilic substitution (S_N2), epoxide ring-opening, and reductive dehalogenation.[11] Representative reactions catalyzed by bacterial GSTs are illustrated in Figure 1-2.

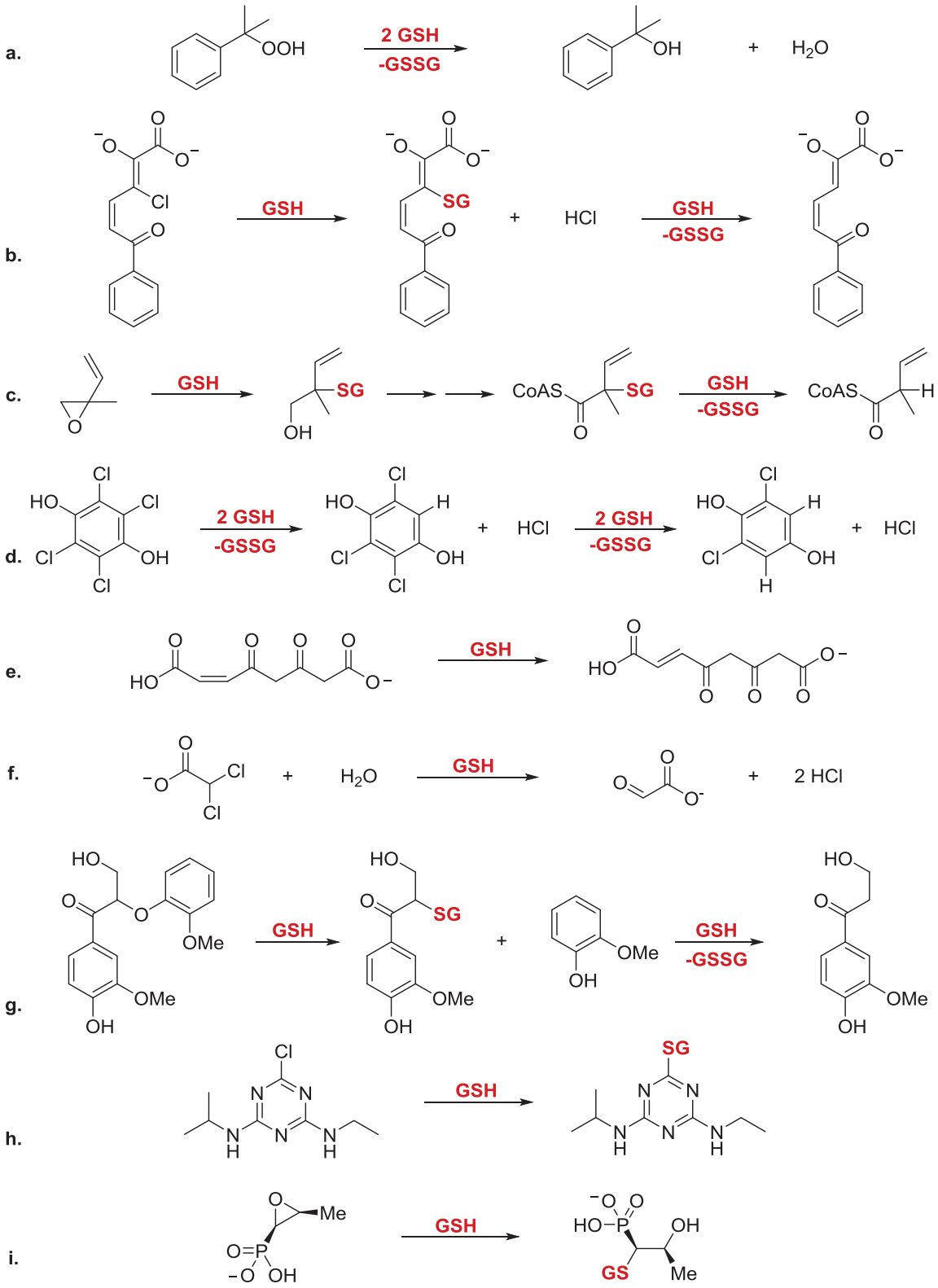

Figure 1-2 (a.-i.): Examples of reactions catalyzed by bacterial GSTs.

Three enzymes from *E. coli*, GST B1-1 (beta class), YfcF (class unassigned), and YfcG (nu class), have been found to display glutathione peroxidase activity toward cumene hydroperoxide (Figure 1-2a). Additionally, cell lines were more susceptible to oxidative damage when the individual genes were separately knocked out.[26,27] Interestingly, YfcG bears extensive structural similarity to *E. coli* YghU, a nu class enzyme that can reduce several organic hydroperoxides. Also, YfcG and YghU displayed disulfide bond reductase activity with the molecule 2-hydroxyethyl disulfide.[27] PmGSTB1-1 was also able to reduce hydrogen peroxide. This activity was supported by the ability of hydrogen peroxide to induce PmGSTB1-1 expression on both the transcriptional and translational levels, and the elevated sensitivity to hydrogen peroxide exhibited by knockout cell lines.[36]

$BphK^{LB400}$ from *Burkholderia xenovorans* strain LB400 is a beta class glutathione transferase that assists in the degradation of biphenyl and chlorophenyl derivatives.[11] These compounds are degraded in aerobic bacteria by the *bph* pathway. When it was discovered that BphK can effectively dechlorinate 4-chlorobenzoate, work was done by the Fortin group to determine whether the enzyme could dechlorinate 3-chloro-2-hydroxy-6-oxo-6-phenyl-2,4-dienoate (3-Cl HOPDA), an inhibitor of the final hydrolysis step in the *bph* pathway.[37] 3-Cl HOPDA (Figure 1-2b) is produced when polychlorinated biphenyls (PCBs) are co-metabolized with biphenyl compounds. The finding was that BphK was successful in dechlorinating 3-Cl HOPDA and 5-Cl HOPDA, but not 4-Cl HOPDA. Fortin proposed two dehalogenation mechanisms. The first is addition of the glutathione thiolate, followed by elimination of the chloride anion. The second is a concerted bimolecular substitution reaction.[37]

Two GSTs from *Rhodococcus* sp. strain AD45, a bacterium that can thrive on isoprene, are involved in the metabolism of isoprene, an unsaturated hydrocarbon that is naturally produced and released by organisms in the environment. Isoprene is initially oxidized by Phase I monooxygenases to yield the more soluble epoxide products, such as *cis*-1,2-dichloroepoxyethane and isoprene monoxide. IsoI catalyzes the GSH-dependent ring-opening of the epoxide isoprene monoxide to produce 1-hydroxy-2-glutathionyl-2-methyl-3-butene (Figure 1-2c). IsoJ then removes the glutathione moiety from the conjugate. This activity is unique because Gram-positive bacteria such as this *Rhodococcus* strain do not typically exhibit detectable levels of glutathione.[38,39]

Tetrachlorohydroquinone dehalogenase (TCHQ dehalogenase) from *Sphingomonas chlorophenolica* is an essential enzyme in the metabolism of the dangerous oxidative phosphorylation uncoupling agent pentachlorophenol (PCP). PCP is a common antifungal agent used for wood preservation. During Phase I metabolism of PCP, pentachlorophenol hydroxylase generates tetrachlorohydroquinone (TCHQ). TCHQ is then reductively dehalogenated to trichlorohydroquinone (TriCHQ) by TCHQ dehalogenase, with the concomitant oxidation of two glutathione molecules to glutathione disulfide. Next, TriCHQ is reductively dehalogenated to yield 2,6-dichlorohydroquinone (DCHQ) in an identical manner (Figure 1-2d). DCHQ undergoes a ring-cleavage step to produce the end product of the degradation pathway, 2,4-dichloro-3-hydroxy-*cis,cis*-muconic semialdehyde (DCHMS).[40]

It was discovered that TCHQ dehalogenase from *S. chlorophenolica* also possesses maleylacetoacetate isomerase activity. In certain organisms, including bacteria and fungi, phenylalanine and tyrosine are broken down via the homogentisate pathway.

The intermediate homogentisate is produced and converted to maleylacetoacetate. Maleylacetoacetate isomerase catalyzes the reaction in which the *cis*-double bond of maleylacetoacetate is isomerized to a *trans*-double bond, producing fumarylacetoacetate (Figure 1-2e). The isomerization reaction requires the participation of one molecule of glutathione. The same TCHQ dehalogenase has also been found to catalyze the conversion of dichloroacetate, a carcinogen produced during water sanitization, to glyoxylate (Figure 1-2f). Mammalian zeta class GSTs in human and rat have been confirmed to possess this activity.[11,40]

The *ligDFEG* gene cluster from *Sphingomonas paucimobilis* SYK-6 is responsible for the bacterial lignin degradation pathway. Lignin is a phenol-based polymer linked through β-aryl ether bonds, and is considered to be the most prevalent aromatic material in nature. The *ligDFEG* cluster contains two glutathione transferases, β-etherases LigE and LigF, and a glutathione lyase, LigG. LigF was found to be inactive with the archetypal GST substrates CDNB, *p*-nitrobenzyl chloride, and 1,2-epoxy-3-*p*-nitrophenoxypropane. Nonetheless, Masai and co-workers reported a 500-fold increase in β-etherase activity when LigF was added to a mixture of GSH and lignin.[41] HPLC and ESI-MS analysis revealed that LigF functions by mediating the nucleophilic attack of GSH on the beta carbon of lignin catabolite α-(2-methoxyphenoxy)-β-hydroxypropiovanillone (MPHPV) to form the GSH conjugate glutathionyl-β-hydroxypropiovanillone (GS-HPV) (Figure 1-2g). LigE is also able to catalyze this reaction, but its specific activity was estimated to be 170 times lower than that of LigF. LigG is a glutathione lyase that catalyzes the removal of the glutathionyl moiety from GS-HPV to produce the HPV product.[42]

Certain bacteria are capable of metabolizing the popular herbicide atrazine. GSTs initiate the process by catalyzing the dechlorination of the molecule, producing an atrazine-GSH conjugate (Figure 1-2h). *Ochrobactrum anthropi* is an aerobic Gram-negative bacterium that possesses the beta class enzyme OaGST. OaGST catalyzes the dechlorination of atrazine and enables the microorganism to survive with only atrazine as the carbon source. Favaloro and co-workers observed an increase in the expression of OaGST upon the addition of atrazine to cell culture.[43]

Arca and co-workers isolated the 32 kDa dimeric enzyme FosA from a clinical bacteria sample that is understood to confer resistance to the broad-spectrum antibiotic fosfomycin.[44] Fosfomycin is a competitive inhibitor of the enzyme MurA. MurA ligates the enolpyruvate group of phosphoenolpyruvate with uridine diphospho-*N*-acetylglucosamine, catalyzing the first-committed step of bacterial peptidoglycan biosynthesis. While it was discovered that FosA is unable to bind GSH-affinity resin and catalyzed GSH and CDNB conjugation, it was proven through GSH-derivitization and HPLC that the enzyme facilitates GSH-mediated epoxide-opening of fosfomycin, resulting in a fosfomycin-GSH conjugate which no longer inhibits MurA (Figure 1-2i).[44] Using Electron Paramagnetic Resonance (EPR) spectroscopy, Armstrong and co-workers subsequently discovered that FosA is specifically a manganese metalloglutathione transferase wherein each subunit contains a divalent magnesium cation in the active site that coordinates fosfomycin, His7, and Glu113. Interestingly, FosA was found to operate optimally in the presence of monovalent potassium cation.[45]

Theta class GSTs are found in mammals, but enzymes resembling theta class members are present in bacteria. Theta class GSTs cannot conjugate GSH and CDNB and

do not bind glutathione affinity matrices. Their active sites contain a Ser residue which is responsible for the activation of the glutathione nucleophile.[46] In methylotrophic bacteria *Methylobacterium* DM4 and *Methylophilus* DM11, theta class-like GSTs known as dichloromethane dehalogenases catalyze the conjugation of dichloromethane and other methyl halides. In this manner, these bacterial species may subsist with dichloromethane as the only carbon source. The reaction of GSH with dihalomethanes like dichloromethane proceeds via an S_N2 mechanism, producing *S*-chloromethylglutathione. This intermediate is typically intercepted by water, resulting in *S*-hydroxymethyl-glutathione, which is subsequently converted to formaldehyde and free glutathione. Gisi and colleagues found that the *S*-chloromethylglutathione intermediate can form genotoxic DNA adducts.[47,48] Stourman and colleagues corroborated this finding by elucidating the exact mechanism of dichloromethane metabolism by *Methylophilus* DM11.[49] The order of catalytic efficiency for dihalomethanes is strongly correlated with leaving group efficacy.[48]

The activity of DM11 GST with ethyl halides has been thoroughly investigated. For monohaloethanes, catalytic efficiency corresponds to leaving group propensity, with brominated compounds exhibiting better kinetic parameters than chlorinated ones. 1,2-Dihaloethanes, also known as vicinal dihalides, are also substrates for this enzyme. However, the catalytic efficiency cannot wholly be explained by leaving group ability. Wheeler and colleagues found that unexpectedly, 1-bromo-2-chloroethane outperformed 1,2-dibromoethane, followed by 1,2-dichloroethane.[50] The mechanism for 1,2-dihaloethane metabolism is more complicated than that of the dihalomethanes. Initially, GSH reacts with the electrophile to produce an *S*-haloethylglutathione intermediate. The

intermediate undergoes an intramolecular nucleophilic substitution reaction, forming a glutathione episulfide. The episulfide may be attacked by a variety of nucleophiles, including another molecule of glutathione (forming *S,S*-ethylene-bis-glutathione), a water molecule (forming *S*-hydroxyethylglutathione), or DNA (forming a genotoxic adduct).[50]

GstB from *Escherichia coli*

Bromoacetate Degradation

GstB from *Escherichia coli* is a GST that remains relatively uncharacterized. GstB is encoded by the gene *yliJ/gst*B and is located in the cytosol. It is a homodimer comprised of two 23,713 Da subunits. Each subunit consists of 208 amino acid residues. Its theoretical isoelectric point is 5.05, indicating that this enzyme exhibits a net negative charge under physiological conditions.[51] GstB cannot catalyze the conjugation of GSH and CDNB and does not display binding affinity toward GSH resin (Stourman, unpublished results). Using genetic selection and *E. coli* single-gene knockout Keio screening, Desai and Miller made the discovery that the enzyme GstB, encoded by the gene *yliJ*, catalyzes the conjugation of glutathione and the toxicant bromoacetate (Figure 1-3).[52] Bromoacetate, along with other haloacetic acids, is a common water disinfection by-product (DBP). Other haloacetic acid DBPs include chloroacetate, iodoacetate, dichloroacetate, dibromoacetate, trichloroacetate, and tribromoacetate.

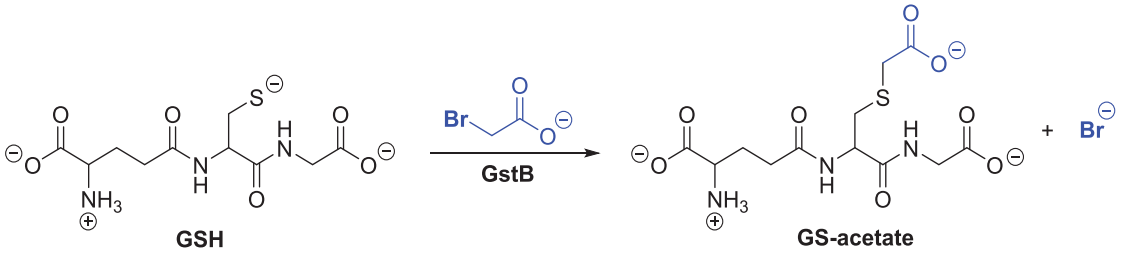

Figure 1-3: Conjugation of bromoacetate and glutathione catalyzed by GstB.

Bromoacetate has been found to be mutagenic in bacteria and mammalian cells *in vitro*.[53] The conjugation of bromoacetate and glutathione proceeds spontaneously at a rate of 1.4 x 10^{-2} $M^{-1}s^{-1}$, while GstB provides marked rate enhancement of 5.4 x 10^{3} $M^{-1}s^{-1}$. It is likely that the GstB-mediated reaction proceeds via a basic S_N2 mechanism. Kinetic analysis allowed for the calculation of a Michaelis constant (K_M) of 5 mM and a turnover number (k_{cat}) of 27 s^{-1}, with respect to bromoacetate.[52] Kinetic studies were also carried out with the halogenated carboxylate compounds chloroacetate, iodoacetate, 2-bromopropionate, and 3-bromopropionate (Table 1-1). GstB displayed appreciable activity with only iodoacetate. Additionally, bromoacetamide was tested, and it was concluded that GstB did not accept the amide functionality. To supplement their kinetic findings, the authors conducted compound sensitivity studies. They separately created the knockout mutants *GstB*$^-$ and *GshA*$^-$. *GshA* encodes glutamate-cysteine ligase, the enzyme that catalyzes the first step of glutathione biosynthesis. *GstB*$^-$, *GshA*$^-$, and the wild-type bacteria were plated on media containing bromoacetate, iodoacetate, and bromoacetamide. The results indicated that *GstB*$^-$ was more sensitive to bromoacetate than the wild-type, but not quite as sensitive as *GshA*$^-$. Both mutants were sensitive to iodoacetate. *GstB*$^-$ was resistant to bromoacetamide, while *GshA*$^-$ was sensitive to the compound. After analysis of both the kinetic and compound sensitivity studies, it was concluded that the probable physiological substrate for GstB is a small carboxylated molecule.[52]

Table 1-1: Results of GstB activity screening.[52]

Compound	Activity (μmoles min^{-1} mg^{-1})
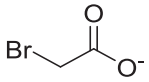	10.5
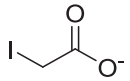	48.9
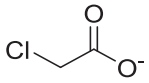	<0.07
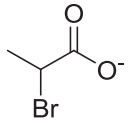	<0.07
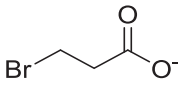	<0.07
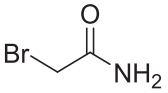	<0.07

Arsenate Detoxication

In 2015, Chrysostomou et al. described the ability of GstB from *E. coli* to reduce pentavalent arsenate to trivalent arsenite.[54] *E. coli* possess the *arsC* gene that encodes an enzyme to accomplish this reduction, rendering the arsenite product more suitable for cellular efflux by the arsenite transporter protein ArsB. This enzyme relies on the action of glutaredoxin. The authors overexpressed GstB in *arsC*-null mutants, and discovered that GstB is capable of reducing arsenate to arsenite, relying solely upon glutathione for reducing power.

Chrysostomou et al. sought to interrogate the GstB active site residues that are responsible for binding the arsenate substrate. The X-ray crystal structure of GstB has not

yet been solved. The authors used a solved X-ray crystal structure of an orthologous GST from *Salmonella enterica* to study the GstB H-site, as this protein bears 83% sequence identity to GstB. The crystal structure highlighted the presence of three arginine residues, Arg7, Arg111, and Arg119, within 7 Å of the G-site. Arg7 is known to be a part of the G-site, so its role was not investigated. A Chimera view of this crystal structure with bound glutathione is displayed in Figure 1-4. Single mutants of Arg111 and Arg119 were generated in which the mutant residue was glutamine. A double mutant in which both Arg111 and Arg119 were mutated to glutamine was also created. The Arg119Gln mutant was more sensitive to arsenate than the Arg111Gln mutant and was unable to grow on media that contained more than 2 mM sodium arsenate. The double mutant resulted in a complete loss of arsenate resistance. Additionally, this mutant did not display any activity toward the previously described GstB substrate bromoacetate. The authors concluded that Arg111 and Arg119 are essential for adequate electrophile binding by GstB.[54]

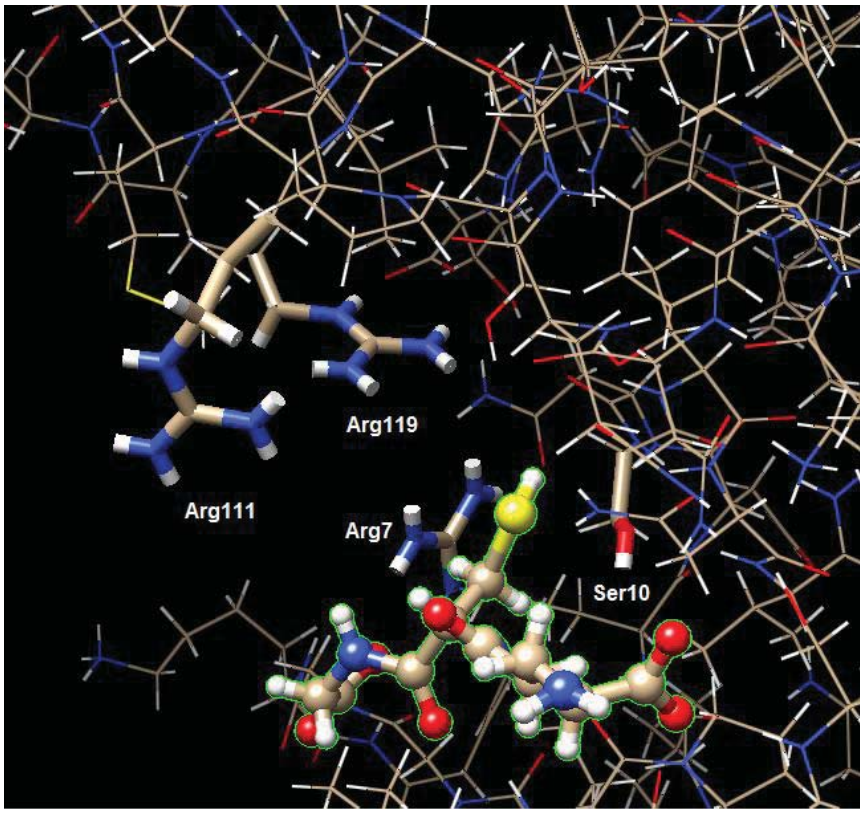

Figure 1-4: Chimera 1.11-generated image of the active site of YliJ from *S. enterica.*

Bacterial GST Bioremediation

It is essential that more bacterial GSTs are fully characterized because of their important applications. In addition to their implication in antibiotic resistance, GSTs are being investigated for their use in bioremediation. Bioremediation is the utilization of biological systems to protect the environment via the elimination of pollutant compounds. It is a cost-effective alternative to current methods of remediation, such as incineration, which are expensive.[55] Bacterial GSTs are excellent candidates for bioremediation because they are relatively robust enzymes, functioning over a broad range of both temperature and pH. If more is discerned about the relationship between the identity of

H-site amino acid residues and substrate specificity, then GSTs could potentially be engineered to detoxify target toxic compounds in the environment.

In 2004, Rui et al. successfully engineered an eight-gene metabolic pathway in *E. coli* that can degrade both *cis*- and *trans*-1,2-dichloroethylenes and trichloroethylene with greater efficiency than has been previously observed.[56] Particularly, *cis*-1,2-dichloroethylene was degraded 3.5-fold more rapidly. During traditional degradation of these compounds, promiscuous oxygenases, such as toluene *ortho*-monooxygenase (TOM) produce chlorinated epoxyethanes. These are dangerous alkylating agents that promote cell death. Rui and colleagues included the five-gene TOM-green system and IsoILR1, a GST from *Rhodococcus* sp. strain AD45, in their engineered pathway that functioned to intercept the chlorinated epoxyethane intermediate via formation of an inactive glutathione conjugate. They also included γ-glutamylcysteine synthetase to allow for enhanced glutathione availability.[56] This bioengineering work highlights the practicality of using glutathione transferases to mitigate dangerous natural processes.

Rather than working to engineer entire degradative pathways, McGuinness et al. have been employing the technique of site-directed mutagenesis to interrogate specific GST amino acid residues and improve GST efficiency toward compounds of environmental concern.[57-59] Using site-directed mutagenesis, they created mutants of the GST $BphK^{LB400}$ from the Gram-negative bacterium *Burkholderia xenovorans,* which is a known degrader of polychlorinated biphenyls (PCBs). In their 2006 study, McGuinness and co-workers mutated two residues that were found to be highly conserved across enzymes from PCB-degrading bacteria. The mutants were Ser152Thr and Ala180Pro. The Ala180Pro mutant greatly outperformed the wild-type in catalyzing the conjugation

of GSH to 1-chloro-2,4-dinitrobenzene (CDNB), a classic GST substrate. Additionally, this mutant possessed far more activity toward 3-chlorobenzoate, 4-chlorobenzoate, and 3-chloro-2-hydroxy-6-oxo-6-phenyl-2,4-dienoate, metabolites of the breakdown of PCBs and herbicides, as well as the herbicides 2,4-dichlorophenoxyacetate and atrazine.[57] The Ala180Pro mutant was further evaluated in a plant inoculation study. First, the activity of the Ala180Pro mutant toward pentanochlor, Clean-up®, chloromequat chloride, and triphenyltin chloride was assessed. Mutant BphK activity increased 1.4-fold for both pentanochlor and chloromequat, and 1.1-fold for Clean-up®. Next, pea plants were injected with *E. coli* that overexpressed either wild-type BphK or the Ala180Pro mutant. After 25 days of exposure to increasing concentrations of chloromequat chloride, plant root biomass and length were measured. Both the wild-type and mutant BphK-containing strains displayed better growth parameters than the plants inoculated with normal *E. coli.*[58] In a 2009 study, the same authors produced the Cys10Phe mutant of $BphK^{LB400}$ on the basis that Cys10 was observed in 61 aligned GSTs. It was discovered that this mutant displayed nearly 5-fold greater activity with CDNB than the wild-type. The authors intend to examine the activity of the Cys10Phe mutant toward the chlorinated pesticides that they previously investigated in their study of the Ala180Pro mutant.[59]

In 2010, Federici and colleagues analyzed a solved crystal structure of PmGST from *Proteus mirabilis* to create four PmGST mutants that demonstrated excellent stability across a wide range of both temperature and pH.[60] The mutations were carried out on residues that faced the PmGST H-site. The mutants were screened for activity with substrates representative of different reaction mechanisms, including S_N2, S_NAr, Michael addition, and hydroperoxide reduction. Most notably, the Trp164Ala mutant displayed

the greatest activity with both CDNB and FDNB. It was also the most active mutant toward ethacrynic acid, with which GSH conjugation proceeds through Michael addition.[60] These pioneering investigations on GSTs in the bioremediation process provide a promising rationale for further work in this area.

Statement of Purpose

Bacterial glutathione transferases remain relatively unexplored to date. The glutathione transferase GstB from *Escherichia coli* is the focal point of this work. Three research goals will guide the study of GstB. The first goal is to improve the purification of the native GstB enzyme by assessing the efficacy of various protein precipitation strategies.

The second goal is to characterize the substrate scope of GstB. The enzyme activity with a variety of compounds bearing different functional groups will be assessed. This will enable a more thorough understanding of the function of this enzyme. Potential GstB substrates will be evaluated both *in vitro* and *in vivo*.

The third goal is to examine the potential relationship between GstB electrophile-binding site amino acid residue identity and substrate specificity. This will be accomplished via site-directed mutagenesis of the arginine at position 119, a residue that has been implicated in electrophilic substrate binding. The residue substitutions will include alanine, histidine, glutamine, and serine, all sterically and electronically diverse. Alteration of GstB substrate specificity in this manner can be utilized as the basis for pollutant-targeted enzyme engineering for bioremediation purposes.

CHAPTER 2. MATERIALS & METHODS

Materials

Protein Expression & Purification: The expression vector *pET20b(gstB)* was provided by Dr. Nina V. Stourman. *Escherichia coli* BL21 (DE3) cells were purchased from Invitrogen (Carlsbad, CA). *Escherichia coli* DH5α cells were a gift from Dr. Jonathan Caguiat. Luria-Bertani (LB) medium, SOB medium, bacteriological agar, isopropyl β-D-1-thiogalactopyranoside (IPTG), ampicillin sodium salt, DL-dithiothreitol (DTT), ethylenediaminetetraacetic acid (EDTA), ammonium sulfate, and streptomycin sulfate were purchased from Amresco (Solon, Ohio). Hydroxylapatite was purchased from Bio-Rad (Hercules, CA), and Q-Sepharose was purchased from GE Healthcare (Piscataway, NJ).

Site-directed Mutagenesis: The QuikChange II Site-directed Mutagenesis Kit was purchased from Agilent Technologies (Santa Clara, CA), and custom DNA oligonucleotide primers were purchased from Thermo Fisher Scientific (Waltham, MA). The QIAprep Spin Miniprep Kit was purchased from Qiagen (Germantown, MD).

Buffers & Reagents: Sodium phosphate monobasic (anhydrous), sodium phosphate dibasic (anhydrous), TRIS, TRIS-HCl, sodium dodecyl sulfate (SDS), *N,N,N'N'*-tetramethylethylenediamine (TEMED), glycerol, sodium chloride, and chloramphenicol were purchased from Amresco (Solon, OH). Acrylamide (40%) was purchased from Fisher Scientific (Hampton, NH). Reduced L-glutathione, 5,5'-dithio-bis(2-nitrobenzoic acid) (DTNB), iodoacetamide, iodoacetic acid, phosphomycin disodium salt, and 1-chloro-2,4-dinitrobenzene (CDNB) were purchased from Sigma-Aldrich (St. Louis, MO). Chloroacetic acid and dichloroacetic acid were purchased from Alfa-Aesar (Haverhill,

MA). Bromoacetic acid and dimethyl sulfoxide (DMSO) were purchased from Acros Organics (NJ). Page Ruler® protein ladder was purchased from Thermo Fischer Scientific (Waltham, MA). Acrylic acid, 2-bromobutyric acid, 3-bromo-1-propanol were purchased from Aldrich Chemical Company (Milwaukee, WI). *trans*-Cinnamic acid and ethyl bromoacetate were purchased from Sigma-Aldrich (St. Louis, MO).

Metal Salts: Gold (III) chloride, potassium chromate, cobalt (II) chloride, cadmium (II) chloride, sodium arsenite, and sodium selenite were provided by Dr. Jonathan Caguiat (Youngstown State University). Sodium arsenate dibasic heptahydrate was purchased from Sigma-Aldrich (St. Louis, MO). Silver nitrate was purchased from Reagent World (Irvine, CA). Copper (II) sulfate and mercury (II) chloride were purchased from Fisher Scientific (Fair Lawn, NJ). Terbium (III) nitrate hydrate and cerium (III) nitrate hexahydrate were purchased from Alfa Aesar (Haverhill, MA), Ammonium molybdate tetrahydrate was purchased from J. T. Baker (Phillipsburg, NJ). Lead (II) acetate, manganese (II) sulfate monohydrate, nickel (II) nitrate, and tin (II) chloride were purchased from Mallinckrodt (St. Louis, MO). Barium oxide was purchased from Acros Organics (NJ).

Instrumentation: An HP Agilent 8453 Diode Array spectrophotometer (Santa Clara, CA) was used for all spectrophotometric analysis and assays.

Methods

PART I. EXPRESSION & PURIFICATION OF WILD TYPE GSTB

Expression of Wild Type GstB

A 50 mL liquid Luria-Bertani (LB) medium containing 100 µg/mL ampicillin was inoculated with BL21 (DE3) cells containing pET20-*gstB*. The culture was incubated at 37 ºC with shaking at 200 rpm for 18 h. Three separate 12-mL aliquots of the culture were diluted into three flasks containing 1.2 L LB with 100 µg/mL ampicillin. The 1.2-L cultures were incubated at 37 ºC with shaking at 200 rpm until the OD_{600} was between 0.6 and 0.8. Protein expression was initiated by the addition of isopropyl-β-D-1-thiogalactopyranoside (IPTG) to a final concentration of 0.30 mM, and the cultures were incubated at 37 ºC with shaking at 175 rpm for 19 h. The cells were pelleted via centrifugation at 10,000 x g and 4 ºC for 10 min. The resulting pellets were stored at -20 ºC. In an effort to optimize ammonium sulfate precipitation conditions, the six cell pellets were separated and treated with different concentrations of ammonium sulfate, as described below.

Ammonium Sulfate Precipitation 1

The frozen cell pellet was resuspended in 15 mL of 10 mM Tris, pH 7.0, containing 2 mM EDTA and 1 mM DTT. The suspension was subjected to eight cycles consisting of 30 s of sonication and 1 min of stirring on ice. The cell lysate was centrifuged at 11,000 x g and 4 ºC for 20 min. The pellet was discarded. To promote the precipitation of nucleic acids, streptomycin sulfate in 10 mM Tris, pH 7.0, containing 2 mM EDTA and 1 mM DTT was added dropwise to the supernatant to obtain a final

concentration of 1% (w/v). After centrifugation at 11,000 x g and 4 ºC for 30 min, the pellet was discarded and 4.28 g of ammonium sulfate (45% saturation) were slowly added to the supernatant with vigorous stirring. The resulting suspension was centrifuged at 10,000 x g and 4 ºC for 30 min. The pellet was discarded. Further precipitation was encouraged by the addition of 3.59 g of ammonium sulfate (75% saturation). Centrifugation at 10,000 x g and 4 ºC and for 30 min yielded the protein pellet.

Ammonium Sulfate Precipitation 2

The frozen cell pellet was resuspended in 15 mL of 10 mM Tris, pH 7.0, containing 2 mM EDTA and 1 mM DTT. The suspension was subjected to eight cycles consisting of 30 s of sonication and 1 min of stirring on ice. The cell lysate was centrifuged at 10,000 x g and 4 ºC for 30 min. The pellet was discarded. To promote the precipitation of nucleic acids, streptomycin sulfate in 10 mM Tris, pH 7.0, containing 2 mM EDTA and 1 mM DTT was added dropwise to the supernatant to obtain a final concentration of 1% (w/v). After centrifugation at 10,000 x g and 4 ºC for 30 min, the pellet was discarded and 2.28 g of ammonium sulfate (25% saturation) were slowly added to the supernatant with vigorous stirring. The resulting suspension was centrifuged at 10,000 x g and 4 ºC for 30 min. The pellet was discarded. Further precipitation was encouraged by the addition of 3.21 g of ammonium sulfate (60% saturation). Centrifugation at 10,000 x g and 4 ºC for 40 min yielded the protein pellet.

Ammonium Sulfate Precipitation 3

A total of four frozen cell pellets were resuspended in 60 mL of 10 mM Tris, pH 7.0, containing 2 mM EDTA and 1 mM DTT. The suspension was subjected to eight cycles consisting of 30 s of sonication and 1 min of stirring on ice. The resulting cell lysate was centrifuged at 10,000 x g and 4 ^{o}C for 30 min. The pellet was discarded. To promote the precipitation of nucleic acids, streptomycin sulfate in 10 mM Tris, pH 7.0, containing 2 mM EDTA and 1 mM DTT was added dropwise to the supernatant to obtain a final concentration of 1% (w/v). After centrifugation at 10,000 x g and 4 ^{o}C for 30 min, the pellet was discarded and 27.47 g of ammonium sulfate (75% saturation) were slowly added to the supernatant with vigorous stirring. The suspension was left to stand on ice for an additional 10 min. Centrifugation at 10,000 x g and 4 ^{o}C for 40 min yielded the protein pellet. The pellet was resuspended in a minimal volume of 20 mM Tris, pH 7.4, containing 1 mM DTT and dialyzed against 3 L of the same buffer for 16 h.

Anion Exchange Column Chromatography

A Q-Sepharose Fast Flow anion exchange column (3 x 12 cm) was equilibrated with 500 mL of 20 mM Tris, pH 7.4, containing 1 mM DTT. The dialyzed protein sample was centrifuged at 10,000 x g and 4 ^{o}C for 10 min, and the supernatant was applied to the column. The column was washed with 500 mL of 20 mM Tris, pH 7.4, containing 1 mM DTT. The protein was eluted with a 400-mL gradient of 0 to 400 mM sodium chloride in 20 mM Tris, pH 7.4, containing 1 mM DTT, and 3-mL fractions were collected. The fractions were analyzed by measuring the absorbance at 280 nm and SDS-PAGE. Fractions containing an appreciable amount of pure GstB were pooled and concentrated

via centrifugation at 10,000 x g and 4 ^{o}C using an Amicon Ultra centrifugal filter unit (MWCO: 10,000 Da).

PART II. WILD TYPE GSTB KINETICS

Initial Activity Screening

The CDNB activity assay was adapted from the protocol published by Habig and colleagues[61]. A solution of 58 mM CDNB was prepared in 95% ethanol. The spontaneous reactions consisted of 960 µL of 50 mM NaP_i, pH 7.0, 20 µL of 100 mM GSH, and 20 µL of 58 mM CDNB. Upon the addition of CDNB, the absorbance at 340 nm was recorded every 30 s for 10 min. The catalyzed reactions consisted of 940 µL of 50 mM NaP_i, pH 7.0, 20 µL of 100 mM GSH, 20 µL of enzyme, and 20 µL of 58 mM CDNB. Upon the addition of CDNB, the absorbance at 340 nm was recorded every 30 s for 10 min.

Enzyme activity with all other substrates tested was measured via a discontinuous spectrophotometric assay using 5,5'-dithio-bis-(2-nitrobenzoic acid) (DTNB), or Ellman's reagent. The absorbance at 412 nm was measured, as 412 nm is the λ_{max} for the 2-nitro-5-thiobenzoate anion (TNB^{2-}; ε = 13,600 $M^{-1}cm^{-1}$). Before each measurement, a quartz cuvette containing 925 µL of 200 mM Tris (pH 8.0) and 50 µL of 5 mM DTNB in ethanol was blanked, and 25 µL of reaction mixture was added to the cuvette.

All potential GstB substrates were initially screened using the same enzyme activity assay protocol described below. Stock solutions of the electrophiles were 100 mM and prepared in 50 mM NaP_i, pH 7.0. Stock solutions of GSH were 50 mM and prepared in 50 mM NaP_i, pH 7.0.

Uncatalyzed Reaction

Each uncatalyzed reaction contained 360 µL of 50 mM NaP_i, pH 7.0, 50 µL of 50 mM GSH, and 90 µL of 100 mM electrophile, added last. The final concentrations of GSH and electrophile in the reaction were 5 mM and 18 mM, respectively. After addition of the electrophile, the reaction was incubated at room temperature for 10 min. Every 2 min, a 25-µL aliquot of reaction mixture was added to the cuvette containing DTNB solution, and the absorbance at 412 nm was measured.

Catalyzed Reaction

Each catalyzed reaction contained 350 µL of 50 mM NaP_i, pH 7.0, 50 µL of 50 mM GSH, 10 µL of 50 µM GstB, and 90 µL of 100 mM electrophile, added last. The final concentrations of GSH, electrophile, and GstB in the reaction were 5 mM, 18 mM, and 1 µM, respectively. After addition of the electrophile, the reaction was incubated at room temperature for 10 min. Every 2 min, a 25-µL aliquot of reaction mixture was added to the cuvette containing DTNB solution, and the absorbance at 412 nm was measured. If the difference in uncatalyzed and catalyzed reaction rates was significant, kinetic assays were performed.

Substrate-Specific Reaction Conditions

Acrylic acid: The reaction mixture contained 4.5 mM GSH, 1.3 μM GstB, and 18 mM acrylic acid.

2-Bromobutyric acid: The reaction mixture contained 4.5 mM GSH, 1.3 μM GstB, and 18 mM 2-bromobutyric acid.

3-Bromo-1-propanol: The reaction mixture contained 3.6 mM GSH, 1.1 μM GstB, and 18 mM 3-bromo-1-propanol.

***Trans*-Cinnamic acid:** The reaction mixture contained 4.4 mM GSH, 1.3 μM GstB, and 18 mM *trans*-cinnamic acid.

Chloramphenicol: The chloramphenicol stock solution was prepared in 50 mM NaP_i, pH 7.0, containing 30% dimethyl sulfoxide (DMSO). The reaction mixture contained 4.6 mM GSH, 1.3 μM GstB, and 9.4 mM chloramphenicol.

Chloroacetic acid: The reaction mixture contained 1.9 mM GSH, 1.4 μM GstB, and 21 mM chloroacetic acid.

Dichloroacetic acid: The reaction mixture contained 3.6 mM GSH, 1.1 μM GstB, and 18 mM dichloroacetic acid. Additional trials were performed in which the concentration of dichloroacetic acid was 4.5 mM, 9.0 mM, 18 mM, and 90 mM.

Ethyl bromoacetate: The reaction mixture contained 4.8 mM GSH, 1.3 μM GstB, and 1.8 mM ethyl bromoacetate.

Fosfomycin: The reaction mixture contained 4.7 mM GSH, 1.5 μM GstB, and 18 mM fosfomycin.

Iodoacetamide: The reaction mixture contained 4.8 mM GSH, 1.5 μM GstB, and 18 mM iodoacetamide.

Michaelis-Menten Kinetics: Varying Electrophile Concentration

Stock solutions of the electrophiles were prepared in 50 mM NaP_i, pH 7.0 and diluted accordingly using the same buffer. Stock solutions of GSH were 50 mM and prepared in 50 mM NaP_i, pH 7.0.

Determination of Initial GSH Concentration

To determine the initial GSH concentration, 50 µL of GSH solution were added to 450 µL 50 mM NaP_i, pH 7.0. The solution was mixed and 25 µL were delivered to the cuvette containing DTNB solution. The absorbance at 412 nm was measured. All initial GSH concentration determinations were performed in duplicate and averaged.

Uncatalyzed Reaction

Each uncatalyzed reaction contained 360 µL of 50 mM NaP_i, pH 7.0, 50 µL of 50 mM GSH, and 90 µL of electrophile at varying concentrations, added last. The final concentrations of each component in the reaction and the allotted reaction times are detailed below. Following the specified 25 °C incubation period, a 25-µL aliquot of reaction mixture was added to the cuvette containing DTNB solution. The absorbance at 412 nm was recorded. All reactions were performed in duplicate and averaged.

Catalyzed Reaction

Each catalyzed reaction contained 350 µL of 50 mM NaP_i, pH 7.0, 50 µL of 50 mM GSH, 10 µL of 50 µM GstB, and 90 µL of electrophile at varying concentrations, added last. The final concentrations of each reaction mixture component and the allotted reaction times are detailed below. Following the specified 25 °C incubation period, a 25-µL aliquot of reaction mixture was added to the cuvette containing DTNB solution. The

absorbance at 412 nm was recorded. All reactions were performed in duplicate and averaged.

Substrate-Specific Reaction Conditions

Bromoacetic acid: The reaction mixtures contained 3.6 mM GSH and 1.3 μM GstB. The concentration of bromoacetic acid was varied from 1.6 to 26 mM. Each reaction was incubated at 25 °C for 2 min.

Chloroacetic acid: The reaction mixtures contained 4.3 mM GSH and 1.4 μM GstB. The concentration of chloroacetic acid was varied from 5.4 to 86 mM. Each reaction was incubated at 25 °C for 4 min.

Iodoacetic acid: The reaction mixtures contained 3.8 mM GSH and 1.5 μM GstB. The concentration of iodoacetic acid was varied from 0.28 to 9.0 mM. Each reaction was incubated at 25 °C for 1 min.

2-Bromobutyric acid: The reaction mixtures contained 1.8 mM GSH and 1.5 μM GstB. The concentration of 2-bromobutyric acid was varied from 0.60 to 18 mM. Each reaction was incubated at 25 °C for 4 min.

Iodoacetamide: The reaction mixtures contained 3.6 mM GSH and 1.0 μM GstB. The concentration of iodoacetamide was varied from 3.3 to 40 mM. Each reaction was incubated at 25 °C for 3 min.

Michaelis-Menten Kinetics: Varying GSH Concentration

Stock solutions of glutathione were prepared in 50 mM NaP_i, pH 7.0 and diluted accordingly using the same buffer. Stock solutions of the electrophiles were 100 mM and prepared in 50 mM NaP_i, pH 7.0.

Determination of Initial GSH Concentration

To determine the initial GSH concentration, 50 µL of GSH solution were added to 450 µL of 50 mM NaP_i, pH 7.0. The solution was mixed and 25 µL were delivered to the cuvette containing DTNB solution. The absorbance at 412 nm was recorded. All initial GSH concentration determinations were performed in duplicate and averaged.

Uncatalyzed Reaction

Each uncatalyzed reaction contained 360 µL of 50 mM NaP_i, pH 7.0, 50 µL of GSH at varying concentrations, and 90 µL of 100 mM electrophile (unless otherwise specified), added last. The final concentrations of each component in the reaction and the allotted reaction times are detailed below. Following the specified 25 °C incubation period, a 25-µL aliquot of reaction mixture was added to the cuvette containing DTNB solution. All reactions were performed in duplicate and averaged.

Catalyzed Reaction

Each catalyzed reaction contained 350 µL of 50 mM NaP_i, pH 7.0, 50 µL of GSH at varying concentrations, 10 µL of 50 µM GstB, and 90 µL of 100 mM electrophile (unless otherwise specified), added last. The final concentrations of each reaction mixture component and the allotted reaction times are detailed below. Following the specified 25 ° C incubation periods, a 25-µL aliquot of reaction mixture was added to the cuvette containing DTNB solution. All reactions were performed in duplicate and averaged.

Substrate-Specific Reaction Conditions

Bromoacetic acid: The reaction mixtures contained 18 mM bromoacetic acid and 1.5 μM GstB. The concentrations of GSH were varied from 0.80 to 14 mM. Each reaction was incubated at 25 °C for 1 min.

Chloroacetic acid: The reaction mixtures contained 21 mM chloroacetic acid and 1.3 μM GstB. The concentrations of GSH were varied from 0.60 to 8.3 mM. Each reaction was incubated at 25 °C for 4 min.

Iodoacetic acid: The reaction mixtures contained 18 mM iodoacetic acid and 1.5 μM GstB. The concentrations of GSH were varied from 0.80 to 19 mM. Each reaction was incubated at 25 °C for 1 min. Aliquots of the final two reactions (highest concentrations of GSH) were diluted 5-fold and 10-fold, respectively, before addition to the cuvette containing DTNB solution.

2-Bromobutyric acid: The reaction mixtures contained 18 mM 2-bromobutyric acid and 1.3 μM GstB. The concentrations of GSH were varied from 0.30 to 13 mM. Each reaction was incubated at 25 °C for 4 min. Aliquots of reactions in which the concentration of GSH was 5.0, 10, and 15 mM were diluted 10-fold before addition to the cuvette containing DTNB solution.

Iodoacetamide: The reaction mixtures contained 18 mM iodoacetamide and 1.3 μM GstB. The concentrations of GSH were varied from 0.50 to 15 mM. Each reaction was incubated at 25 °C for 3 min. All reaction aliquots were diluted 4-fold before addition to the cuvette containing DTNB solution.

PART III. WILD TYPE GSTB DISK DIFFUSION SENSITIVITY SCREENING – ELECTROPHILES

Two 2-mL LB liquid media were inoculated with *E. coli* K-12 cells or *E. coli* BW25113Δ*gstB* cells. The cultures were incubated at 37 °C with shaking at 200 rpm for 16 h. 300 µL of each culture were spread on LB-agar Petri dishes (15-cm diameter). Stock solutions of the electrophiles (acrylic acid, bromoacetic acid, 2-bromobutyric acid, chloroacetic acid, *trans*-cinnamic acid, dichloroacetic acid, ethyl bromoacetate, iodoacetamide, and iodoacetic acid) were prepared in 50 mM NaP_i, pH 7.0 at a concentration of 100 mM. The solutions were diluted in 50 mM NaP_i, pH 7.0 to yield solutions at concentrations of 50 mM, 10 mM, and 2 mM. Sterile tweezers were used to place sterile 0.6-cm filter paper disks on the plate, and then 5 µL of each solution were dispensed onto the disks. The plates were incubated at 37 °C for 18 h. The clearance zone diameters were measured.

Electrophiles that displayed kinetic activity with GstB were reevaluated at higher concentrations (bromoacetic acid, 2-bromobutyric acid, chloroacetic acid, dichloroacetic acid, and iodoacetic acid). Two 2-mL LB liquid media were inoculated with *E. coli* K-12 cells or *E. coli* BW25113Δ*gstB* cells. The cultures were incubated at 37 °C with shaking at 200 rpm for 16 h. 100 µL of each culture were spread on LB-agar Petri dishes (10-cm diameter). The stock solutions of the electrophiles prepared in 50 mM NaP_i, pH 7.0 at a concentration of 500 mM. The solutions were diluted in 50 mM NaP_i, pH 7.0 to yield solutions at concentrations of 250 mM. Sterile tweezers were used to place sterile 0.6-cm filter paper disks on the plate, and then 5 µL of each solution were dispensed onto the disks. The plates were incubated at 37 °C for 18 h. The clearance zone diameters were measured.

PART IV. WILD TYPE GSTB DISK DIFFUSION SENSITIVITY SCREENING – METALS

Four 2-mL LB media were inoculated with either *E. coli* K-12 cells, *E. coli* BW25113Δ*gstB* cells, *E. coli* BL21-pET20 cells, or *E. coli* BL21-pET20(*gstB*) cells. The cultures were incubated at 37 °C with shaking at 200 rpm for 16 h. IPTG was added to both BL21 cultures to a final concentration of 0.3 mM to induce protein expression 30 min before plating. 300 µL of the K-12 and BW25113Δ*gstB* cultures were spread on LB-agar Petri dishes (15-cm diameter). 150 µL of the BL21 cultures were spread on LB-agar Petri dishes (10-cm diameter) containing 100 µg/mL ampicillin. Sterile tweezers were used to place sterile 0.6-cm filter paper disks on the plate, and then 5 µL of each solution were dispensed onto the disks. The metal salts tested were saturated mercury (II) chloride, 0.1 M silver nitrate, saturated lead (II) acetate, 0.05 M gold (III) chloride, 1 M potassium chromate, 1 M cobalt (II) chloride, 0.05 M cadmium (II) chloride, 1 M sodium arsenite, 1 M sodium selenite, 1 M sodium arsenate, 1 M nickel (II) nitrate, 1 M terbium (III) nitrate, saturated ammonium heptamolybdate, 1 M manganese (II) sulfate, saturated tin (II) chloride, saturated barium oxide, and 1 M cerium (III) nitrate. The plates were incubated at 37 °C for 18 h. The clearance zone diameters were measured. Disk diffusion experiments were repeated with metals that produced significant sensitivity differences between bacterial strains using different concentrations of the metal salts.

PART V. SITE-DIRECTED MUTAGENESIS

Transformation of *pET20b(gstB)* into DH5α Competent Cells

A 50-µL aliquot of *E. coli* DH5α competent cells was thawed on ice. The thawed cells were mixed with 2 µL of *pET20b(gstB)* plasmid. The mixture was incubated on ice for 30 min. The cells were heat-shocked at 42 °C for 45 s. The mixture was incubated on ice for 5 min, and then 900 µL of liquid SOC medium were added. The liquid culture was incubated at 37 °C with shaking at 200 rpm for 1 h. 100 µL of the SOC liquid culture were spread on an LB-agar plate containing 100 µg/mL ampicillin, and the plate was incubated at 37 °C for 19 h.

Purification of *pET20(gstB)* Plasmid

A 5-mL aliquot of liquid LB containing 100 µg/mL ampicillin was inoculated with a single colony from the DH5α transformation LB-agar plate. The liquid culture was incubated at 37 °C with shaking at 200 rpm for 15 h. Two 15% glycerol stocks were prepared by adding 450 µL 50% glycerol to 1,000 µL liquid culture.

Plasmid DNA was purified using the QIAprep Spin Miniprep Kit reagents and protocol. The absorbance at 260 nm was measured to calculate DNA concentration.

Polymerase Chain Reaction (PCR)

The DNA primers used for PCR were designed using Agilent Technologies' QuikChange® Primer Design Program and synthesized by Invitrogen (Thermo Fisher Scientific). The following DNA primers were used, with the mutation sites underlined:

Forward R119A: 5'-tcctgatgggattagtcgcaacaccaccggaagagc-3'

Reverse R119A: 5'-gctcttccggtggtgttgcgactaatcccatcagga-3'

Forward R119H: 5'-gatcctgatgggattagtccatacaccaccggaagagcgc-3'

Reverse R119H: 5'-gcgctcttccggtggtgtatggactaatcccatcaggatc-3'

Forward R119Q: 5'-gatcctgatgggattagtccagacaccaccggaagagcgc-3'

Reverse R119Q: 5'-gcgctcttccggtggtgtctggactaatcccatcaggatc-3'

Forward R119S: 5'-tgatgggattagtcagcacaccaccggaagagc-3'

Reverse R119S: 5'-gctcttccggtggtgtgctgactaatcccatca-3'

Site-directed mutagenesis was performed according to the QuikChange II Site-Directed Mutagenesis Kit protocol. Each of four PCR reactions contained 5 µL 10X reaction buffer, 5 µL 5 ng/µL *pET-20(gstB)* template, 1 µL dNTP mix, 29 µL sterile deionized water, 5 µL 25 ng/µL forward primer, and 5 µL 25 ng/µL reverse primer. To each reaction mixture was added 1 µL of 2.5 U/µL PfuUltra HF DNA polymerase. The reaction mixtures were mixed via pipetting and centrifuged at 13,000 x g for 30 s. The PCR reactions were conducted in a Techne TC-312 thermocycler configured with the program displayed in Table 2-1.

Table 2-1: Thermocycler settings for PCR.

Segment	Cycles	Temperature	Time
1	1	95 °C	30 s
2	16	95 °C	30 s
2	16	55 °C	1 min
2	16	68 °C	4 min 20 s

Template DNA Digestion

Following PCR, the reaction mixtures were cooled on ice for 2 min, and 1 µL of 10 U/µL DpnI restriction enzyme was added to each. The reactions were mixed by pipetting and centrifuged at 13,000 x g for 1 min. The reactions were incubated at 37 °C for 1 h.

Transformation into *E. coli* XL1-Blue Supercompetent Cells

XL1-Blue supercompetent cells were thawed on ice. The competent cells were deposited into pre-chilled 15-mL BD Falcon polypropylene round-bottom tubes in 50-µL aliquots. The thawed cells were mixed with 1 µL of the DpnI-digested PCR reaction mixture and incubated on ice for 30 min. The tubes were heat-shocked at 42 °C for 45 s and then incubated on ice for 2 min. SOC broth was preheated to 42 °C and a 0.5-mL aliquot was added to each transformation tube. The cultures were incubated at 37 °C with shaking at 225 rpm for 1 h. Following incubation, 250 µL of each transformation mixture were spread onto each of two LB plates containing 100 µg/mL ampicillin. The plates were incubated at 37 °C for 22 h.

Purification of Mutant Plasmid DNA

Three different colonies from each transformation were picked and used to inoculate three 2-mL LB media containing 100 µg/mL ampicillin. The cultures were incubated at 37 °C with shaking at 200 rpm for 16 h. Mutant plasmid DNA was purified using the QIAprep Spin Miniprep Kit following the manufacturer protocol. The purified DNA was submitted to the Plant-Microbe Genomics Facility at The Ohio State

University for DNA sequencing (Sanger Capillary Sequencing using 3730 DNA Analyzer from Applied Biosystems, Inc. and BigDye® Terminator Cycle Sequencing chemistry).

Transformation into *E. coli* BL21 (DE3) Competent Cells

Four tubes, each containing 100-µL aliquots of *E. coli* BL21 (DE3) competent cells, were thawed on ice. The thawed cells were mixed with 1.5 µL purified mutant plasmid DNA, and the tubes were incubated on ice for 30 min. The cells were heat-shocked at 42 °C for 45 s, the tubes were incubated on ice for 5 min, and then 900 µL SOC broth were added to each. The mixtures were transferred to culture tubes and incubated at 37 °C with shaking at 200 rpm for 1 h. Following incubation, 100 µL of each liquid culture were spread on an LB plate containing 100 µg/mL ampicillin. The plates were incubated at 37 °C for 18 h.

Overexpression Study of Mutant Proteins

Different colonies were chosen to inoculate 2-mL LB media containing 100 µg/mL ampicillin. The cultures were incubated at 37 °C with shaking at 200 rpm for 16 h. Each culture was diluted 100-fold into LB media containing 100 µg/mL ampicillin. The cultures were incubated at 37 °C with shaking at 200 rpm until the OD_{600} was between 0.6 and 0.8, and 400-µL aliquots of each culture were saved for analysis. Protein production was initiated by the addition of IPTG to a final concentration of 0.3 mM, and the cultures were incubated at 37 °C with shaking at 200 rpm for 4 h. After 4 h, 100-µL aliquots of each culture were collected for analysis.

The 400-µL (-)-IPTG aliquots and the 100-µL (+)-IPTG aliquots were centrifuged at 13,000 x g for 5 min. The pellets were resuspended in 2X SDS loading dye, heated at 100 °C for 5 min, and centrifuged at 13,000 x g for 5 min. Two SDS-PAGE gels (18 % resolving gel, 4.5 % stacking gel) were loaded with 15 µL of each sample and 5 µL of molecular weight marker. The gels were run at 200 V for 1.2 h and visualized with Coomassie brilliant blue stain. This entire protocol was followed for a larger-scale expression study, in which the liquid culture size was 100 mL.

Purification of Mutant Proteins (R119S & R119Q)

A single colony of transformed BL21 (DE3) cells was used to inoculate a 50-mL LB medium containing 100 µg/mL ampicillin. The culture was incubated at 37 °C with shaking at 200 rpm for 16 h. The culture was diluted 100-fold into three 1.2-L LB media containing 100 µg/mL ampicillin and incubated at 37 °C with shaking at 150 rpm for 5 h until the OD_{600} was between 0.6 and 0.8. Protein expression was initiated by the addition of IPTG to a final concentration of 0.6 mM, and the cultures were incubated at 37 °C with shaking at 150 rpm for 21 h.

The cells were harvested via centrifugation at 6,000 x g and 4 °C for 10 min. The frozen cell pellets were resuspended in 80 mL of 10 mM Tris, pH 7.0, containing 2 mM EDTA and 1 mM DTT. The suspension was subjected to twelve cycles consisting of 30 s of sonication and 1 min of stirring on ice. The cell lysate was centrifuged at 10,000 x g and 4 ^{o}C for 30 min. The pellet was discarded. To promote the precipitation of nucleic acids, streptomycin sulfate in 10 mM Tris, pH 7.0, containing 2 mM EDTA and 1 mM DTT was added dropwise to the supernatant to obtain a final concentration of 1% (w/v).

After centrifugation at 10,000 x g and 4 ºC for 30 min, the pellet was discarded and 36.63 g of ammonium sulfate (75% saturation) were slowly added to the supernatant with vigorous stirring. Centrifugation at 10,000 x g and 4 °C for 30 min yielded the protein pellet, which was stored at -20 °C.

Anion Exchange Column Chromatography

The protein pellets were dissolved in 23 mL of 20 mM Tris, pH 7.4, containing 1 mM DTT and dialyzed against 3 L of 20 mM Tris, pH 7.4, containing 1 mM DTT at 4 °C for 18 h. A Q-Sepharose Fast Flow anion exchange column (3 x 12 cm) was equilibrated with 500 mL of 20 mM Tris, pH 7.4, containing 1 mM DTT. After centrifugation at 10,000 x g and 4 °C for 10 min, the supernatant was applied to the column. The column was washed with 500 mL of 20 mM Tris, pH 7.4, containing 1 mM DTT. The protein was eluted with a 400-mL gradient of 0 to 400 mM sodium chloride in 20 mM Tris, pH 7.4, containing 1 mM DTT, and 3-mL fractions were collected. The fractions were analyzed by measuring the absorbance at 280 nm and SDS-PAGE. Fractions containing an appreciable amount of pure mutant GstB were pooled and concentrated via centrifugation at 10,000 x g and 4 ºC using an Amicon Ultra centrifugal filter unit (MWCO: 10,000 Da).

Hydroxylapatite Column Chromatography

The R119H and R119Q mutants required additional purification by hydroxylapatite column chromatography, following the Hydroxylapatite Chromatography Alternate Protocol I.[61] The Bio-Gel HTP matrix was prepared by suspension and settling

in 10 mM NaP_i, pH 6.8, with decantation of the fines. The column was equilibrated via washing with 125 mL of 10 mM NaP_i, pH 6.8. After centrifugation at 10,000 x g and 4 °C, 1 mL of protein was loaded onto the column. The column was washed with 240 mL of 10 mM NaP_i, pH 6.8, containing 1 mM DTT. Then, a step-gradient elution was carried out, in which the column was washed with 60 mL each of 0.025 M, 0.050 M, 0.25 M, and 0.40 M NaP_i, pH 6.8, containing 1 mM DTT. After 15% SDS-PAGE analysis, the 10 mM NaP_i and 0.025 M NaP_i washes were pooled and concentrated via centrifugation at 10,000 x g and 4 ^oC using an Amicon Ultra centrifugal filter unit (MWCO: 10,000 Da).

PART VI. ACTIVITY SCREENING OF GSTB MUTANTS

The GstB mutants were initially screened for activity with CDNB using the same protocol detailed in Part II. Then, the mutants were screened for activity with all other electrophiles using the discontinuous DTNB spectrophotometric assay protocol described in Part II. Screening reaction times were either 12-16 min, with reaction aliquots taken every 2 min, or 15 min with reaction aliquots taken every 5 min. The concentration of GSH in the screening reactions was between 3.0 and 4.0 mM, while the concentration of electrophile was between 15 and 23 mM, with the exception of ethyl bromoacetate at 1.8 mM. The concentration of mutant enzyme in the reaction was between 0.80 and 2.0 µM. Wild type GstB was screened each time so that a comparative rate could be obtained under identical reaction conditions.

Michealis-Menten kinetic assays were performed for all four mutants with respect to both iodoacetamide and GSH. For reactions in which iodoacetamide was varied, GSH was held constant at a concentration between 3.0 and 4.0 mM in the reaction, the

concentration of enzyme remained constant at concentrations between 0.30 and 2.6 μM, and the concentration of iodoacetamide was varied from 0.50 to 60 mM. For reactions in which GSH was varied, iodoacetamide was held constant near 18 mM, the concentration of enzyme remained constant at concentrations between 1.0 and 2.3 μM, and the concentration of GSH was varied from 0.50 to 15 mM.

Iodoacetamide Mode of Inhibition Studies: WT GstB and R119H Mutant

Determination of Initial GSH Concentration

To determine the initial GSH concentration, 50 μL of GSH solution were added to 450 μL of 50 mM NaP_i, pH 7.0. The solution was mixed and 25 μL were delivered to the cuvette containing DTNB. The absorbance at 412 nm was recorded. All initial GSH concentration determinations were performed in duplicate and averaged.

A 500-μL mixture containing 437 μL of 50 mM NaP_i, pH 7.0, 50 μL of 50 mM iodoacetamide in 50 mM NaP_i, pH 7.0, and 13 μL of 2.0 mM wild type GstB was incubated at room temperature for 120 min. The incubated enzyme's efficacy in the conjugation of GSH and bromoacetate was examined by transferring 10 μL of the mixture to a reaction tube immediately (0 min) and after 15, 30, 60, and 120 min of incubation with iodoacetamide. Each reaction also contained 350 μL of 50 mM NaP_i, pH 7.0, 50 μL of 50 mM GSH, and 90 μL of 60 mM bromoacetate, added last. The final concentrations of bromoacetate, GSH, and GstB in the reaction were 11 mM, 5.0 mM, and 1.0 μM, respectively. After addition of bromoacetate, the reaction incubated at room temperature for 3 min. Then, a 25-μL aliquot of reaction mixture was added to the cuvette containing DTNB solution. The absorbance at 412 nm was recorded.

PART VII. DISK DIFFUSION SENSITIVITY TESTING OF GSTB MUTANTS

Six 2-mL LB liquid media containing 100 μg/mL ampicilin were inoculated with *E. coli* BL21-pET20, BL21-pET20(*gstB*), BL21-pET20(*gstB-R119A*), BL21-pET20(*gstB-R119H*), BL21-pET20(*gstB-R119Q*), and BL21-pET20(*gstB-R119S*) cells. The cultures were incubated at 37 °C with shaking at 200 rpm for 16 h. IPTG was added to each liquid culture to a final concentration of 1 mM, and the cultures were incubated at 37 °C with shaking at 200 rpm for 30 min. 150 μL of each liquid culture were spread onto LB-agar Petri dishes (10-cm diameter) containing 100 μg/mL ampicilin. Stock solutions of the electrophiles were prepared in 50 mM NaP_i, pH 7.0. The electrophile solutions used were 470 mM bromoacetate, 500 mM 2-bromobutyrate, 100 mM ethyl bromoacetate, 500 mM chloroacetate, 300 mM iodoacetamide, and 580 mM iodoacetate. Sterile tweezers were used to place sterile 0.6-cm filter paper disks on the plate, and then 4 μL of each solution were dispensed onto the disks. The plates were incubated at 25 °C for 6 h, and then at 37 °C for 18 h. Bacterial growth clearance diameters were measured.

Electrophiles that produced significant bacterial growth clearance differences were reevaluated at lower concentrations. Six 2-mL LB liquid media containing 100 μg/mL ampicilin were inoculated with *E. coli* BL21-pET20, BL21-pET20(*gstB*), BL21-pET20(*gstB-R119A*), BL21-pET20(*gstB-R119H*), BL21-pET20(*gstB-R119Q*), and BL21-pET20(*gstB-R119S*) cells. The cultures were incubated at 37 °C with shaking at 200 rpm for 16 h. IPTG was added to each liquid culture to a final concentration of 1 mM, and the cultures were incubated at 37 °C with shaking at 200 rpm for 30 min. 150 μL of each liquid culture were spread onto LB-agar Petri dishes (10-cm diameter) containing 100 μg/mL ampicilin. Stock solutions of the electrophiles were prepared in 50 mM NaP_i, pH

7.0. The electrophile solutions used were 150 mM iodoacetamide, 100 mM iodoacetate, and 230 mM bromoacetate. Sterile tweezers were used to place sterile 0.6-cm filter paper disks on the plate, and then 4 µL of each solution were dispensed onto the disks. The plates were incubated at 25 °C for 6 h, and then at 37 °C for 18 h. Bacterial growth clearance diameters were measured.

CHAPTER 3. RESULTS

PART I. EXPRESSION AND PURIFICATION OF WILD TYPE GSTB

Ammonium Sulfate Precipitation

A GstB purification procedure was designed by Collins Aboagye, a previous graduate student.[62] Modification of this protocol was carried out to optimize the ammonium sulfate precipitation conditions. Following protein expression, six cell pellets (Samples 1-6) were harvested via culture centrifugation. Prior to ammonium sulfate addition, Samples 1-6 underwent sonication and were treated with 1% streptomycin to precipitate nucleic acids. Then, various ammonium sulfate precipitation protocols were attempted.

During the first optimization procedure, ammonium sulfate was first added to 45% saturation. Then, protein was precipitated from the supernatant with the addition of ammonium sulfate to 75% saturation. Analysis of the SDS-PAGE gel (Figure 3-1, Lanes 6 and 7) reveals that this particular step-wise precipitation approach was inefficient. GstB appears at 23 kDa, the molecular weight of an individual subunit. The 45% ammonium sulfate pellet contained a substantial amount of a higher molecular weight impurity protein near 55 kDa.

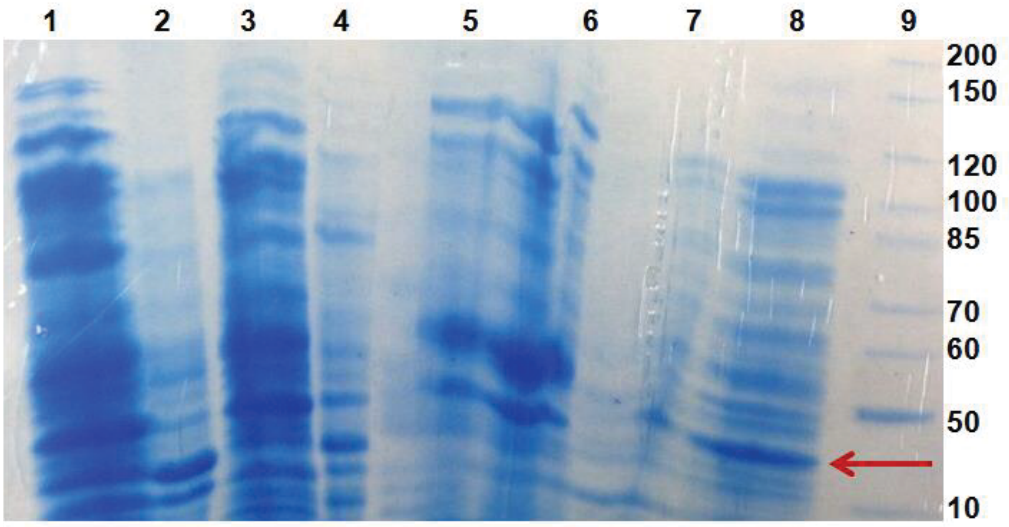

Figure 3-1: 12.5% SDS-PAGE of samples from protein purification of Sample 1 (45%, 75% ammonium sulfate precipitation). Lane 1: sonication supernatant; Lane 2: sonication pellet; Lane 3: streptomycin supernatant; Lane 4: streptomycin pellet; Lane 5: 45% ammonium sulfate supernatant; Lane 6: 45% ammonium sulfate pellet; Lane 7: 75% ammonium sulfate supernatant; Lane 8: 75% ammonium sulfate pellet; Lane 9: MW marker.

Protein precipitation of Sample 2 was also conducted in a step-wise fashion. After sonication and nucleic acid precipitation with streptomycin sulfate, ammonium sulfate was added to 25% saturation in an attempt to precipitate the 55 kDa impurity protein. The precipitation of this protein was not achieved, as it appeared in the 25% supernatant (Figure 3-2, Lane 6). Next, ammonium sulfate was added to 60% saturation, which removed some of the undesired proteins (Figure 3-2, Lane 9).

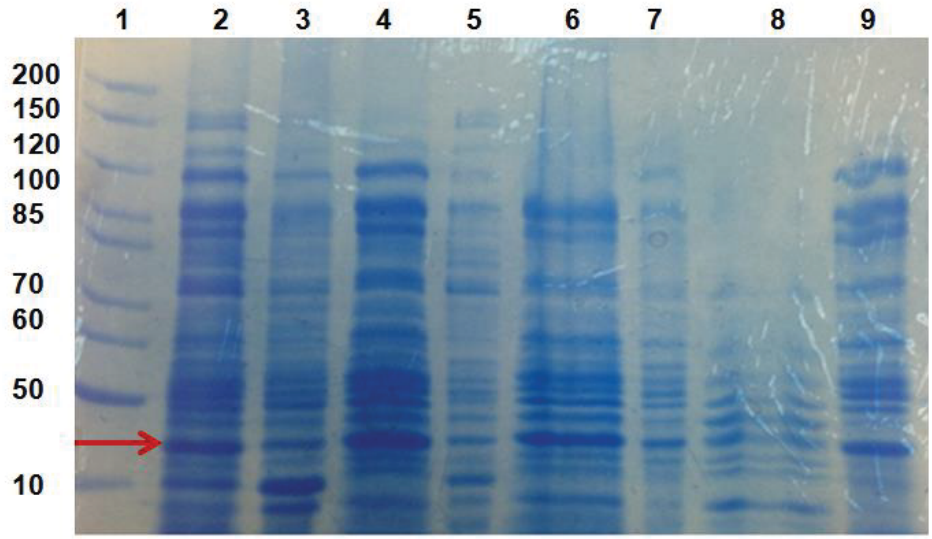

Figure 3-2: 12.5 % SDS-PAGE of samples from protein purification of Sample 2 (25%, 60% ammonium sulfate precipitation). Lane 1: MW marker; Lane 2: sonication supernatant; Lane 3: sonication pellet; Lane 4: streptomycin supernatant; Lane 5: streptomycin pellet; Lane 6: 25% ammonium sulfate supernatant; Lane 7: 25% ammonium sulfate pellet; Lane 8: 60% ammonium sulfate supernatant; Lane 9: 60% ammonium sulfate pellet.

Samples 3-6 were combined, sonicated, and treated with streptomycin sulfate to remove nucleic acids. Instead of step-wise precipitation, there was a single addition of ammonium sulfate to 75% saturation. There was a significant amount of GstB present in the sonication pellet (Figure 3, Lane 2), which was large in size, indicating that the sonication procedure, eight cycles consisting of 30 s sonication and 1 min stirring on ice, may not have been completely effective with the sonicator available. All of the sonication pellets from Samples 1-6 were subjected to additional sonication cycles and re-purified with a single 75% ammonium sulfate precipitation. All future GstB protein purification was conducted using the optimized protocol consisting of 12 cycles of sonication and one treatment of ammonium sulfate to 75% saturation.

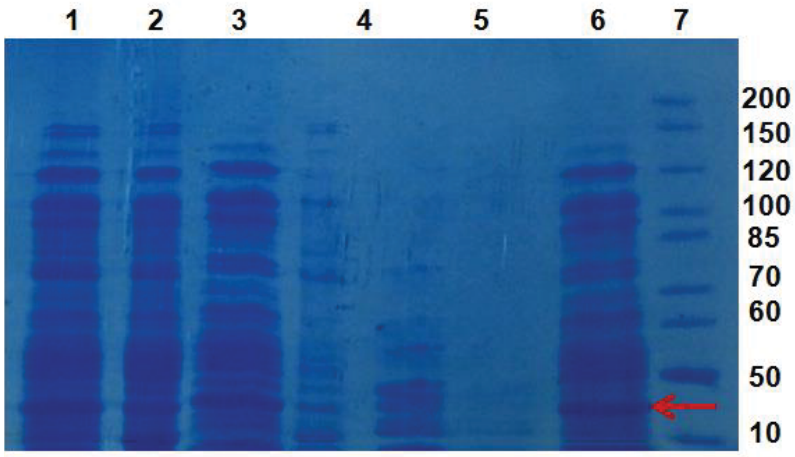

Figure 3-3: 12.5% SDS-PAGE of samples from protein purification of Samples 3-6 (75% ammonium sulfate precipitation). Lane 1: sonication supernatant; Lane 2: sonication pellet; Lane 3: streptomycin supernatant; Lane 4: streptomycin pellet; Lane 5: 75% ammonium sulfate supernatant; Lane 6: 75% ammonium sulfate pellet; Lane 7: MW marker.

Anion Exchange Column Chromatography

Anion exchange column chromatography was the final step in the purification of GstB. The theoretical isoelectric point (pI) of GstB is 5.05, and the operating pH during this step was 7.4. Therefore, GstB had a net negative charge. Negatively charged GstB was electrostatically bound to the positively charged trimethylammonium-substituted agarose matrix. GstB was eluted from the column with a 0-400 mM sodium chloride gradient. Figure 3-4 reveals that very little GstB was present in the flow-through and wash fractions. Analysis of fractions via absorbance at 280 nm and SDS-PAGE indicated that fractions 91-110 contained sufficiently pure GstB (Figure 3-5).

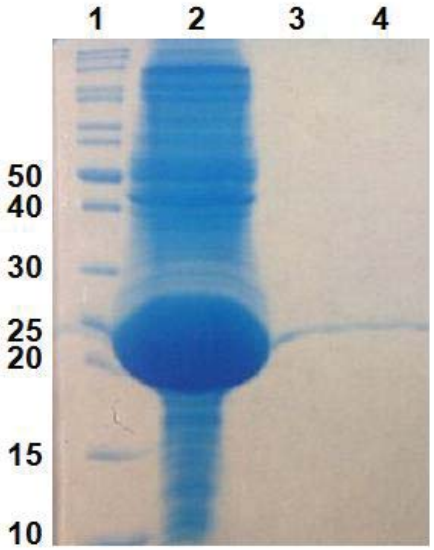

Figure 3-4: 18% SDS-PAGE of anion exchange column chromatography fractions. Lane 1: MW marker; Lane 2: load; Lane 3: flow-through; Lane 4: wash.

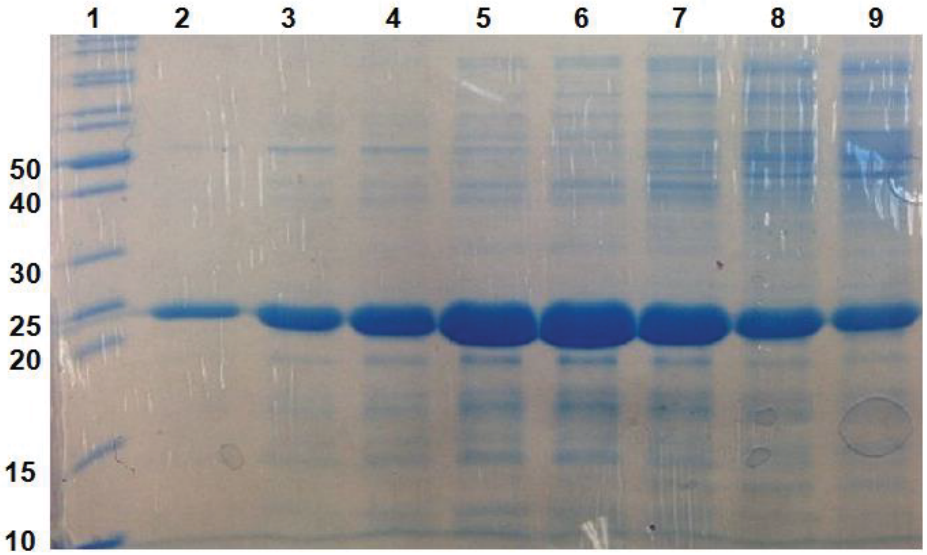

Figure 3-5: 18% SDS-PAGE of anion exchange column chromatography 0-400 mM NaCl wash fractions. Lane 1: MW marker; Lane 2: fraction #92; Lane 3: fraction #95; Lane 4: fraction #97; Lane 5: fraction #100; Lane 6: fraction #102; Lane 7: fraction #107; Lane 8: Fraction #110; Lane 9: fraction #111.

Following anion exchange column chromatography, fractions containing the largest amount of purified GstB were pooled and concentrated. After protein concentration, several dilutions were prepared and analyzed via SDS-PAGE. The 1:100 dilution is most representative of the working concentration of GstB required for enzyme activity assays. GstB is the dominant protein present at this concentration, and the sample is virtually free of other proteins (Figure 3-6, Lane 6).

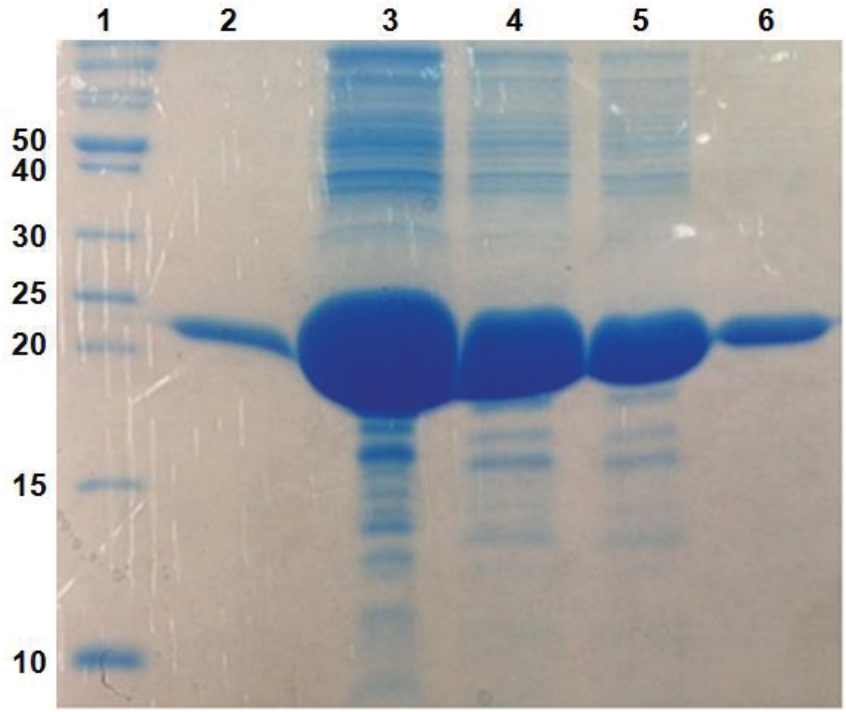

Figure 3-6: 18% SDS-PAGE of concentrated anion exchange column chromatography fractions. Lane 1: MW marker; Lane 2: flow-through; Lane 3: concentrate diluted 5-fold; Lane 4: concentrate diluted 10-fold; Lane 5: concentrate diluted 20-fold; Lane 6: concentrate diluted 100-fold.

PART II. WILD TYPE GSTB KINETICS

Initial Activity Screening

The reaction between GSH and CDNB results in the formation of a GS-DNB conjugate that has a maximum absorbance at 340 nm (GS-DNB conjugate Ɛ = 9,600 $M^{-1}cm^{-1}$), as shown in Figure 3-7. Wild type GstB did not display activity with CDNB, as there was essentially no difference in the rate data between the spontaneous and catalyzed trials. Therefore, it can be concluded that GstB does not catalyze the conjugation reaction between GSH and CDNB.

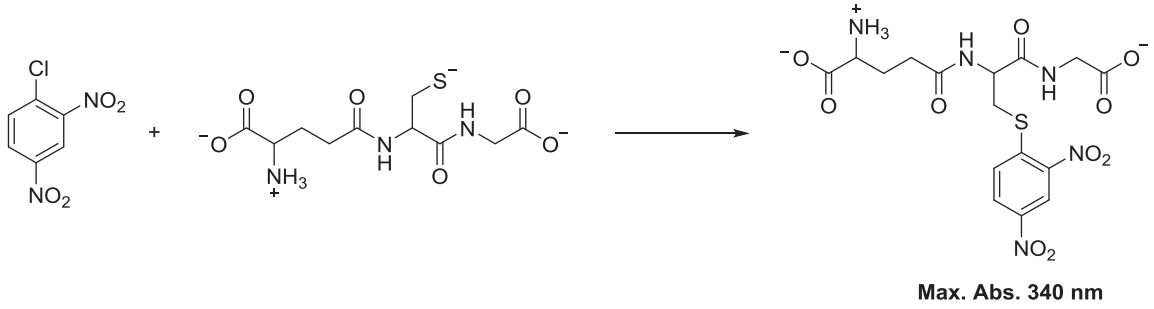

Figure 3-7: CDNB and GSH conjugation reaction.

Use of a discontinuous spectrophotometric assay allowed for the determination of the initial and final concentrations of GSH for each reaction. When 5,5'-dithio-bis-(2-nitrobenzoic acid) (DTNB) reacts with GSH, a mixed disulfide product is formed, as well as the 2-nitro-5-thiobenzoate dianion (TNB^{2-}), which has a maximum absorbance at 412 nm and a molar extinction coefficient of 13,600 $M^{-1}cm^{-1}$ (Figure 3-8). GSH can readily react with electrophilic molecules in the absence of enzyme. Therefore, two 15-minute screening reactions, a spontaneous reaction and a catalyzed reaction, were performed. During these reactions, aliquots were taken every two minutes and the absorbance at 412 nm was measured. When the difference between the spontaneous and catalyzed rates was insignificant, it was concluded that the electrophile did not serve as a substrate for GstB.

Figure 3-9 displays the chemical structures of the electrophiles with which GstB was inactive.

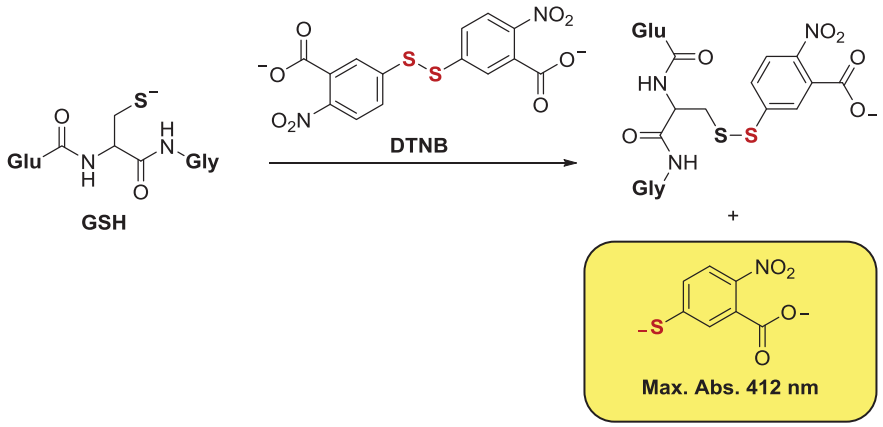

Figure 3-8: Reaction of GSH with DTNB.

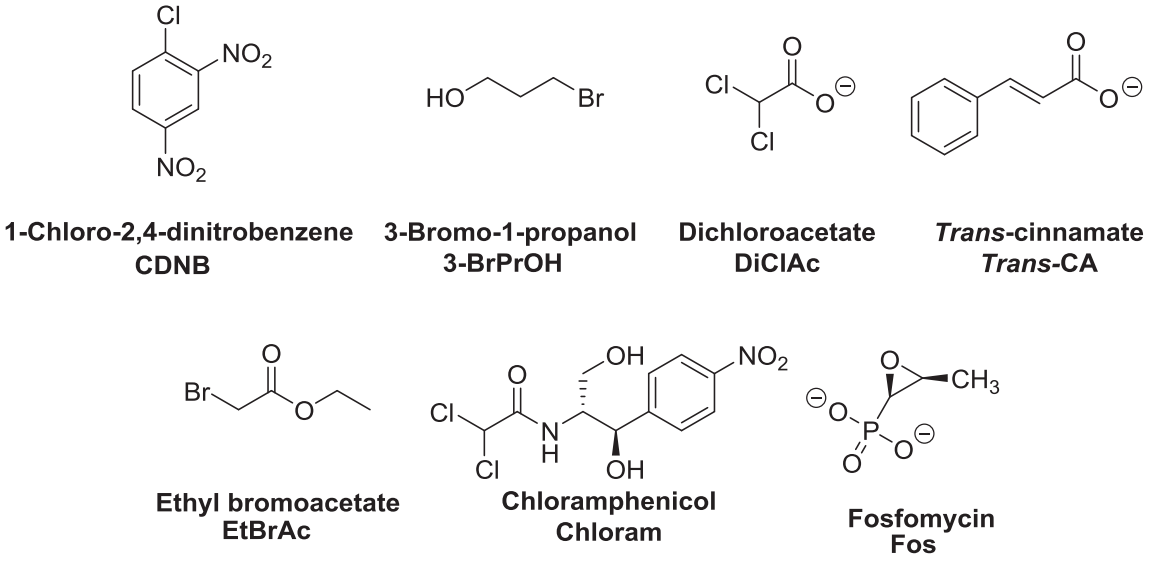

Figure 3-9: Chemical structures of electrophilic compounds that were not GstB substrates.

Michaelis-Menten Kinetics: Varying Electrophile Concentration

Figure 3-10 displays the chemical structures of the electrophiles that were GstB substrates. As GstB catalyzes a bisubstrate reaction, Michaelis-Menten kinetic assays using DTNB were carried out by maintaining one substrate at a constant non-limiting concentration and varying the concentration of the other. For the following assays, GSH was held constant near 3.50 mM, while the concentration of the electrophile was varied. These assays were conducted for the electrophiles bromoacetate (Figure 3-11), chloroacetate (Figure 3-12), iodoacetate (Figure 3-13), 2-bromobutyrate (Figure 3-14), and iodoacetamide (Figure 3-15). The red diamonds in these figures represent the experimental data.

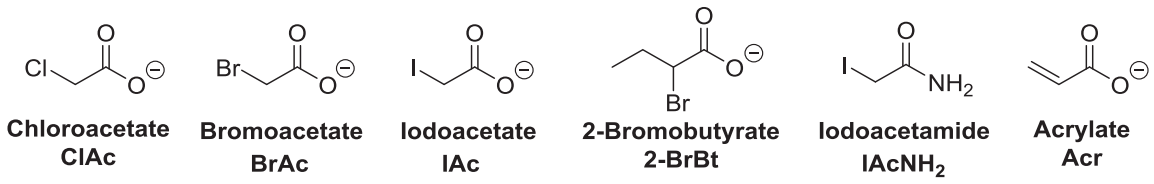

Figure 3-10: Chemical structures of electrophilic compounds that were GstB substrates.

Michaelis-Menten Kinetics Data Analysis

The absorbance measurements at 412 nm were used to calculate the initial and final concentrations of GSH according to Beer's Law (Equation 1).

$$\boldsymbol{Equation\ 1}:$$

$$\boldsymbol{c\ (in\ mM) = A_{412} \times 13,600\ M^{-1}cm^{-1} \times 1\ cm\ \times 1,000\ \times dilution\ factor,}$$

where c is the concentration of GSH, A_{412} is the absorbance at 412 nm, Ɛ is the molar extinction coefficient of the TNB^{2-} thiolate dianion (13,600 M^{-1} cm^{-1}), and l is the cuvette path length (1 cm). The concentration of GSH remaining after the reaction was subtracted from the initial concentration of GSH. This value was then divided by the reaction time to obtain the rate (ΔC/t). The rate of the uncatalyzed reaction was subtracted from the catalyzed reaction rate to obtain the adjusted rate.

Determining Kinetic Parameters with Michaelis-Menten Modeling

Kinetic Parameters without Inhibition

The rate data were fit to the Michaelis-Menten equation (Equation 2), where v_0 is initial velocity, V_{max} is maximal velocity, [S] is substrate concentration, and K_M is the Michaelis constant: the concentration of substrate at half-maximal velocity, via nonlinear regression analysis using Equation 3.

$$\boldsymbol{Equation\ 2}: \qquad \boldsymbol{v_0 = \frac{V_{max}[S]}{K_M + [S]}}$$

$$\boldsymbol{Equation\ 3}: \qquad \boldsymbol{y = \frac{V_{max}}{\left(1 + \frac{K_M}{x}\right)}}$$

Values for the Michaelis constant ($K_M^{el.}$), maximal velocity ($V_{max}^{el.}$), and turnover number ($k_{cat}^{el.}$) were determined by obtaining a coefficient of determination (R^2) value that

approached 1.0. The substrates chloroacetate (Figure 3-12), iodoacetate (Figure 3-13), and 2-bromobutyrate (Figure 3-14) did not inhibit GstB and were modeled in this manner. The experimental data points are red diamonds, and the model data points are black diamonds.

Kinetic Parameters with Inhibition

The rate data were fit to the Michaelis-Menten equation, accounting for substrate inhibition (Equation 4), where v_0 is initial velocity, V_{max} is maximal velocity, [S] is substrate concentration, and K_M is the Michaelis constant: the concentration of substrate at half-maximal velocity, and K_I is the inhibition constant: the concentration of inhibitor at half-maximal inhibition, via nonlinear regression analysis using Equation 5.

$$\textbf{Equation 4:} \qquad v_0 = \frac{V_{max}[S]}{[K_M] + [S]\left(1 + \frac{[S]}{K_I}\right)}$$

$$\textbf{Equation 5:} \qquad y = \frac{V_{max}}{\left(\frac{x + K_m}{x} + \frac{x}{K_I}\right)}$$

Values for the Michaelis constant (K_M^{GSH}), maximal velocity (V_{max}^{GSH}), and turnover number (k_{cat}^{GSH}) were determined by obtaining a coefficient of determination (R^2) value that approached 1.0. The substrates bromoacetate (Figure 3-10) and iodoacetamide (Figure 3-14) inhibited GstB at high concentrations and were modeled with inhibition.

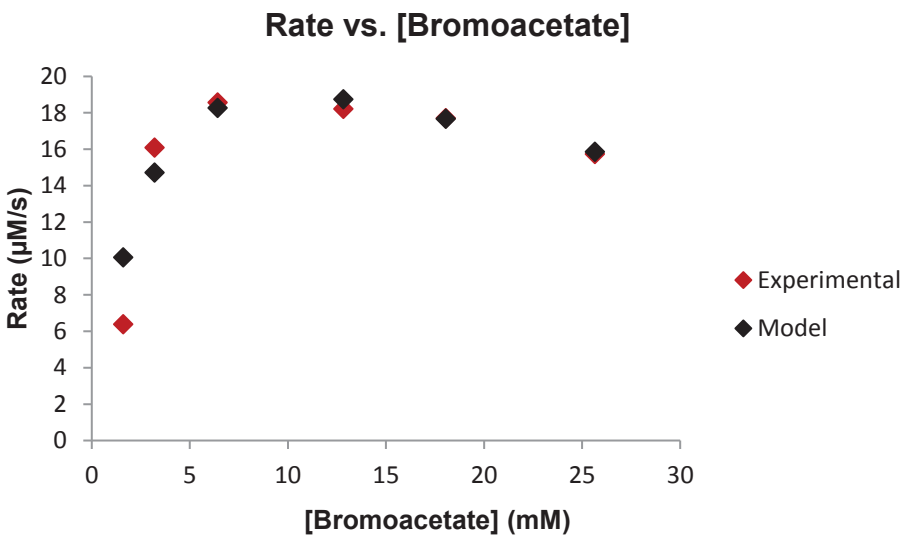

Figure 3-11: A plot of the rate of bromoacetate-GSH conjugation versus bromoacetate concentration with experimental rate (red) and model rate with substrate inhibition (black). [GSH]: 3.6 mM; [GstB]: 1.3 μM; reaction time: 2 min; R^2: 0.990.

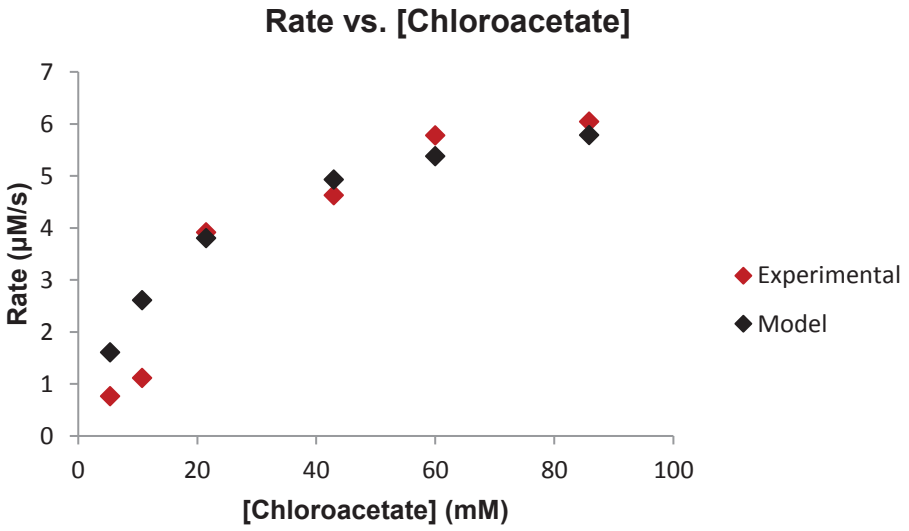

Figure 3-12: A plot of the rate of chloroacetate-GSH conjugation versus chloroacetate concentration with experimental rate (red) and model rate without substrate inhibition (black). [GSH]: 4.3 mM; [GstB]: 1.4 μM; reaction time: 4 min; R^2: 0.971.

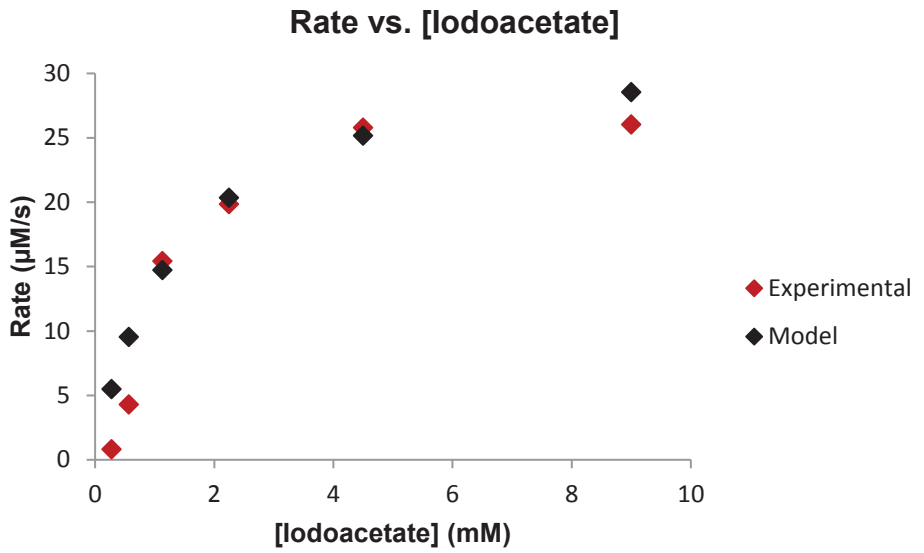

Figure 3-13: A plot of the rate of iodoacetate-GSH conjugation versus iodoacetate concentration with experimental rate (red) and model rate without substrate inhibition (black). [GSH]: 3.8 mM; [GstB]: 1.5 µM; reaction time: 1 min; R^2: 0.975.

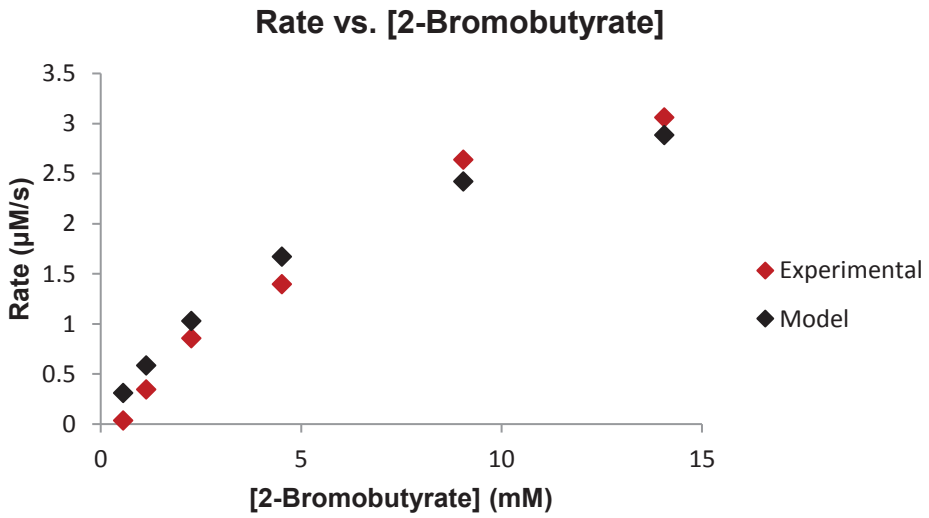

Figure 3-14: A plot of the rate of 2-bromobutyrate-GSH conjugation versus 2-bromobutyrate concentration with experimental rate (red) and model rate without substrate inhibition (black). [GSH]: 3.1 mM; [GstB]: 0.80 µM; reaction time: 4 min; R^2: 0.983.

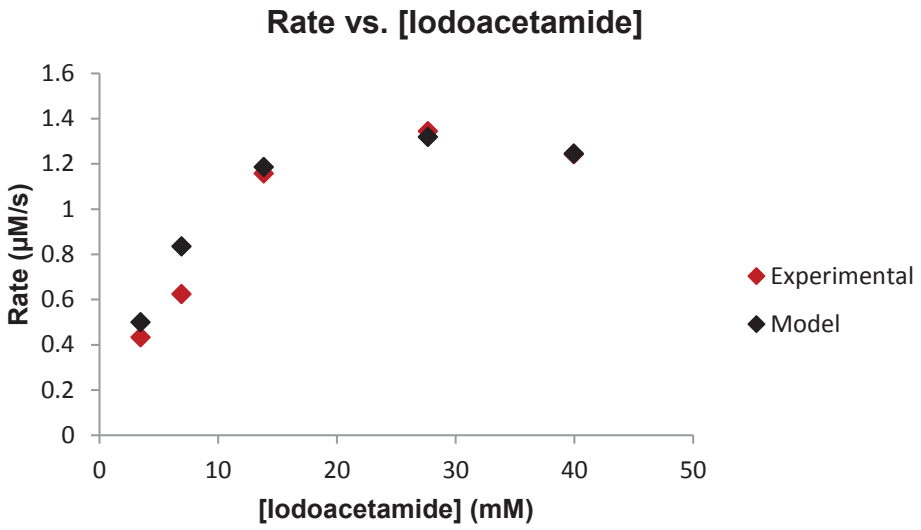

Figure 3-15: A plot of the rate of iodoacetamide-GSH conjugation versus iodoacetamide concentration with experimental rate (red) and model rate with substrate inhibition (black). [GSH]: 3.6 mM; [GstB]: 0.80 μM; reaction time: 3 min; R^2: 0.991.

Table 3-1: Kinetic parameters with respect to electrophile substrate.

Electrophile	$K_M^{El.}$ (mM)	$k_{cat}^{El.}$ (s^{-1})	$k_{cat}^{El.}/K_M^{El.}$ ($mM^{-1}s^{-1}$)	$K_I^{El.}$ (mM)
ClAc	18.0	21.2	1.18	--
BrAc	3.50	33.4	10.0	29.0
IAc	1.40	22.6	16.1	--
2-BrBt	5.53	4.38	0.820	--
$IAcNH_2$	18.4	4.21	0.230	34.5

Table 3-1 includes the kinetic parameters obtained using the modeling process, specific to the enzyme-substrate pair. The electrophiles bromoacetate and iodoacetamide inhibited wild type GstB at higher concentrations, with bromoacetate acting more potently. The data for these reactions was fit using the Michaelis-Menten equation with inhibition. Wild type GstB had the highest affinity for iodoacetate ($K_M^{El.}$: 1.40 mM) and relatively low affinity for chloroacetate and iodoacetamide ($K_M^{El.}$: 18.0 mM and 18.4 mM, respectively). Turnover number ranged from as low as 4.21 s^{-1} for iodoacetamide to as high as 33.4 s^{-1} for bromoacetate. Wild type GstB displayed the highest catalytic efficiency with iodoacetate ($k_{cat}^{El.}/K_M^{El.}$: 16.1 $mM^{-1}s^{-1}$) was least catalytically efficient with iodoacetamide ($k_{cat}^{El.}/K_M^{El.}$: 0.230 $mM^{-1}s^{-1}$).

Michaelis-Menten Kinetics: Varying GSH Concentration

A second set of DTNB assays was conducted in which the concentration of the electrophile remained constant and the concentration of GSH was varied so that the kinetic parameters with respect to the GstB-GSH enzyme-substrate pair could be calculated. The electrophiles in these reactions were bromoacetate (Figure 3-16), chloroacetate (Figure 3-17), iodoacetate (Figure 3-18), 2-bromobutyrate (Figure 3-19), and iodoacetamide (Figure 3-20). All five of these experimental data sets were fit using Equation 5, as GSH substrate inhibition was observed.

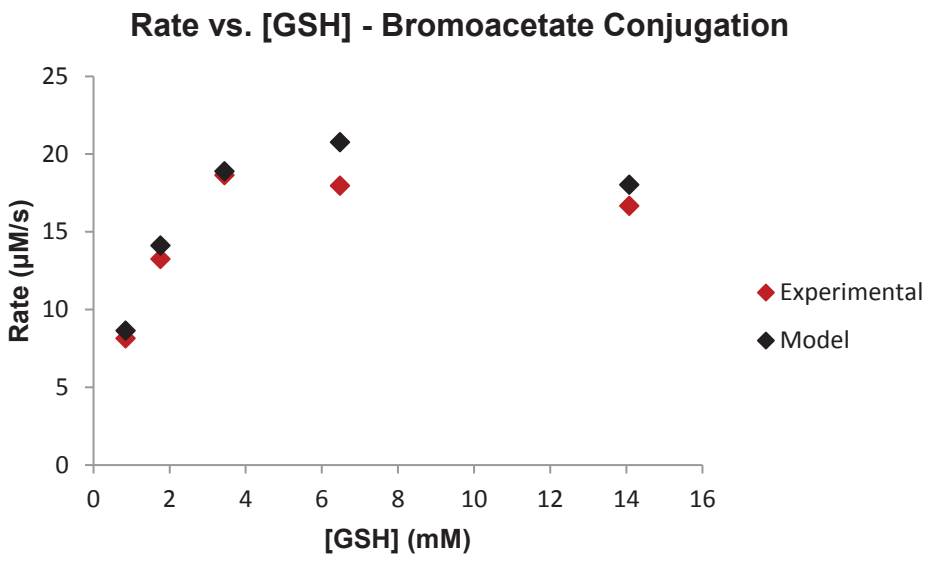

Figure 3-16: A plot of the rate of bromoacetate-GSH conjugation versus GSH concentration with experimental rate (red) and model rate with substrate inhibition (black). [Bromoacetate]: 18 mM; [GstB]: 1.5 µM; reaction time: 1 min; R^2: 0.992.

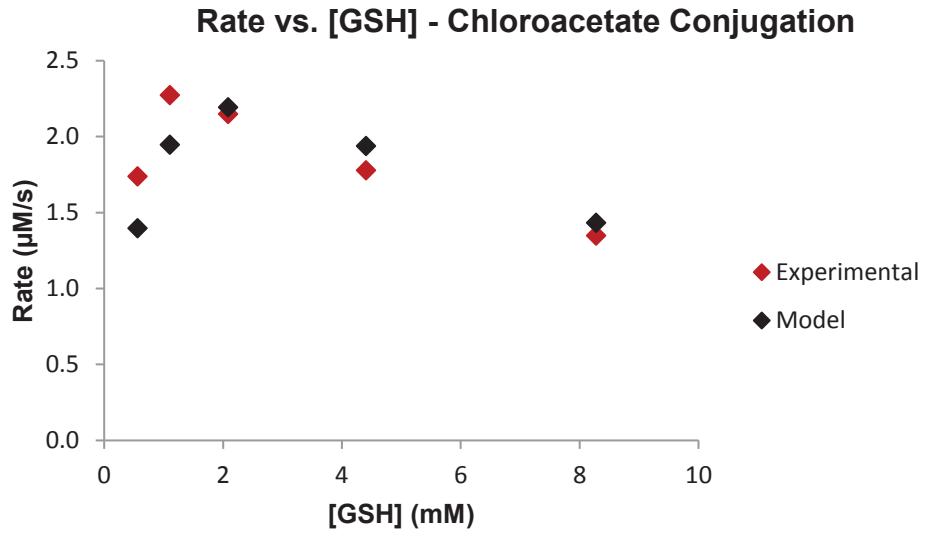

Figure 3-17: A plot of the catalyzed rate of chloroacetate-GSH conjugation versus GSH concentration with experimental rate (red) and model rate with substrate inhibition (black). [Chloroacetate]: 21 mM; [GstB]: 1.3 µM; reaction time: 4 min; R^2: 0.984.

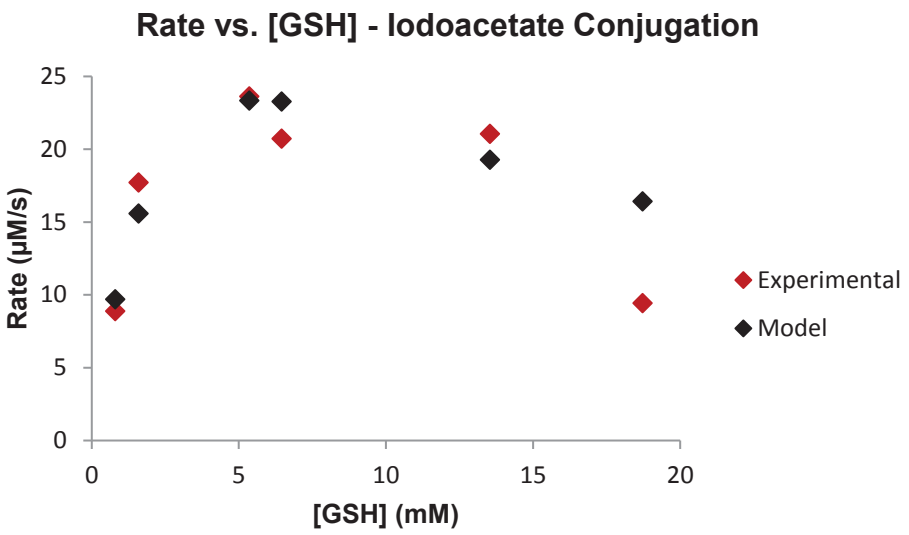

Figure 3-18: A plot of the rate of iodoacetate-GSH conjugation versus GSH concentration with experimental rate (red) and model rate with substrate inhibition (black). [Iodoacetate]: 18 mM; [GstB]: 1.5 μM; reaction time: 1 min; R^2: 0.970.

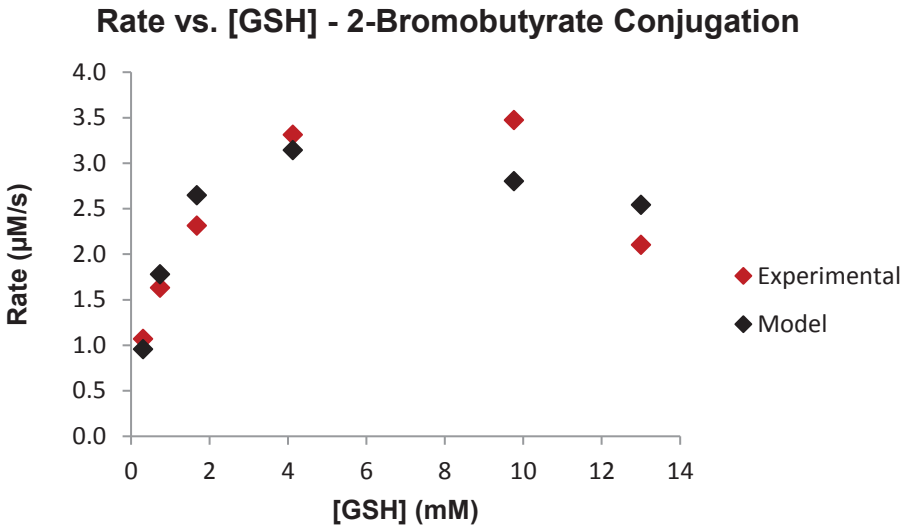

Figure 3-19: A plot of the rate of 2-bromobutyrate-GSH conjugation versus GSH concentration with experimental rate (red) and model rate with substrate inhibition (black). [2-Bromobutyrate]: 18 mM; [GstB]: 1.3 μM; reaction time: 4 min; R^2: 0.977.

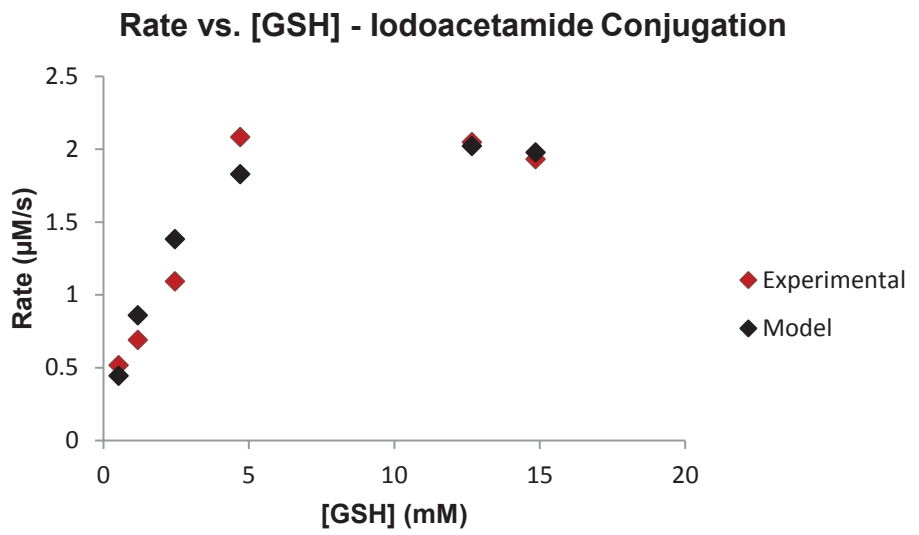

Figure 3-20: A plot of the rate of iodoacetamide-GSH conjugation versus GSH concentration with experimental rate (red) and model rate with substrate inhibition (black). [Iodoacetamide]: 18 mM; [GstB]: 1.3 µM; reaction time: 3 min; R^2: 0.987.

These results indicate that there is a threshold concentration of GSH beyond which GstB experiences inhibition. The inhibition constants for GSH were obtained (Table 3-2). This inhibition is strongest for the chloroacetate conjugation reaction (K_I^{GSH}: 4.00 mM) and weakest for the iodoacetamide conjugation reaction (K_I^{GSH}: 30.5 mM). The wild type enzyme had the highest affinity for GSH when chloroacetate and 2-bromobutyrate were the electrophilic substrates (K_M^{GSH}: 1.20 mM, 1.30 mM). Turnover number with respect to GSH was lowest for chloroacetate conjugation (k_{cat}^{GSH}: 3.68 s^{-1}) and highest for iodoacetate conjugation (k_{cat}^{GSH}: 34.3 s^{-1}). Finally, catalytic efficiency was lowest for iodoacetamide conjugation (k_{cat}^{GSH}/K_M^{GSH}: 0.890 $mM^{-1}s^{-1}$) and highest for iodoacetate conjugation (k_{cat}^{GSH}/K_M^{GSH}: 10.5 $mM^{-1}s^{-1}$).

Table 3-2: Kinetic parameters with respect to GSH substrate.

Electrophile	K_M^{GSH} (mM)	k_{cat}^{GSH} (s^{-1})	k_{cat}^{GSH}/K_M^{GSH} ($mM^{-1}s^{-1}$)	K_I^{GSH} (mM)
ClAc	1.20	3.68	3.07	4.00
BrAc	3.00	27.4	9.13	14.0
IAc	3.25	34.3	10.5	10.0
2-BrBt	1.30	3.76	2.89	15.0
$IAcNH_2$	4.85	4.47	0.890	30.5

PART III. WILD TYPE GSTB DISK DIFFUSION SENSITIVITY SCREENING – ELECTROPHILES

Wild type *E. coli* strain K-12 and *E. coli* BW25113Δ*gstB* knockout cells were exposed to the electrophiles evaluated for GstB enzymatic activity to compare their *in vitro* and *in vivo* effects. Figure 3-21 and Table 3-3 indicate that the wild type cells were more sensitive to iodoacetamide than the knockout cells, as a greater clearance zone was observed at 50 and 100 mM. Compounds with which GstB displayed no kinetic activity, including ethyl bromoacetate, *trans*-cinnamate, and acrylate did not impact the growth of either strain.

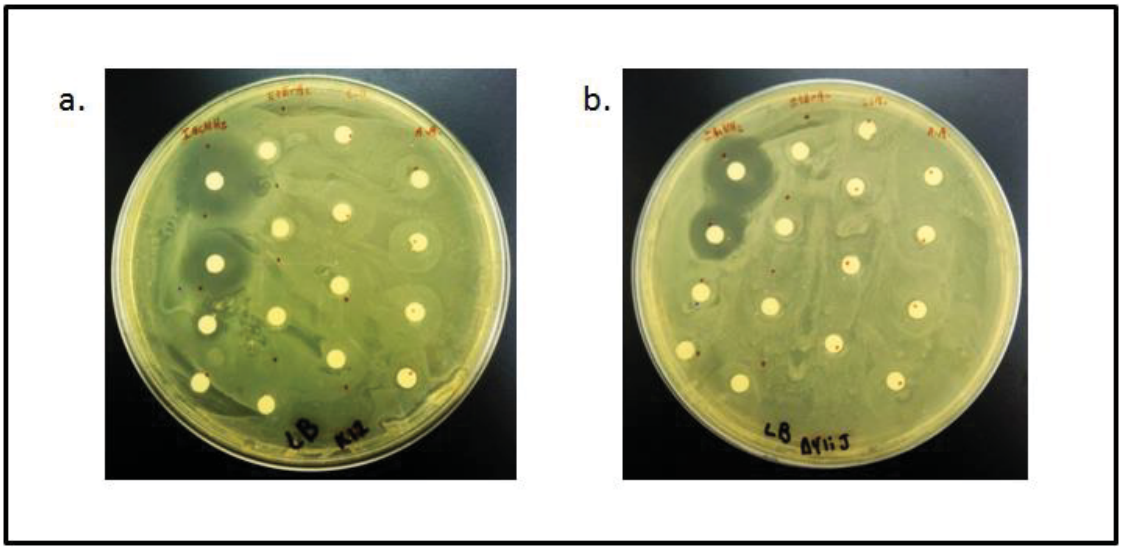

Figure 3-21: Disk diffusion sensitivity screening of *E. coli* K-12 (a.) and *E. coli* BW25113Δ*gstB* (b.) with 100 mM, 50 mM, 10 mM, and 2 mM solutions of iodoacetamide, ethyl bromoacetate, *trans*-cinnamic acid, and acrylic acid (left to right on plates).

Table 3-3: Clearance zone diameters for *E. coli* K-12 and *E. coli* BW25113Δ*gstB* with electrophiles.

Electrophile	K-12 (mm)	Δ*gstB* (mm)
100 mM $IAcNH_2$	35.0	26.5
100 mM EtBrAc	None	None
100 mM *trans*-CA	None	None
100 mM Acr	None	None

Figure 3-22 and Table 3-4 show that the knockout cells were more sensitive to bromoacetate and iodoacetate. High concentrations of chloroacetate and 2-bromobutyrate, compounds that were found to be GstB substrates, had no effect on cell growth for either strain. Both cell lines were resistant to dichloroacetate.

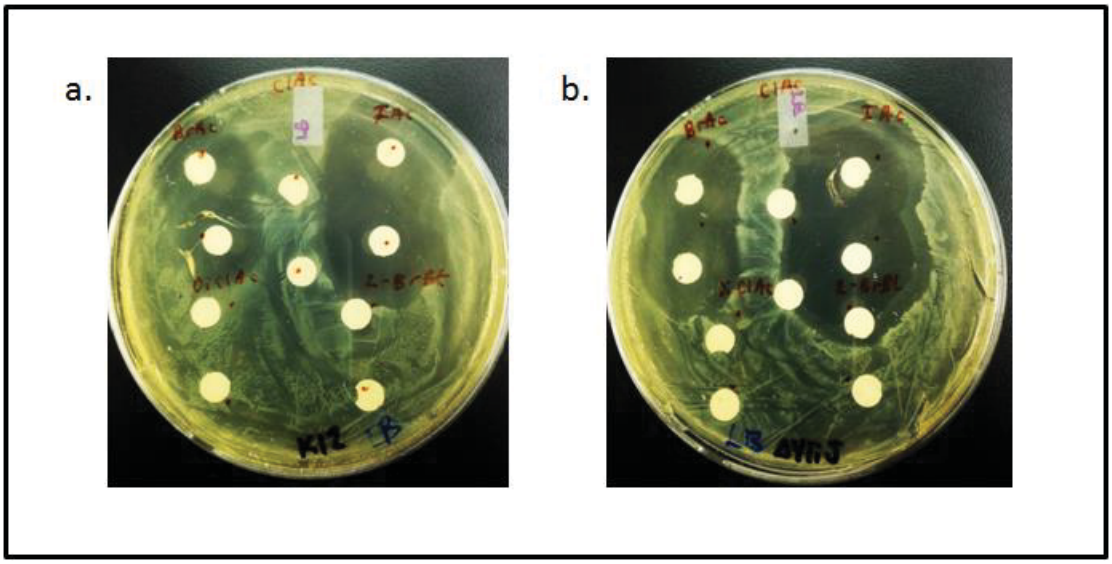

Figure 3-22: Disk diffusion sensitivity screening of *E. coli* K-12 (a.) and *E. coli* BW25113Δ*gstB* (b.) with (from top left of plates) bromoacetate: 500 mM, 250 mM, chloroacetate: 500 mM, 250 mM, iodoacetate: 500 mM, 250 mM, (from bottom left of plates) dichloroacetate: 500 mM, 250 mM and 2-bromobutyrate: 500 mM, 250 mM.

Table 3-4: Clearance zone diameters for *E. coli* K-12 and *E. coli* BW25113Δ*gstB* with electrophiles.

Electrophile	K-12 (mm)	Δ*gstB* (mm)
250 mM BrAc	19.0	24.0
260 mM ClAc	None	None
250 mM IAc	26.0	34.0
500 mM DiClAc	None	None
500 mM 2-BrBt	None	None

PART IV. WILD TYPE GSTB DISK DIFFUSION SENSITIVITY SCREENING - METALS

E. coli K-12 and E. coli BW25113ΔgstB with Pb^{2+}, Hg^{2+}, Ag^{+}, Au^{3+}, Cr^{6+}, Co^{2+}, Cd^{2+}, Cu^{2+}, Se^{4+}, As^{3+}

GSH and certain GSTs are known to interact with metals by reducing, sequestering, or transporting them. Initial screening of *E. coli* K-12 and *E. coli* BW25113Δ*gstB* with metals revealed that the knockout strain was more sensitive to both Cr^{6+} and As^{3+} (Figure 3-23). Table 3-5 below displays the clearance zone diameters. Therefore, the disk diffusion sensitivity testing of these cell lines was performed again with varying concentrations of Cr^{6+} and As^{3+}.

The results of the second experiment with varied concentrations of the metal ions As^{3+} and Cr^{6+} indicated that the *E. coli* BW25113Δ*gstB* strain was more sensitive to As^{3+} than the K-12 strain at all concentrations tested (Figure 3-24 and Table 3-6). The BW25113Δ*gstB* and K-12 strains experienced similar degrees of sensitivity for the three different Cr^{6+} concentrations that were tested.

The results of the third experiment with varied concentrations of the metal ions Hg^{2+} and As^{3+} demonstrated that there was no difference in Hg^{2+} sensitivity between the *E. coli* BW25113Δ*gstB* and K-12 strains (Figure 3-25 and Table 3-7). This experiment also provided duplicate confirmation that the *E. coli* BW25113Δ*gstB* strain was more sensitive than the K-12 strain to all concentrations of As^{3+} tested (Figure 3-25 and Table 3-7).

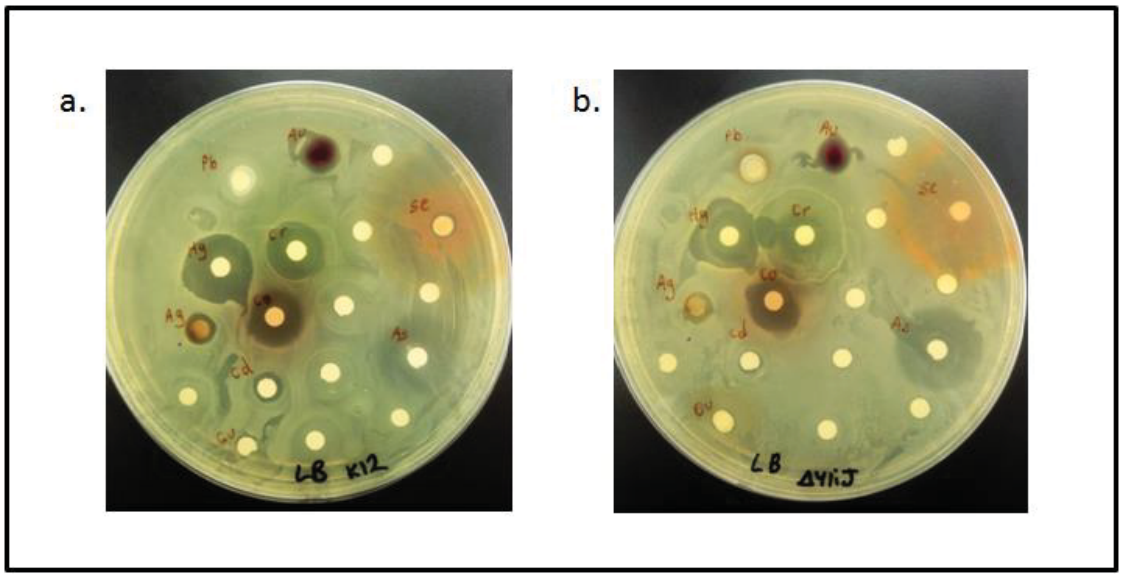

Figure 3-23: Disk diffusion sensitivity screening of *E. coli* K-12 (a.) and *E. coli* BW25113Δ*gstB* (b.), with sat. Pb^{2+}, sat. Hg^{2+}, 0.10 M Ag^{+}, 0.050 M Au^{3+}, 1.0 M Cr^{6+}, 1.0 M Co^{2+}, 0.050 M Cd^{2+}, 0.10 M Cu^{2+}, 1.0 M Se^{4+}, and 1.0 M As^{3+}.

Table 3-5: Clearance zone diameters for *E. coli* K-12 and *E. coli* BW25113Δ*gstB* with metals.

Metal Species	**K-12 (mm)**	**Δ*gstB* (mm)**
Sat. Pb^{2+}	9.0	9.0
Sat. Hg^{2+}	23.5	22.0
0.10 M Ag^{+}	10.0	10.0
0.050 M Au^{3+}	12.5	11.0
1.0 M Cr^{6+}	19.0	31.0
1.0 M Co^{2+}	16.0	15.5
0.050 M Cd^{2+}	10.5	9.5
0.10 M Cu^{2+}	None	None
1.0 M Se^{4+}	50.0	51.0
1.0 M As^{3+}	25.0	28.5

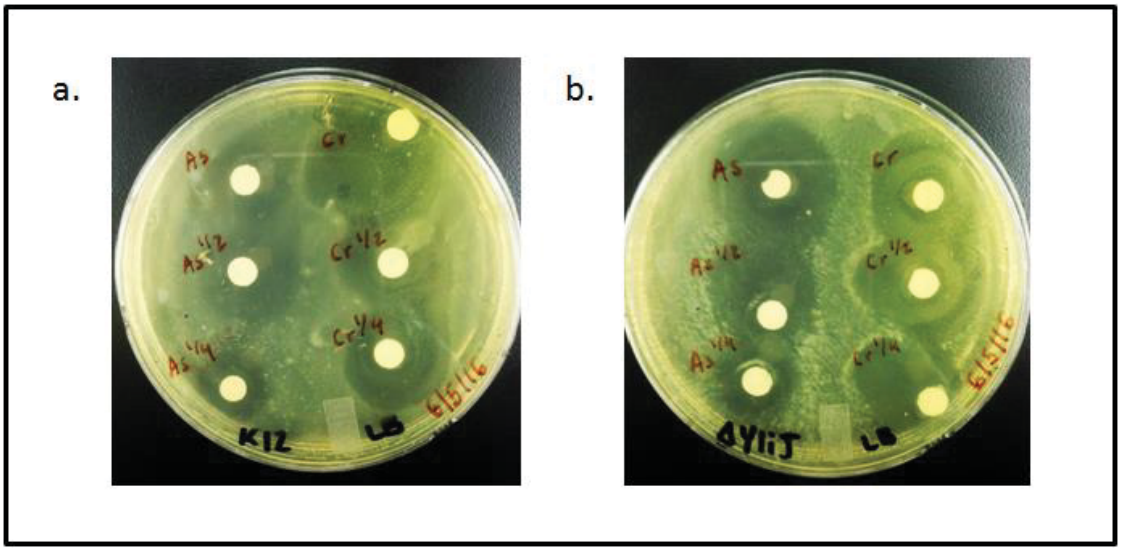

Figure 3-24: Disk diffusion sensitivity screening of *E. coli* K-12 (a.) and *E. coli* BW25113Δ*gstB* (b.) with 1.0 M As^{3+}, 0.50 M As^{3+}, 0.25 M As^{3+}, 1.0 M Cr^{6+}, 0.50 M Cr^{6+}, and 0.25 M Cr^{6+}.

Table 3-6: Clearance diameters for *E. coli* K-12 and *E. coli* BW25113Δ*gstB* with dilutions of As^{3+} and Cr^{6+}.

Metal Species	**K-12 (mm)**	**Δ*gstB* (mm)**
1.0 M As^{3+}	25.0	28.0
0.50 M As^{3+}	21.0	23.5
0.25 M As^{3+}	15.5	19.5
1.0 M Cr^{6+}	30.5	24.0
0.50 M Cr^{6+}	26.0	28.5
0.25 M Cr^{6+}	21.5	24.0

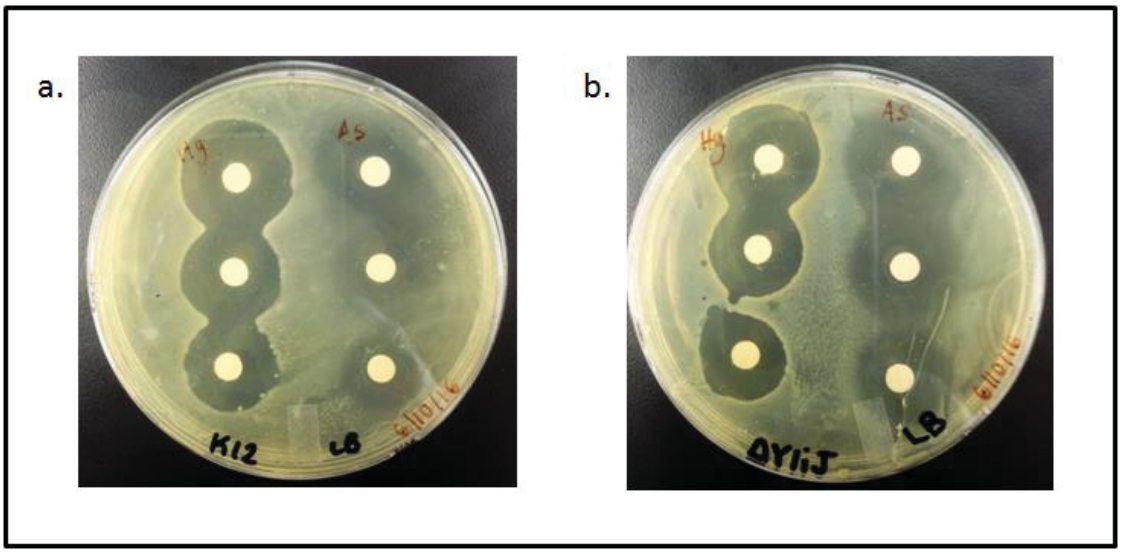

Figure 3-25: Disk diffusion sensitivity screening of *E. coli* K-12 (a.) and *E. coli* BW25113Δ*gstB* (b.) with sat. Hg^{2+}, sat. Hg^{2+} diluted 2-fold, sat. Hg^{2+} diluted 4-fold, 1.0 M As^{3+}, 0.50 M As^{3+}, and 0.25 M As^{3+}.

Table 3-7: Clearance diameters for *E. coli* K-12 and *E. coli* BW25113Δ*gstB* with dilutions of Hg^{2+} and As^{3+}.

Metal Species	**K-12 (mm)**	**Δ*gstB* (mm)**
sat. Hg^{2+}	24.5	23.0
sat. Hg^{2+} diluted 2-fold	22.0	20.5
sat. Hg^{2+} diluted 4-fold	20.0	18.5
1.0 M As^{3+}	25.0	27.5
0.50 M As^{3+}	23.0	25.0
0.25 M As^{3+}	18.5	22.0

***E. coli* BL21 pET-20 and *E. coli* BL21 pET-20(gstB) with Pb^{2+}, Hg^{2+}, Ag^{+}, Au^{3+}, Cr^{6+}, Co^{2+}, Cd^{2+}, Cu^{2+}, Se^{4+}, As^{3+}**

The effect of the metals was also examined in *E. coli* BL21 (DE3) cells that overexpressed GstB. *E. coli* BL21 (DE3) cells that contained the empty pET-20 plasmid served as a control. The only appreciable differences in zone clearance were observed for the metal ions Hg^{2+} (Figure 3-26) and As^{3+} (Figure 3-27). The diameters are listed in Table 3-8. Therefore, disk diffusion experiments were repeated with different concentrations of As^{3+} and Hg^{2+}. The BL21 pET-20 strain was more sensitive to As^{3+} than the BL21 pET-20(*gstB*) strain at all concentrations. This sensitivity pattern was the same at all concentrations of Hg^{2+} tested (Figure 3-28 and Table 3-9).

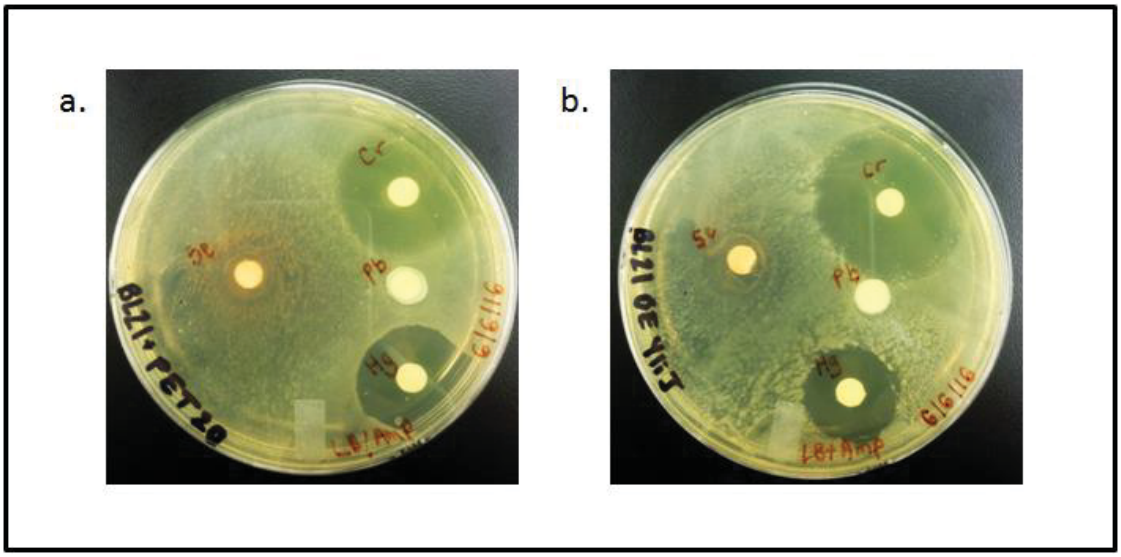

Figure 3-26: Disk diffusion sensitivity screening of *E. coli* BL21 pET-20 (a.) and *E. coli* BL21 pET-20(*gstB*) (right) with 1.0 M Se^{4+}, 1.0 M Cr^{6+}, sat. Pb^{2+}, and sat. Hg^{2+}.

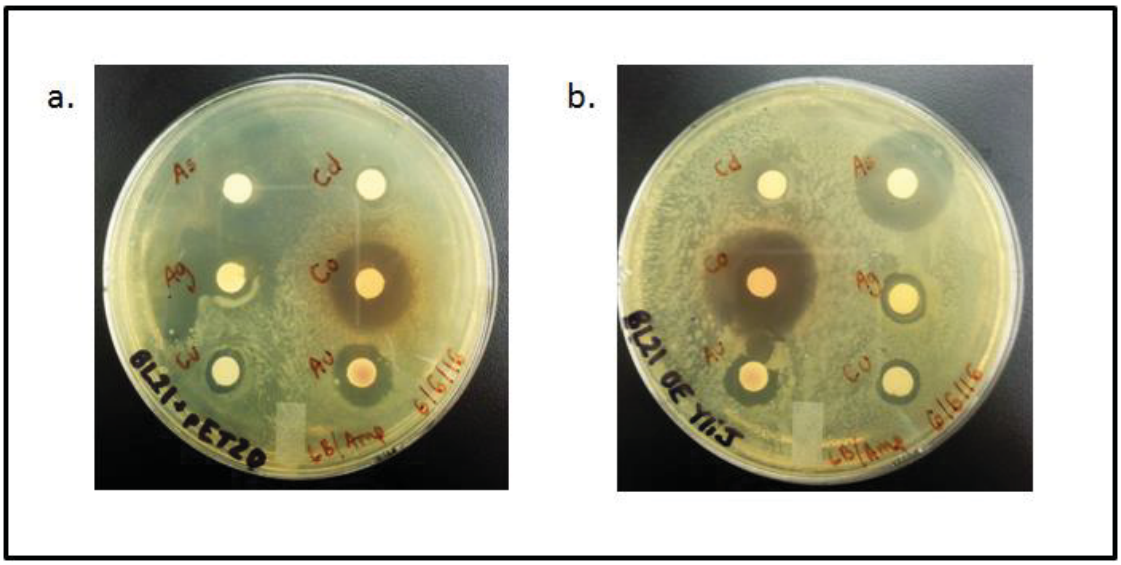

Figure 3-27: Disk diffusion sensitivity screening of *E. coli* BL21 pET-20 (a.) and *E. coli* BL21 pET-20(*gstB*) (b.) with 0.050 M Cd^{2+}, 1.0 M Co^{2+}, 0.050 M Au^{3+}, 1.0 M As^{3+}, 0.10 M Ag^{+}, and 0.10 M Cu^{2+}.

Table 3-8: Clearance diameters for *E. coli* BL21 pET-20(*gstB*) and *E. coli* BL21 pET-20 with metals.

Metal Species	BL21 pET-20(*gstB*) (mm)	BL21 pET-20 (mm)
Sat. Pb^{2+}	None	None
Sat. Hg^{2+}	22.0	25.5
0.10 M Ag^{+}	10.5	None
0.050 M Au^{3+}	14.0	13.5
1.0 M Cr^{6+}	35.0	17.0
1.0 M Co^{2+}	25.5	19.5
0.050 M Cd^{2+}	11.0	10.0
0.10 M Cu^{2+}	9.5	9.5
1.0 M Se^{4+}	None	None
1.0 M As^{3+}	21.5	41.0

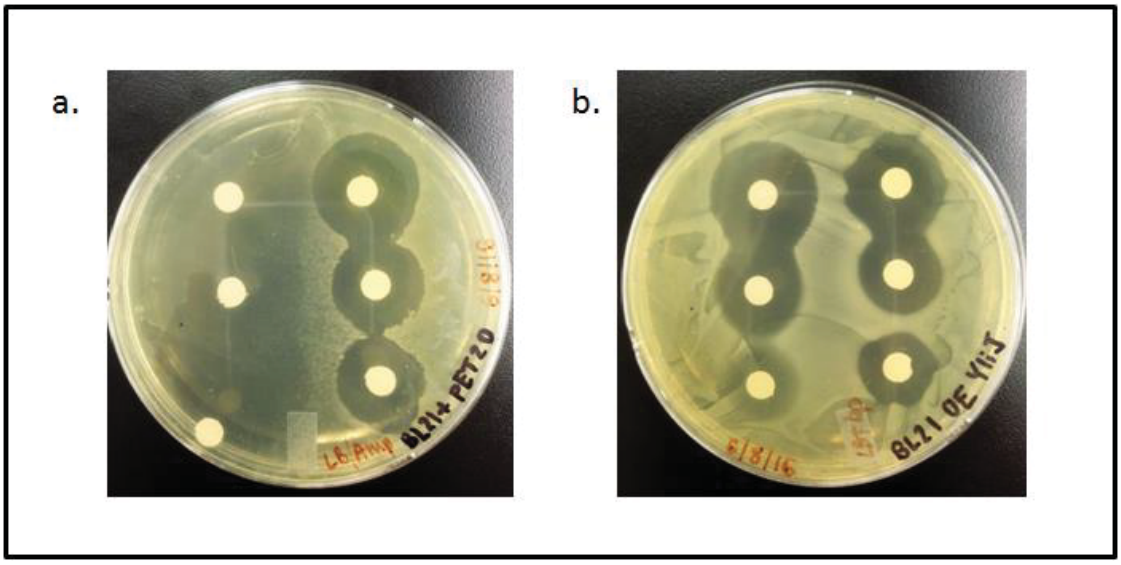

Figure 3-28: Disk diffusion sensitivity screening of *E. coli* BL21 pET-20 (a.) and *E. coli* BL21 pET-20(*gstB*) (b.) with 1.0 M As^{3+}, 0.50 M As^{3+}, 0.25 M As^{3+}, sat. Hg^{2+}, sat. Hg^{2+} diluted 2-fold, and sat. Hg^{2+} diluted 4-fold.

Table 3-9: Clearance diameters for *E. coli* BL21 pET-20(*gstB*) and *E. coli* BL21 pET-20 at various concentrations of As^{3+} and Hg^{2+}.

Metal Species	**BL21 pET-20(*gstB*) (mm)**	**BL21 pET-20 (mm)**
1.0 M As^{3+}	24.0	36.5
0.50 M As^{3+}	21.0	34.0
0.25 M As^{3+}	17.5	30.0
sat. Hg^{2+}	22.0	22.5
sat. Hg^{2+} diluted 2-fold	18.0	20.0
sat. Hg^{2+} diluted 4-fold	17.5	19.0

E. coli K-12, E. coli BW25113ΔgstB, E. coli BL21 pET-20, and E. coli BL21 pET-20(gstB) with As^{5+} and Ni^{2+}

Sensitivity of the K-12 strain to As^{5+} was higher than that displayed by the BW25113Δ*gstB* strain for all concentrations tested (Figure 3-29 and Table 3-10). The BL21 pET-20 strain was more sensitive than the BL21-pET20(*gstB*) strain to all concentrations of As^{5+}. There was no significant difference in clearance for Ni^{2+} (Figure 3-30 and Table 3-10).

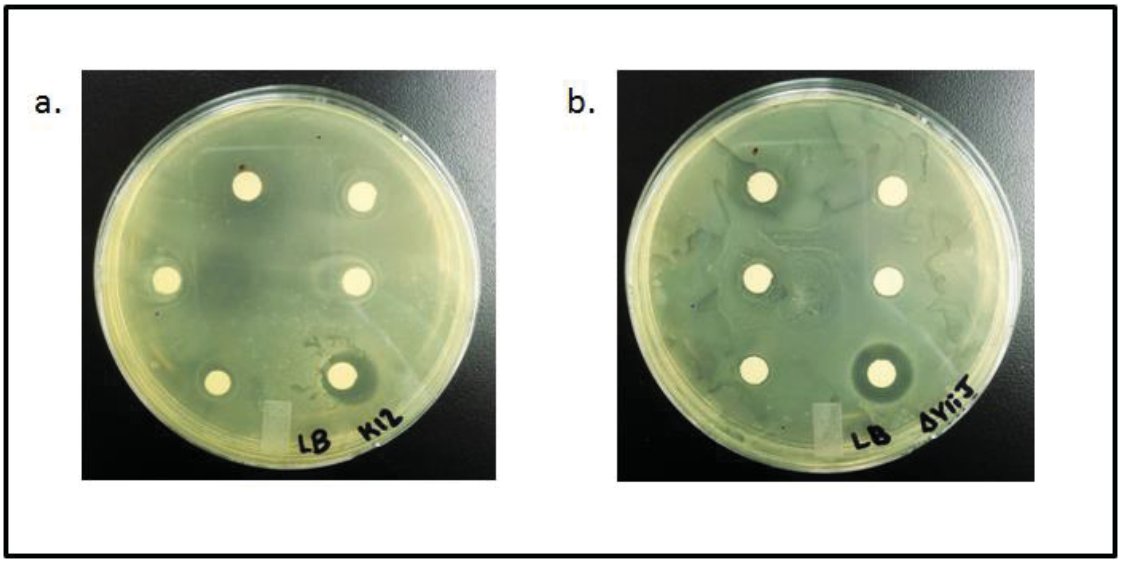

Figure 3-29: Disk diffusion sensitivity screening of *E. coli* K-12 (a.) and *E. coli* BW25113Δ*gstB* (b.) with 1.0 M As^{5+}, 0.50 M As^{5+}, 0.25 M As^{5+}, 0.10 M As^{5+}, 0.070 M As^{5+}, and 1.2 M Ni^{2+}.

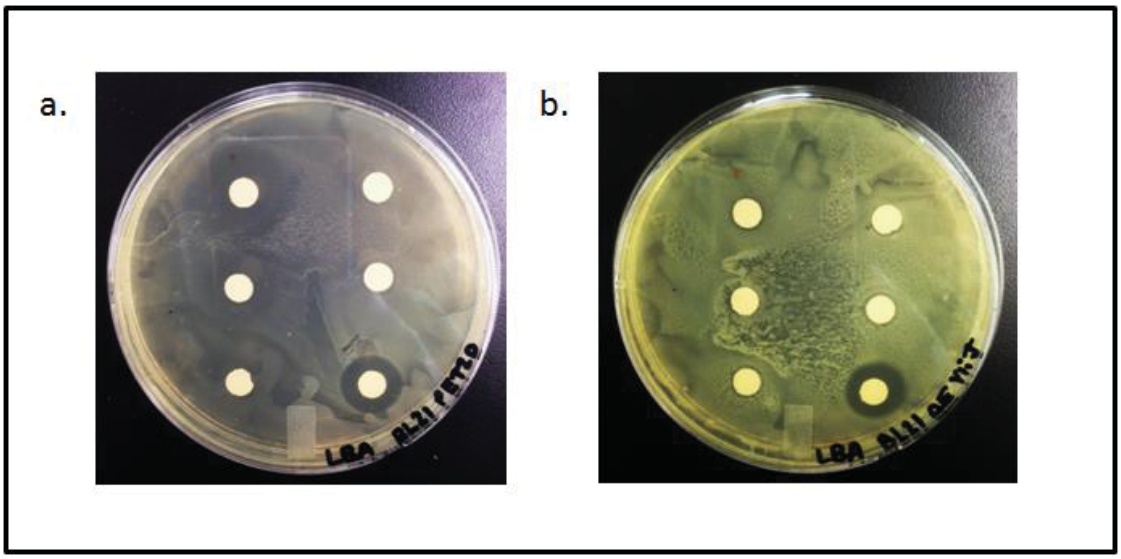

Figure 3-30: Disk diffusion sensitivity screening of *E. coli* BL21 pET-20 (a.) and *E. coli* BL21 pET-20(*gstB*) (b.) with 1.0 M As^{5+}, 0.50 M As^{5+}, 0.25 M As^{5+}, 0.10 M As^{5+}, 0.070 M As^{5+}, and 1.0 M Ni^{2+}.

Table 3-10: Clearance diameters for *E. coli* K-12, *E. coli* BW25113Δ*gstB, E. coli* BL21 pET-20(*gstB*), and *E. coli* BL21 pET-20 with As^{5+} dilutions and Ni^{2+}.

Metal Species	K-12 (mm)	Δ*gstB* (mm)	BL21 pET-20(*gstB*) (mm)	BL21 pET-20 (mm)
1.0 M As^{5+}	20.0	15.5	8.5	22.0
0.50 M As^{5+}	15.5	12.0	None	17.5
0.25 M As^{5+}	10.0	8.5	None	None
0.10 M As^{5+}	12.0	9.0	None	7.5
0.070 M As^{5+}	9.5	9.0	None	8.5
1.2 M Ni^{2+}	13.0	14.0	13.5	14.5

E. coli K-12, E. coli BW25113ΔgstB, E. coli BL21 pET-20, and E. coli BL21 pET-20(gstB) with Tb^{3+}, Mo^{6+}, Mn^{2+}, Sn^{2+}, Ba^{2+}, and Ce^{3+}

The *E. coli* K-12 and BW25113Δ*gstB* cell lines both displayed identical sensitivity to the metals Tb^{3+}, Mo^{6+}, Mn^{2+}, Sn^{2+}, Ba^{2+}, and Ce^{3+}, as indicated in Figure 3-31 and Table 3-11 . Likewise, the *E. coli* BL21 pET-20 and pET-20(*gstB*) cell lines did not differ from each other in their sensitivity to these metals, as indicated in Figure 3-32 and Table 3-12.

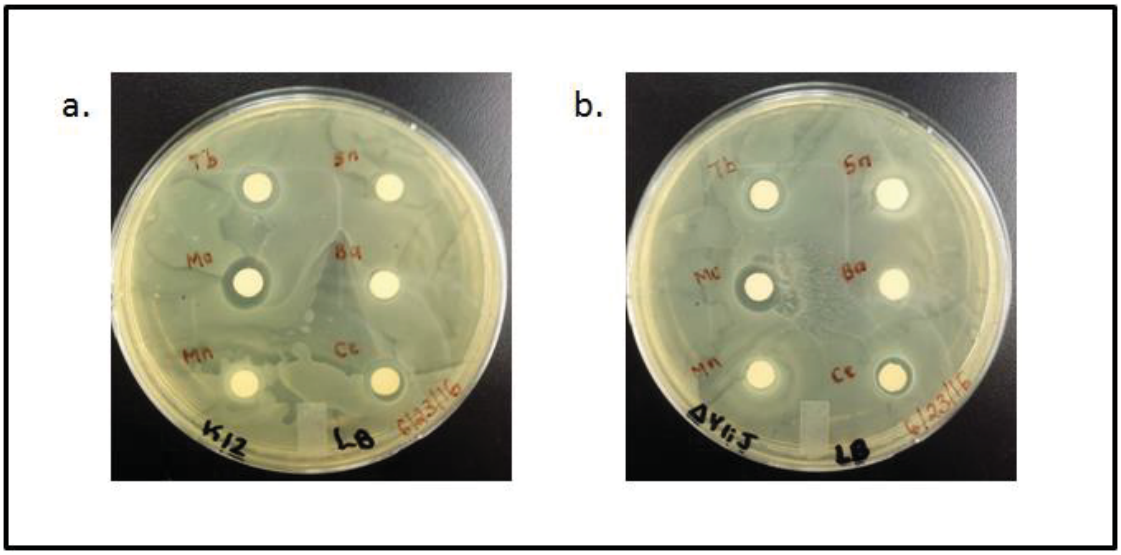

Figure 3-31: Disk diffusion sensitivity screening of *E. coli* K-12 (a.) and *E. coli* BW25113 Δ*gstB* (b.) with 1.0 M Tb^{3+}, sat. Mo^{6+}, 1.0 M Mn^{2+}, sat. Sn^{2+}, sat. Ba^{2+}, and 1.0 M Ce^{3+}.

Table 3-11: Clearance diameters for *E. coli* K-12 and *E. coli* BW25113Δ*gstB* with metals.

Metal Species	K-12 (mm)	Δ*gstB* (mm)
1.0 M Tb^{2+}	10.5	10.5
Sat. Mo^{6+}	11.5	11.0
1.0 M Mn^{2+}	None	None
Sat. Sn^{2+}	None	None
Sat. Ba^{2+}	None	None
1.0 M Ce^{3+}	10.5	10.0

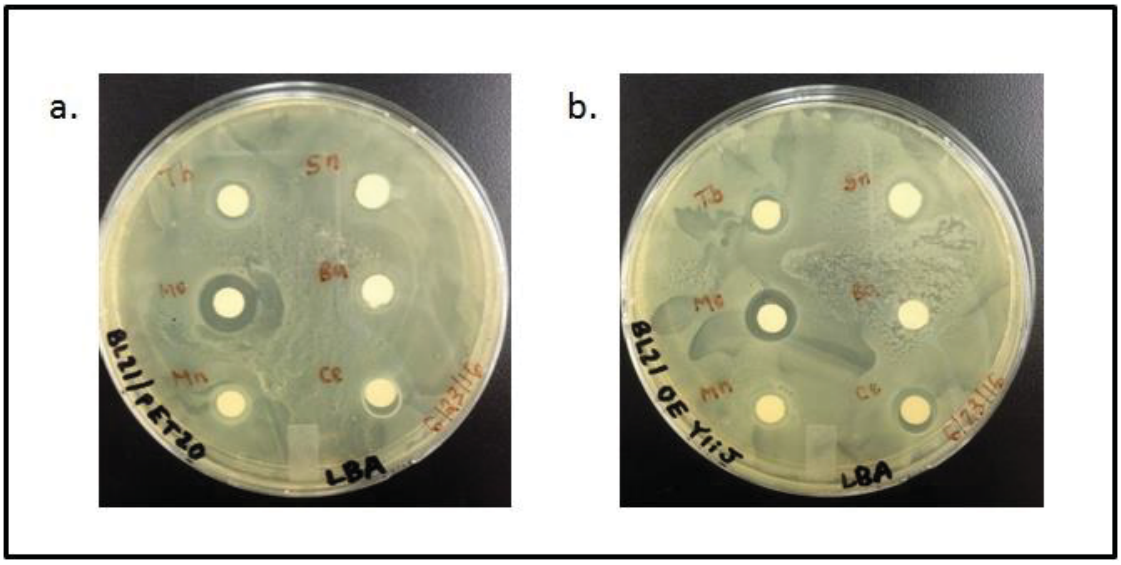

Figure 3-32: Disk diffusion sensitivity screening of *E. coli* BL21 pET-20 (a.) *E. coli* BL21 pET-20(*gstB*) (b.) and with 1.0 M Tb^{3+}, sat. Mo^{6+}, 1.0 M Mn^{2+}, sat. Sn^{2+}, sat. Ba^{2+}, and 1.0 M Ce^{3+}.

Table 3-12: Clearance diameters for *E. coli* BL21 pET-20(*gstB*) and *E. coli* BL21 pET-20 with metals.

Metal Species	BL21 pET-20(*gstB*) (mm)	BL21 pET-20 (mm)
1.0 M Tb^{2+}	9.5	11.5
Sat. Mo^{6+}	12.0	13.0
1.0 M Mn^{2+}	None	None
Sat. Sn^{2+}	None	None
Sat. Ba^{2+}	None	None
1.0 M Ce^{3+}	9.0	9.0

PART V. GSTB SITE-DIRECTED MUTAGENESIS

Mutant Plasmid DNA Sequencing

Site-directed mutagenesis was carried out to create four GstB mutants in which the arginine residue at position 119 was replaced with alanine, histidine, glutamine, and serine. Upon completion of site-directed mutagenesis, plasmid DNA was extracted from the XL1-Superblue competent cell colonies and purified. The DNA samples were sent to the Plant-Microbe Genomics Facility at The Ohio State University for DNA sequencing. The electropherograms were visualized using FinchTV software version 4.0 and comprise Figures 3-33 through 3-36.

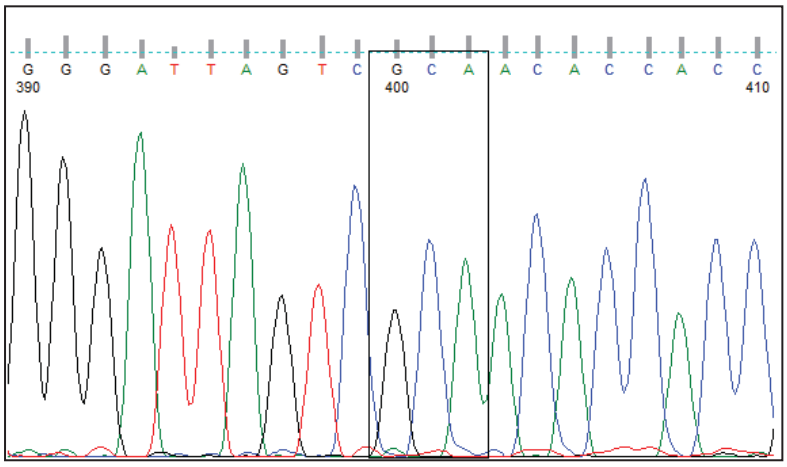

Figure 3-33: Electropherogram from DNA sequencing of the R119A mutant: AGA replaced with CGA.

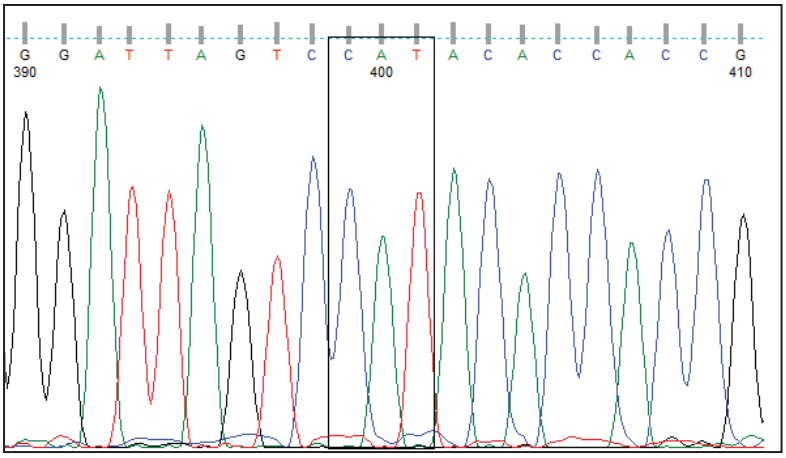

Figure 3-34: Electropherogram from DNA sequencing of the R119H mutant: AGA replaced with CAT.

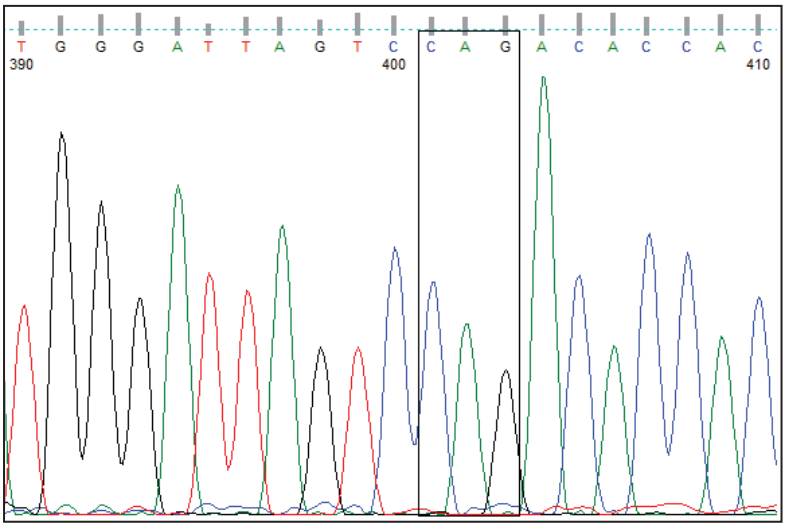

Figure 3-35: Electropherogram from DNA sequencing of the R119Q mutant: AGA replaced with CAG.

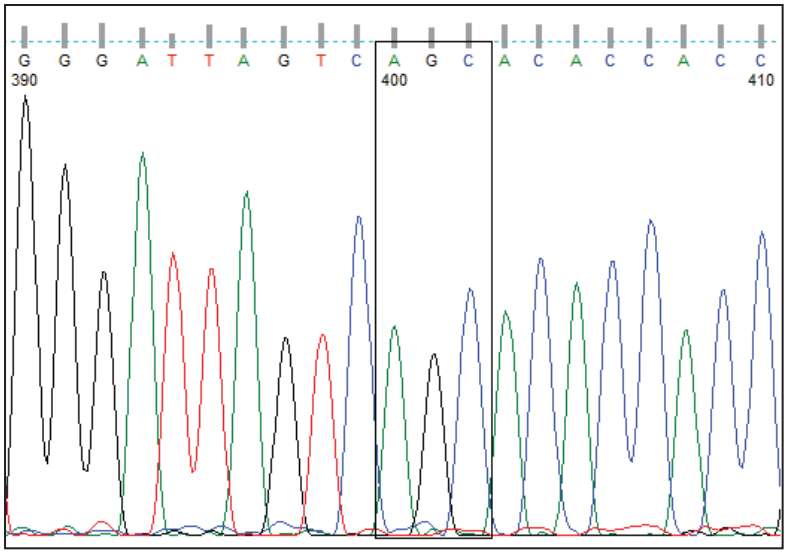

Figure 3-36: Electropherogram from DNA sequencing of the R119S mutant: AGA replaced with AGC.

Overexpression of Mutant Proteins

Once the mutant plasmid DNA sequences were validated, the DNA was transformed into BL21 (DE3) competent cells. Various colonies from each of the transformant plates were screened for protein overexpression. Screening was performed on a small scale (2-mL cultures) and a larger scale (100-mL cultures). The larger-scale protein overexpression studies provided the most conclusive results, confirming that the mutant enzymes could be overexpressed. The R119A and R119H mutants displayed reasonable overexpression (Figure 3-37, Lanes 3 and 7). The R119Q mutant exhibited a similar degree of overexpression (Figure 3-38, Lane 3), while the R119S mutant displayed an impressive degree of overexpression (Figure 3-38, Lane 7).

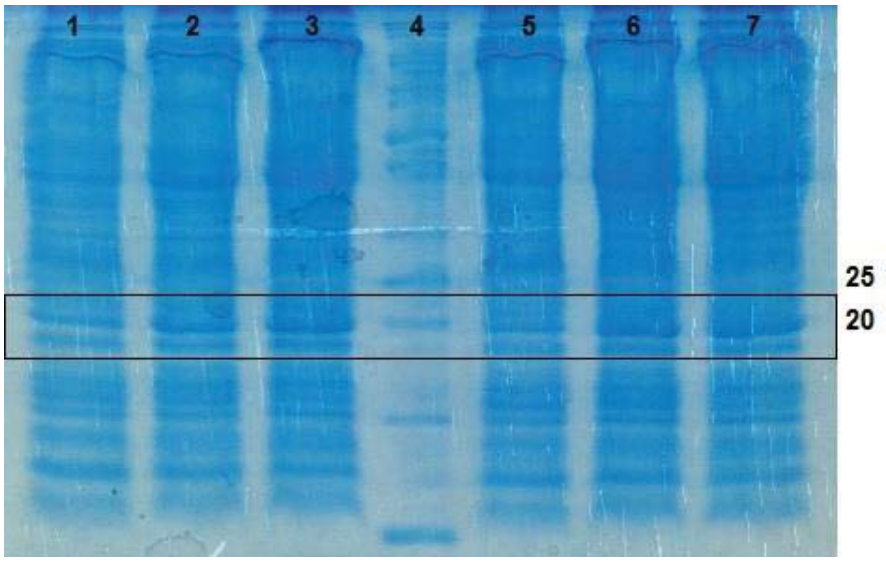

Figure 3-37: 18% SDS-PAGE of R119A and R119H GstB mutants overexpression (100-mL culture). Lane 1: R119A –IPTG; Lane 2: R119A +IPTG after 5.5 h; Lane 3: R119A +IPTG overnight; Lane 4: MW marker; Lane 5: R119H –IPTG; Lane 6: R119H +IPTG after 5.5 h; Lane 7: R119H +IPTG overnight.

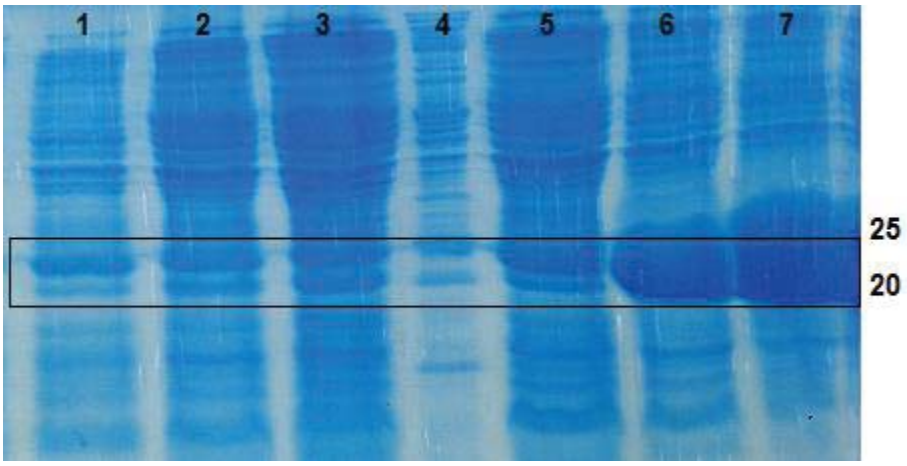

Figure 3-38: 18% SDS-PAGE of R119Q and R119S GstB mutants overexpression (100-mL culture). Lane 1: R119Q –IPTG; Lane 2: R119Q +IPTG after 5.5 h; Lane 3: R119Q +IPTG overnight; Lane 4: MW marker; Lane 5: R119S –IPTG; Lane 6: R119S +IPTG after 5.5 h; Lane 7: R119S +IPTG overnight.

Purification of Mutant Proteins

All four mutants were purified using the same precipitation and anion exchange column chromatography protocols that have been described for wild type GstB. Figure 3-39 demonstrates that the optimized purification protocol for wild type GstB was applicable to the R119Q mutant. Figures 3-40 and 3-41 indicate that many contaminant proteins remained following anion exchange column chromatography and concentration. Therefore, the concentrate was subjected to hydroxylapatite column chromatography to remove impurities (Figure 3-42). Figure 3-43 proves that this additional purification step was successful. Relatively pure R119Q GstB was obtained after concentration of the 8 volume wash and 0.025 M NaP_i, pH 6.8 elution fractions. The R119H mutant also required the additional hydroxylapatite column chromatography purification step.

Figures 3-44 through 3-46 reveal that the optimized protein precipitation protocol and anion exchange chromatography were sufficient to purify the R119S mutant. Thus, no hydroxylapatite chromatography step was performed. The R119A mutant was purified in the same manner as R119S.

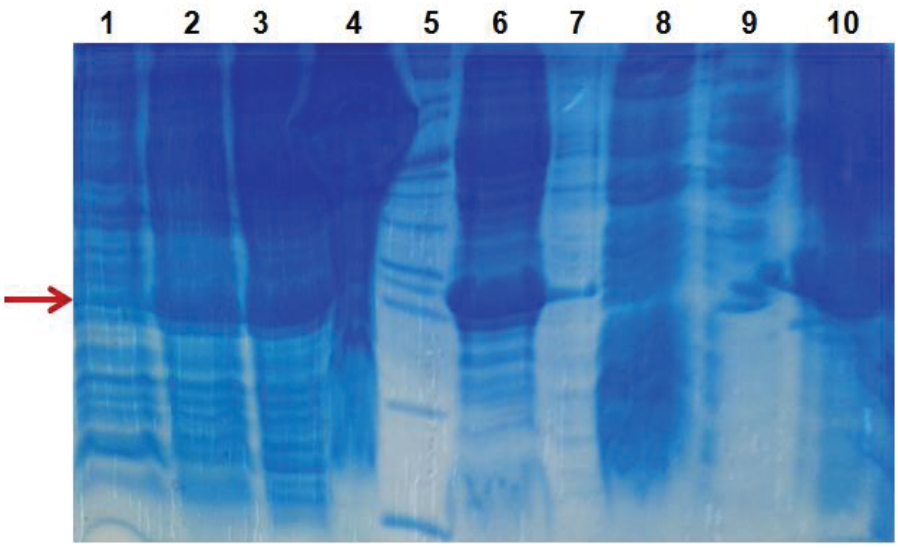

Figure 3-39: 18% SDS-PAGE of R119Q purification. Lane 1: (-)-IPTG; Lane 2: (+)-IPTG overnight; Lane 3: sonication supernatant; Lane 4: sonication pellet; Lane 5: MW marker; Lane 6: streptomycin supernatant; Lane 7: Empty; Lane 8: streptomycin pellet; Lane 9: ammonium sulfate supernatant; Lane 10: ammonium sulfate pellet.

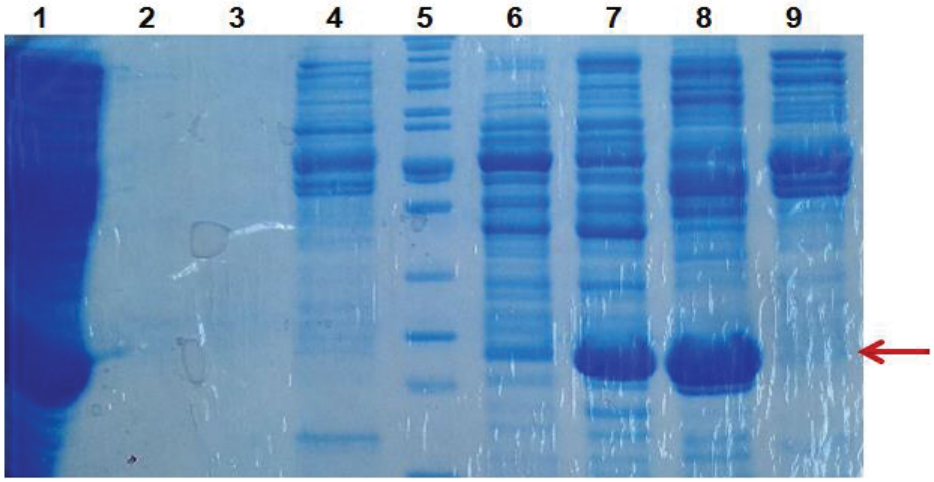

Figure 3-40: 15% SDS-PAGE of R119Q anion exchange column chromatography fractions. Lane 1: load; Lane 2: wash; Lane 3: flow-through; Lane 4: 2 M NaCl; Lane 5: MW marker; Lane 6: fraction #45; Lane 7: fraction #48; Lane 8: fraction #56; Lane 9: fraction #66.

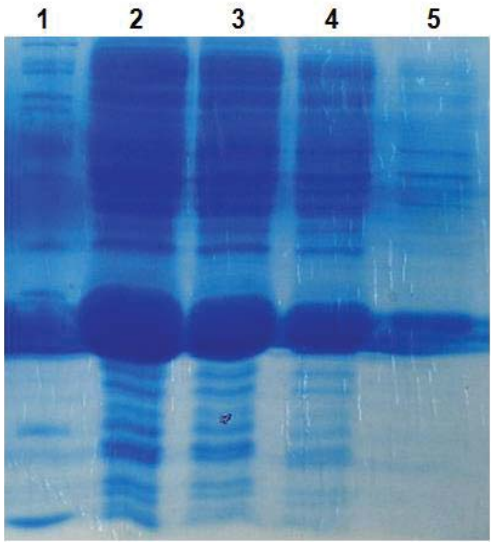

Figure 3-41: 15% SDS-PAGE of concentrated R119Q anion exchange fractions. Lane 1: MW marker; Lane 2: 1:5 dilution; Lane 3: 1:10 dilution; Lane 4: 1:20 dilution; Lane 5: 1:100 dilution.

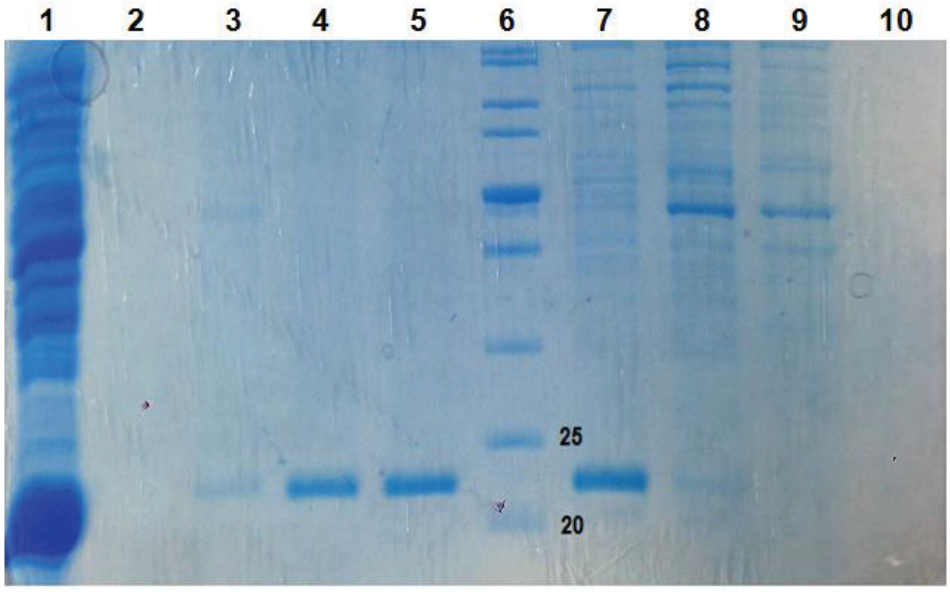

Figure 3-42: 15% SDS-PAGE of R119Q hydroxylapatite column chromatography fractions. Lane 1: load; Lane 2: flow-through; Lane 3: 1.5 vol. 10 mM NaP_i wash; Lane 4: 8 vol. 10 mM NaP_i wash; Lane 5: 0.025 M NaP_i; Lane 6: MW marker; Lane 7: 0.05 M NaP_i; Lane 8: 0.10 M NaP_i; Lane 9: 0.25 M NaP_i; Lane 10: 0.40 M NaP_i.

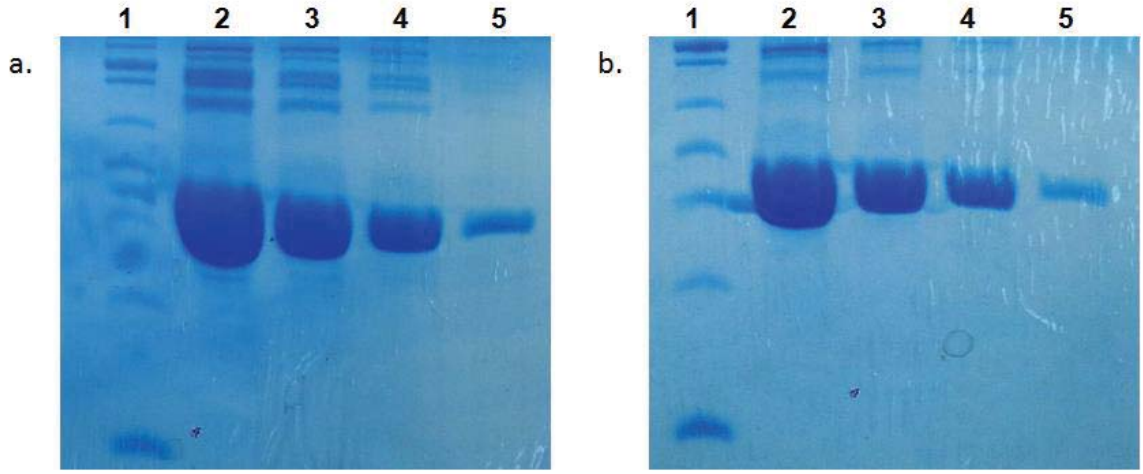

Figure 3-43: 15% SDS-PAGE of concentrated R119Q hydroxylapatite fractions. **a.** 10 mM NaP_i wash: Lane 1: MW marker; Lane 2: 1:5 dilution; Lane 3: 1:10 dilution; Lane 4: 1:20 dilution; Lane 5: 1:100 dilution. **b.** 0.025 M NaP_i wash: Lane 1: MW marker; Lane 2: 1:5 dilution; Lane 3: 1:10 dilution; Lane 4: 1:20 dilution; Lane 5: 1:100 dilution.

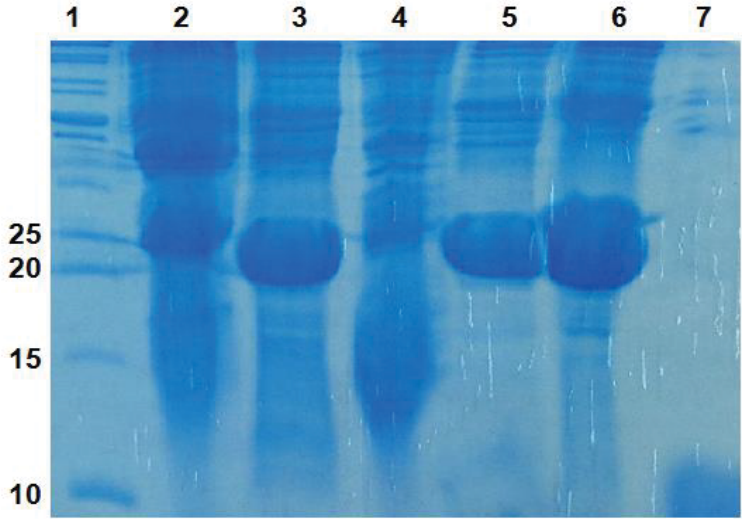

Figure 3-44: 18% SDS-PAGE of R119S purification. Lane 1: MW marker; Lane 2: sonication pellet; Lane 3: sonication supernatant; Lane 4: streptomycin pellet; Lane 5: streptomycin supernatant; Lane 6: ammonium sulfate pellet; Lane 7: ammonium sulfate supernatant.

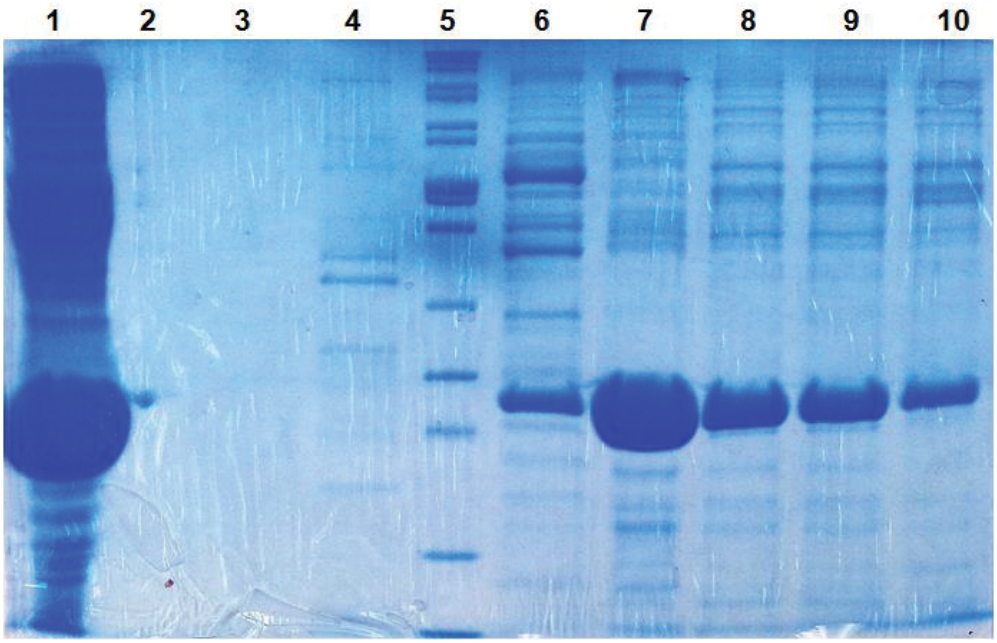

Figure 3-45: 15% SDS-PAGE of R119S anion exchange fractions. Lane 1: load; Lane 2: flow-through; Lane 3: wash; Lane 4: fraction #40; Lane 5: MW marker; Lane 6: fraction #52; Lane 7: fraction #60; Lane 8: fraction #66; Lane 9: fraction #67; Lane 10: fraction #69.

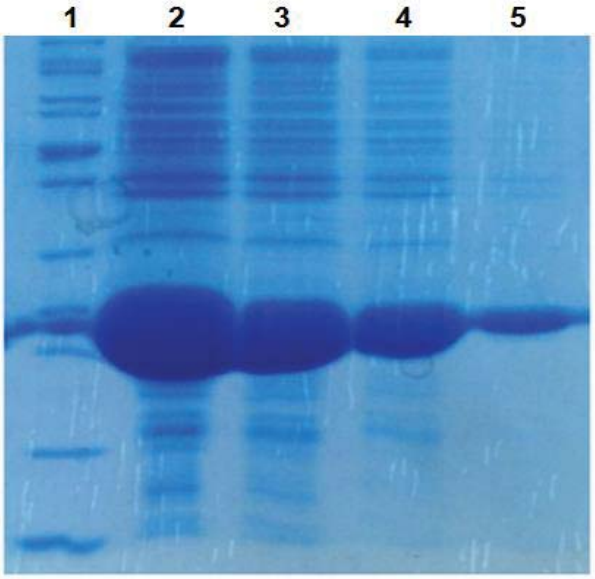

Figure 3-46: 15% SDS-PAGE of concentrated R119S anion exchange fractions. Lane 1: MW marker; Lane 2: 1:5 dilution; Lane 3: 1:10 dilution; Lane 4: 1:20 dilution; Lane 5: 1:100 dilution.

PART VI. ACTIVITY SCREENING OF GSTB MUTANTS

All mutants were initially screened for activity with various electrophiles using the discontinuous DTNB spectrophotometric assay. Reactions with wild type GstB were performed each time, allowing for activity comparison under identical conditions.

R119A

The R119A mutant (green diamonds) was less active with acrylate than the wild type and the other three mutants at all three time points (Figure 3-47). Similar performance was observed for bromoacetate, 2-bromobutyrate, and chloroacetate conjugation reactions (Figures 3-48, 3-50, and 3-52). During the *trans*-cinnamate screening, R119A was more active than the wild type at both the 5 and 10 min time points, but appeared to experience inhibition over time, while wild type GstB did not (Figure 3-54). Figure 3-56 indicates that R119A provided the highest degree of rate enhancement over the wild type compared to the other two mutants tested under the same conditions for iodoacetamide conjugation. While less active with iodoacetate than the wild type, Figure 3-58 demonstrates that R119A slightly outperformed R119H and R119Q under the same conditions.

R119H

The R119H mutant (purple diamonds) was the least active enzyme with respect to acrylate conjugation at both the 5 and 10 min time points. However, at 15 min, its activity nearly matched that of wild type GstB (Figure 3-47). Figure 3-48 shows that R119H was the most active mutant with bromoacetate, though less active than the wild type enzyme. This mutant exhibited virtually no activity with 2-bromobutyrate (Figure 3-51). With respect to *trans*-cinnamate conjugation, R119H was the second most active enzyme at 5

min, but fell to third most active at 15 min (Figure 3-54). R119H was not tested for activity with chloroacetate or ethyl bromoacetate. Its activity with iodoacetamide was very similar to that of R119A; again, exceeding that of wild type GstB (Figure 3-56). R119H suffered some activity loss with iodoacetate compared to the wild type, but it performed similarly to the other two mutants tested under the same conditions (Figure 3-58).

R119Q

The R119Q mutant (blue diamonds) was the most active enzyme in promoting acrylate conjugation (Figure 3-47). Figure 3-48 displays that R119Q , like all mutants, was less active with bromoacetate than the wild type. Specifically, R119Q was more active than R119A, but less active than R119H for this reaction. This mutant was not active with 2-bromobutyrate (Figure 3-51). At the 5 min point for *trans*-cinnamate conjugation, R119Q was the third most active enzyme, and improved to be the second most active enzyme at 15 min. Also, R119Q did not appear to experience inhibition by this molecule over time (Figure 3-54). R119Q was not screened for activity with chloroacetate or ethyl bromoacetate. While outperforming the wild type, R119Q was the least active mutant with iodoacetamide at both the 5 and 10 min time points (Figure 3-56). With respect to iodoacetate conjugation, R119Q activity was nearly identical to the other two mutants tested under the same conditions (Figure 3-58).

R119S

The R119S mutant was the second most active enzyme with respect to acrylate conjugation (Figure 3-47). It was less active than the wild type with bromoacetate (Figure 3-49) and screened separately from the other mutants, so a comparison between them

cannot be accurately made. R119S essentially lacked activity with both 2-bromobutyrate and chloroacetate (Figures 3-50 and 3-53). Interestingly, this mutant was the least active in promoting *trans*-cinnamate conjugation at the 5 min time point, but rose to most active at the 15 min time point (Figure 3-54). R119S had negligible activity with ethyl bromoacetate (Figure 3-55), but was more active with iodoacetamide than wild type GstB (Figure 3-57). Like the other mutants, R119S was less active with iodoacetate than the wild type (Figure 3-59).

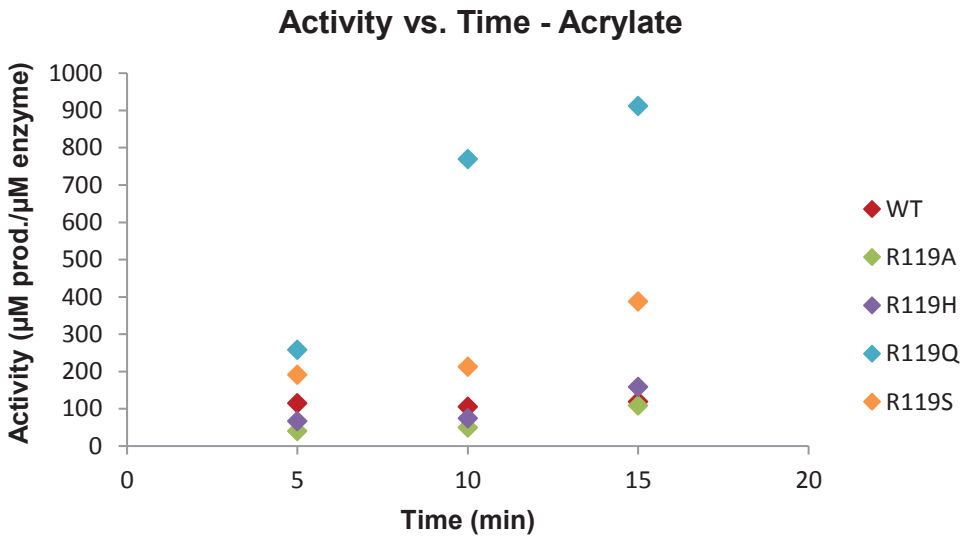

Figure 3-47: A plot of GSH-acrylate conjugation, expressed in µM product formed per µM enzyme, versus time for WT (red), R119A (green), R119H (purple), R119Q (blue), and R119QS (orange). [GSH]: 3.6 mM; [acrylate]: 18 mM.

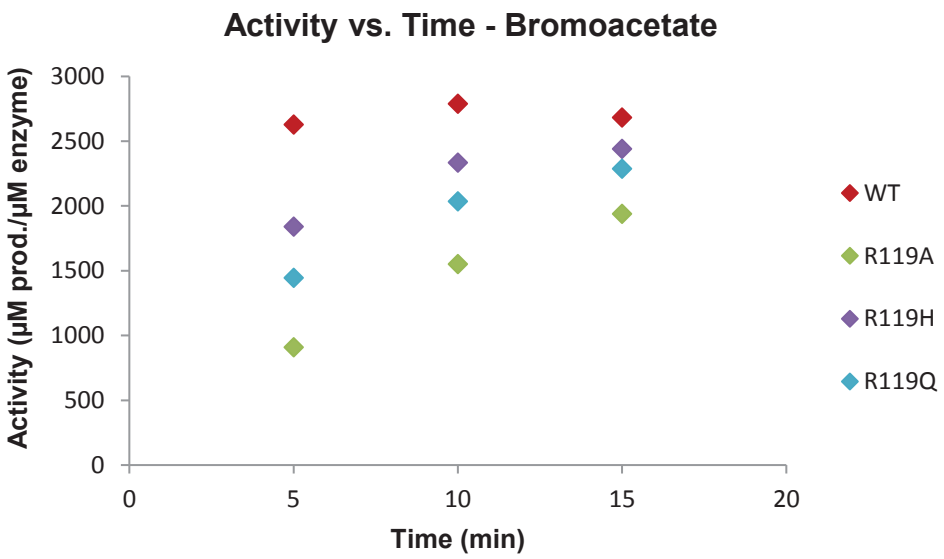

Figure 3-48: A plot of GSH-bromoacetate conjugation, expressed in µM product formed per µM enzyme, versus time for WT (red), R119A (green), R119H (purple), and R119Q (blue). [GSH]: 3.5 mM; [bromoacetate]: 16 mM.

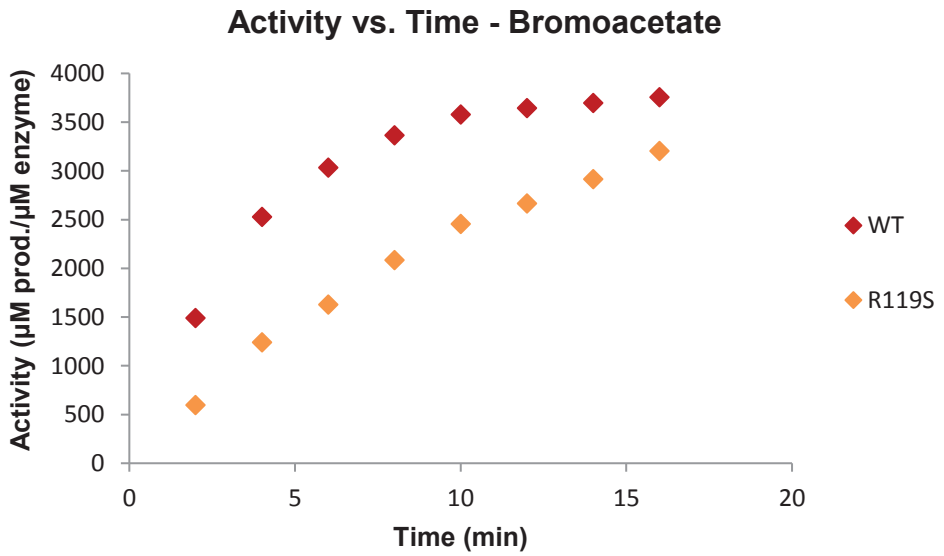

Figure 3-49: A plot of GSH-bromoacetate conjugation, expressed in µM product formed per µM enzyme, versus time for WT (red) and R119S (orange). [GSH]: 3.4 mM; [bromoacetate]: 21 mM.

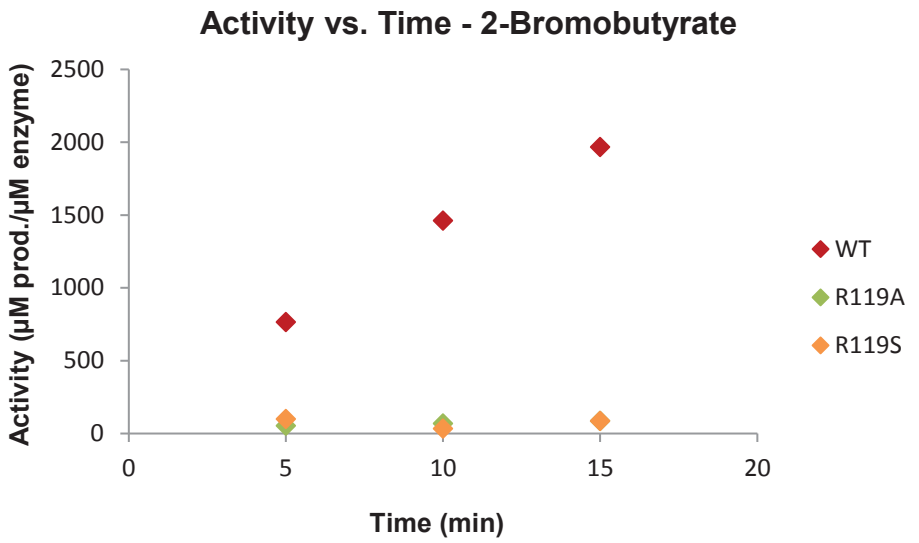

Figure 3-50: A plot of GSH-2-bromobutyrate conjugation, expressed in µM product formed per µM enzyme, versus time for WT (red), R119A (green), and R119S (orange). [GSH]: 3.6 mM; [2-bromobutyrate]: 18 mM.

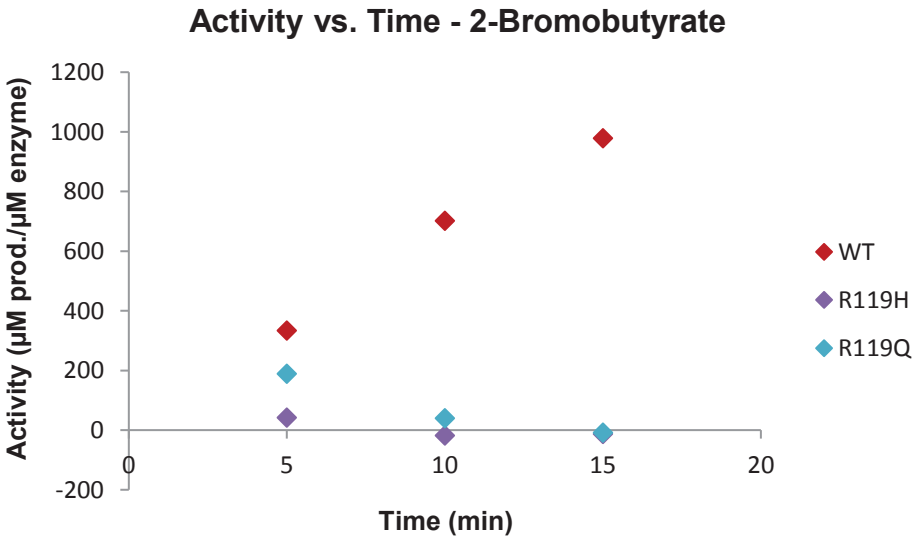

Figure 3-51: A plot of GSH-2-bromobutyrate conjugation, expressed in µM product formed per µM enzyme, versus time for WT (red), R119H (purple), and R119Q (blue). [GSH]: 3.5 mM; [2-bromobutyrate]: 18 mM.

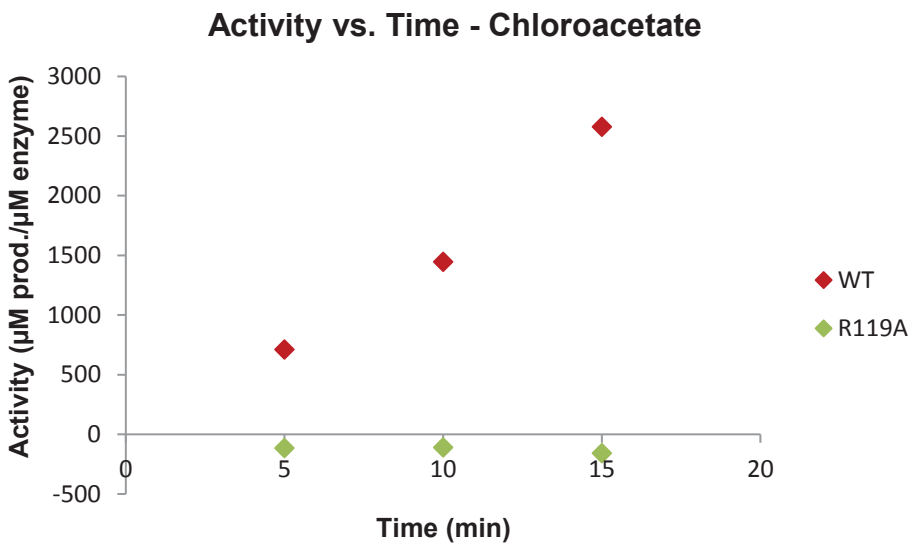

Figure 3-52: A plot of GSH-chloroacetate conjugation, expressed in µM product formed per µM enzyme, versus time for WT (red) and R119A (green). [GSH]: 3.7 mM; [chloroacetate]: 23 mM.

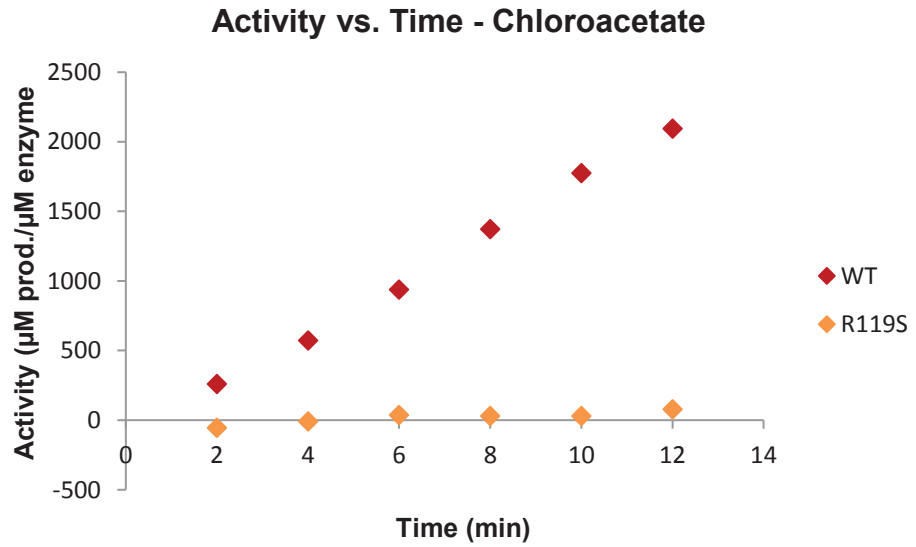

Figure 3-53: A plot of GSH-chloroacetate conjugation, expressed in µM product formed per µM enzyme, versus time for WT (red) and R119S (orange). [GSH]: 3.5 mM; [chloroacetate]: 22 mM.

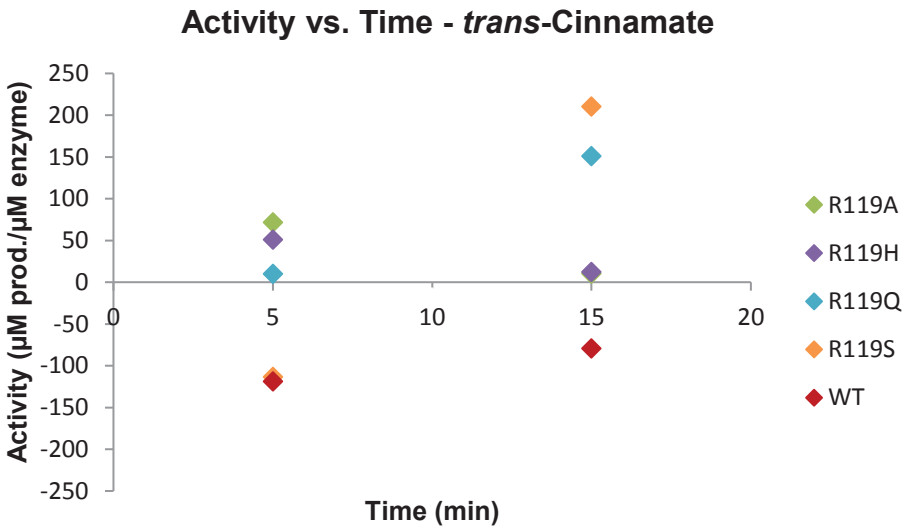

Figure 3-54: A plot of GSH-*trans*-cinnamate conjugation, expressed in µM product formed per µM enzyme, versus time for WT (red), R119A (green), R119H (purple), R119 (blue), and R119QS (orange). [GSH]: 3.6 mM; [*trans*-cinnamate]: 18 mM.

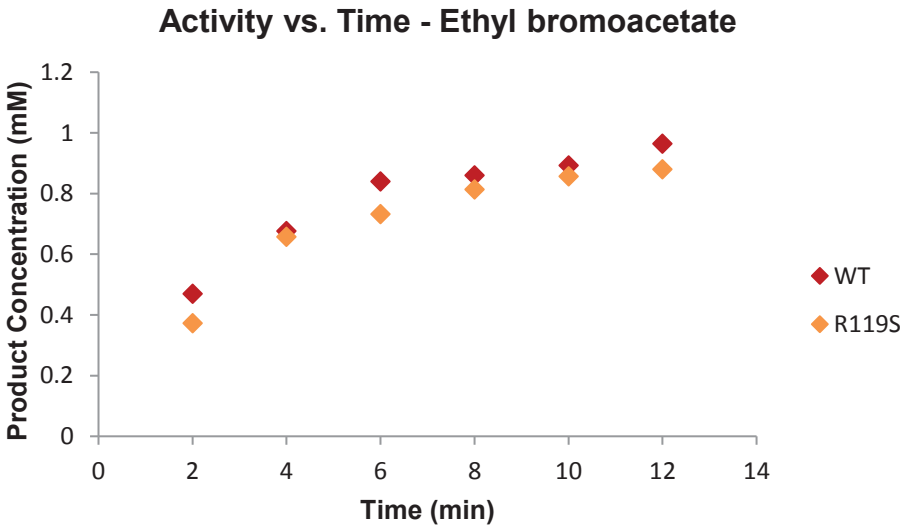

Figure 3-55: A plot of GSH-ethyl bromoacetate conjugation, expressed in mM GS-ethylacetate conjugate, versus time for WT (red), and R119S (orange). [GSH]: 3.5 mM; [ethyl bromoacetate]: 1.8 mM.

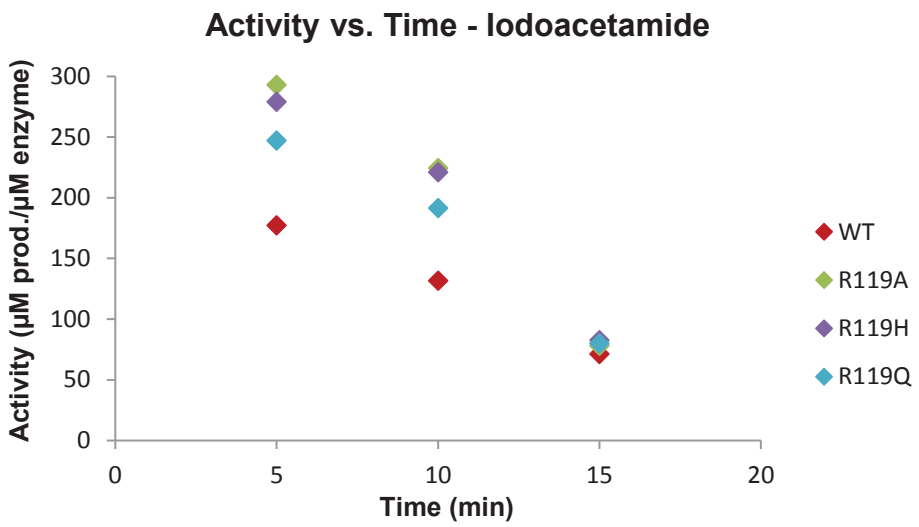

Figure 3-56: A plot of GSH-iodoacetamide conjugation, expressed in µM product formed per µM enzyme, versus time for WT (red), R119A (green), R119H (purple), and R119Q (blue). [GSH]: 3.4 mM; [iodoacetamide]: 18 mM.

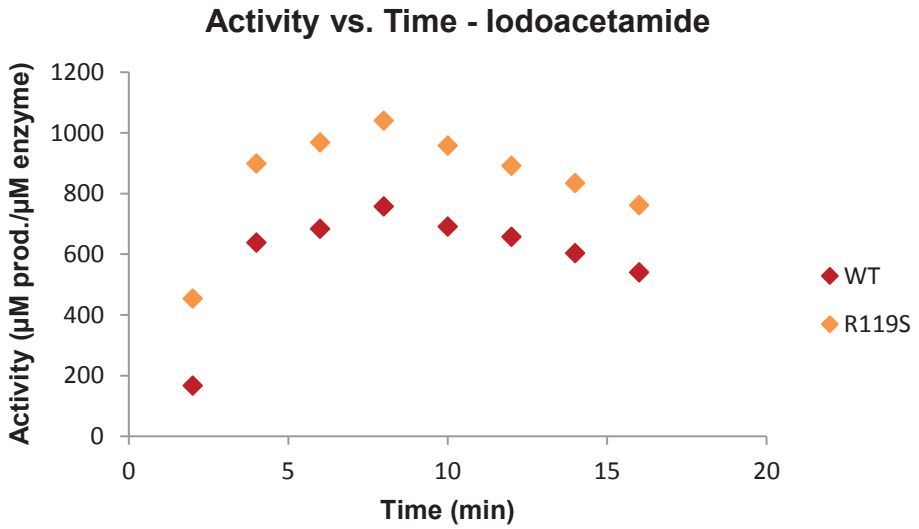

Figure 3-57: A plot of GSH-iodoacetamide conjugation, expressed in µM product formed per µM enzyme, versus time for WT (red), and R119S (orange). [GSH]: 3.5 mM; [iodoacetamide]: 18 mM.

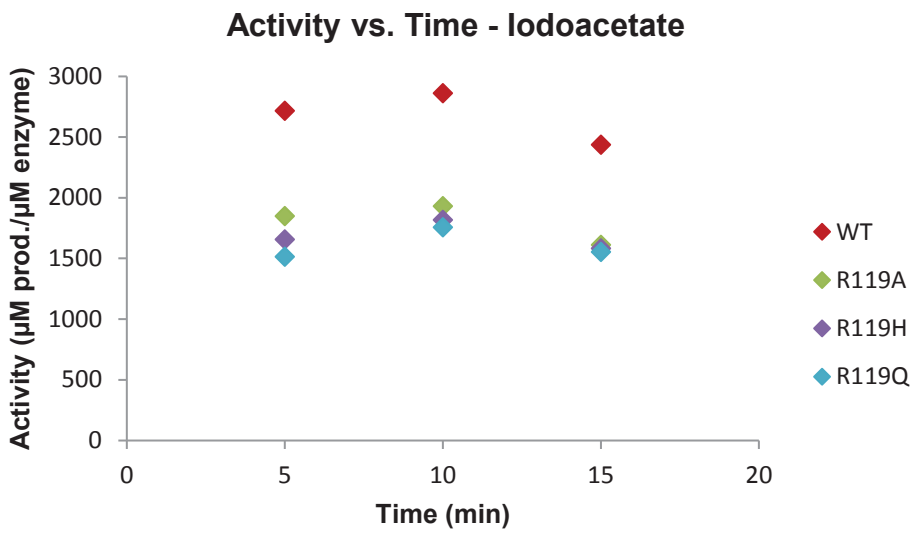

Figure 3-58: A plot of GSH-iodoacetate conjugation, expressed in µM product formed per µM enzyme, versus time for WT (red), R119A (green), R119H (purple), and R119Q (blue). [GSH]: 3.5 mM; [iodoacetate]: 18 mM.

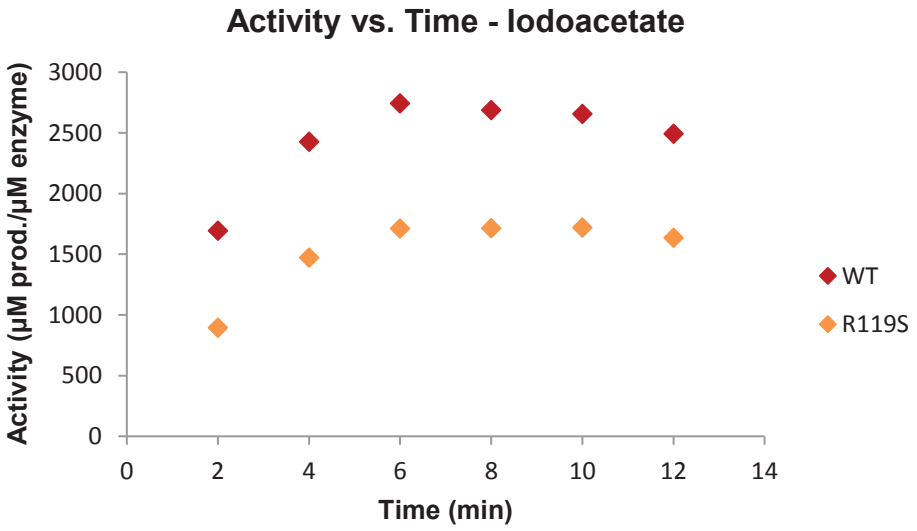

Figure 3-59: A plot of GSH-iodoacetate conjugation, expressed in µM product formed per µM enzyme, versus time for WT (red) and R119S (orange). [GSH]: 3.5 mM; [iodoacetate]: 18 mM.

Comparison of Mutant GstB Enzymatic Activities to Wild Type Activity

Following initial activity screening, it was evident that all four mutants displayed activity with acrylate, bromoacetate, iodoacetate, and iodoacetamide. Figure 3-60 exhibits that, with respect to acrylate conjugation, the R119A and R119H mutants did not provide additional rate enhancement compared to the wild type, operating at 48% and 71% of the wild type activity, respectively. However, the R119Q and R119S mutants displayed 220% and 203% of the wild type activity. None of the mutants outperformed wild type GstB with respect to bromoacetate conjugation. Figure 3-61 indicates that R119A suffered the greatest activity loss at 56% wild type activity, followed by R119Q (73%), R119S (78%), and R119H (84%). Similarly, Figure 3-62 reveals that the mutants did not afford rate enhancement for iodoacetate conjugation, with activites ranging from 61% to 67% of the wild type. Most notably, Figure 3-63 highlights that all four mutants provided rate enhancement for iodoacetamide conjugation, ranging from 146% to 171% wild type activity.

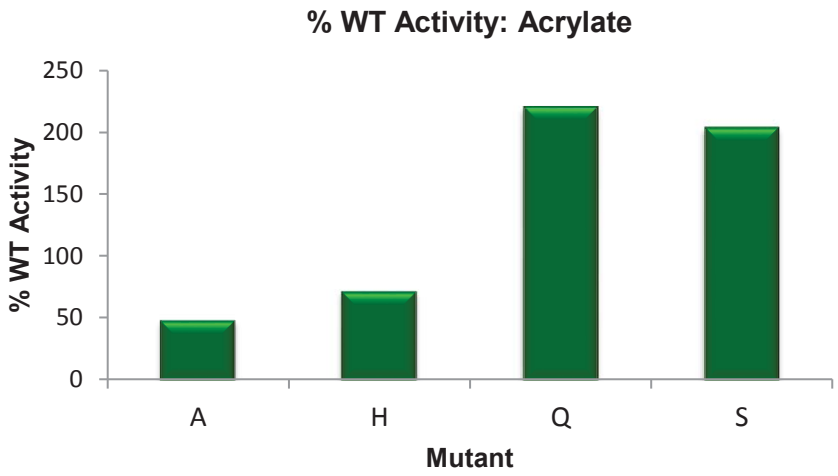

Figure 3-60: The percentage of wild type activity exhibited by each mutant with acrylate after a 10 minute reaction.

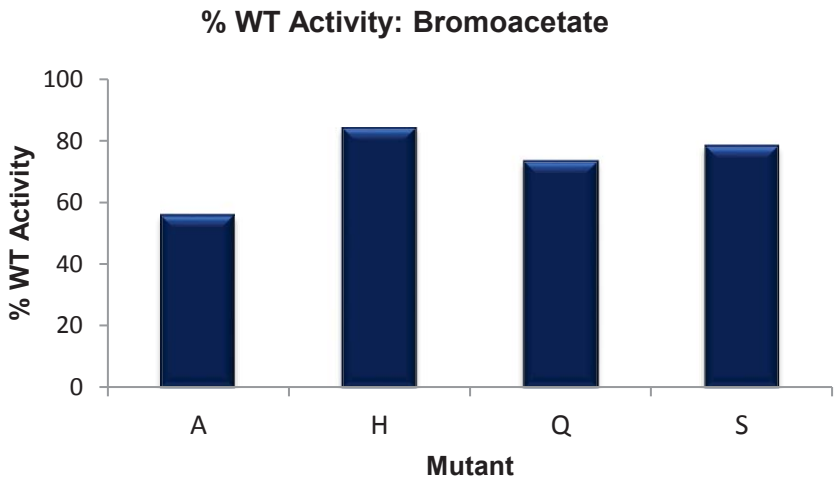

Figure 3-61: The percentage of wild type activity exhibited by each mutant with bromoacetate after a 10 minute reaction.

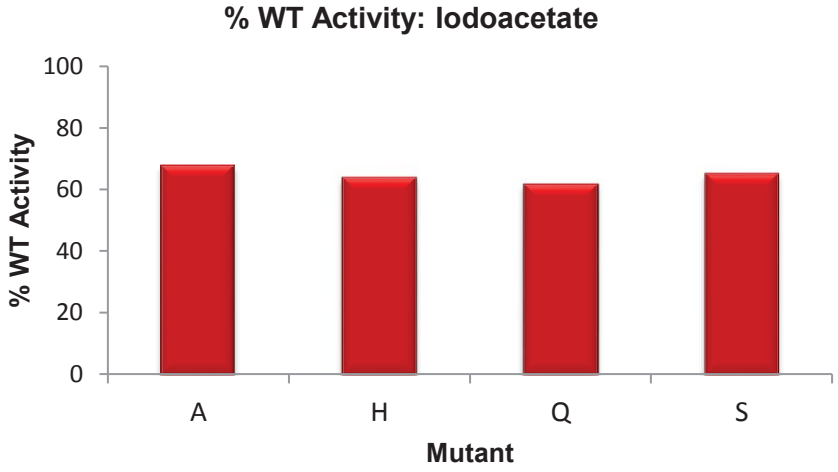

Figure 3-62: The percentage of wild type activity exhibited by each mutant with iodoacetate after a 10 minute reaction.

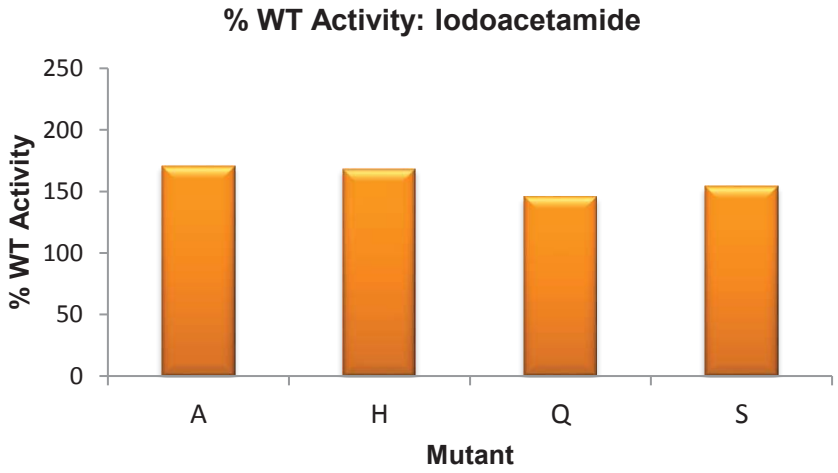

Figure 3-63: The percentage of wild type activity exhibited by each mutant with iodoacetamide after a 10 minute reaction.

Mutant GstB Michaelis-Menten Kinetics

As the initial screening results indicated that all four mutants exhibited greater activity for GSH-iodoacetamide conjugation than wild type GstB, kinetic studies were conducted for this reaction. Michaelis-Menten kinetic parameters are specific for an enzyme-substrate pair. GstB has two substrates; therefore, the kinetic parameters for each mutant were obtained with respect to both iodoacetamide and GSH using the same DTNB assay and data analysis protocols that were described previously.

Varying Iodoacetamide Concentration

Figures 3-64 through 3-67 show the experimental and model Michaelis-Menten curves for the GSH-iodoacetamide conjugation reaction in which the concentration of iodoacetamide is varied. Table 3-13 displays that the R119H mutant had an affinity for iodoacetamide comparable to that of the wild type, while the other mutants demonstrated lower affinities. This is supported by the K_M values: 18.2 mM for the wild type, 18.4 mM

for R119H, 28.1 mM for R119A, 34.9 mM for R119Q, and 38.0 mM for R119S. All four mutants experienced substrate inhibition at higher concentrations of iodoacetamide, as shown in Figures 3-64 through 3-67. The R119Q and R119S mutants were more resistant to this type of inhibition than the wild type, with K_I values of 36.5 and 35.5 mM, respectively, while the wild type K_I value was 34.5 mM. The R119A and R119H mutants were more sensitive to iodoacetamide inhibition, with K_I values of 31.5 and 24.5 mM, respectively.

Turnover number was highest for R119Q at 15.2 s^{-1}, about 3-fold higher than the wild type value of 4.21 s^{-1}. Both R119S and R119H had higher turnover numbers than the wild type enzyme (5.27 and 4.72 s^{-1}, respectively). R119A was the only mutant with a turnover number lower than the wild type (3.85 s^{-1}).

The catalytic efficiency of R119Q (0.436 $mM^{-1}s^{-1}$) was double that of the wild type (0.229 $mM^{-1}s^{-1}$). The catalytic efficiencies of R119A and R119S were about half of that of the wild type (0.137 and 0.139 $mM^{-1}s^{-1}$). The catalytic efficiency of R119H (0.259 $mM^{-1}s^{-1}$) was almost equal to that of the wild type.

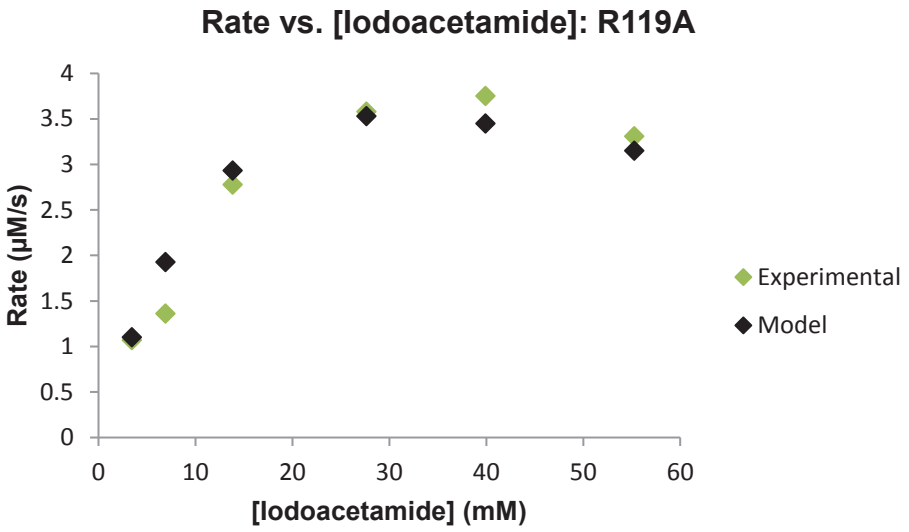

Figure 3-64: A plot of the rate of R119A-catalyzed iodoacetamide-GSH conjugation versus iodoacetamide concentration with experimental rate (green) and model rate with inhibition (black). [GSH]: 3.5 mM; [R119A]: 2.6 μM; reaction time: 3 min; R^2: 0.990.

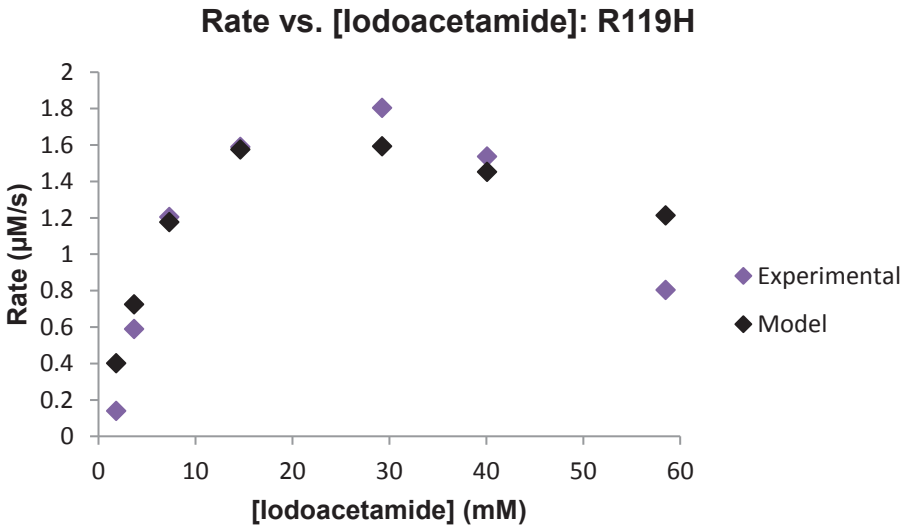

Figure 3-65: A plot of the rate of R119H-catalyzed iodoacetamide-GSH conjugation versus iodoacetamide concentration with experimental rate (purple) and model rate with inhibition (black). [GSH]: 3.6 mM; [R119H]: 0.97 μM; reaction time: 3 min; R^2: 0.972.

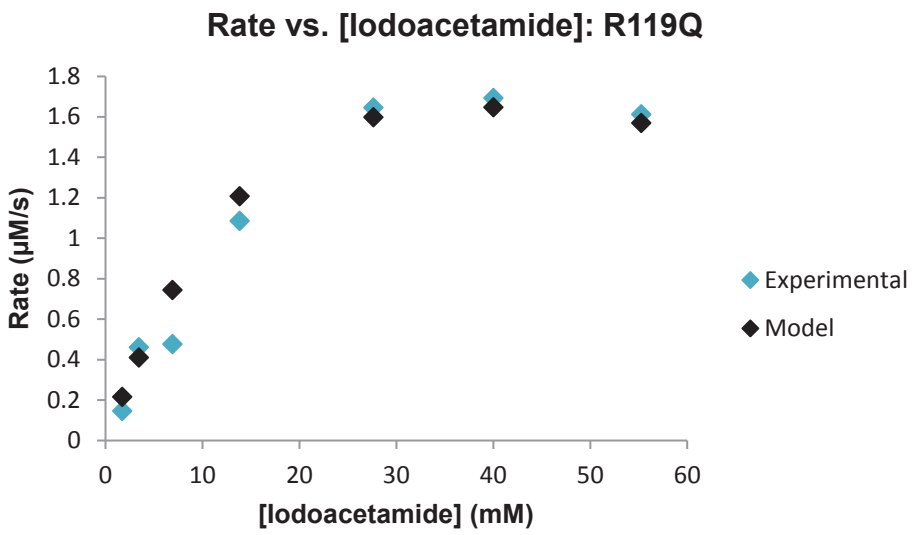

Figure 3-66: A plot of the rate of R119Q-catalyzed iodoacetamide-GSH conjugation versus iodoacetamide concentration with experimental rate (blue) and model rate with inhibition (black). [GSH]: 3.6 mM; [R119Q]: 0.30 μM; reaction time: 3 min; R^2: 0.990.

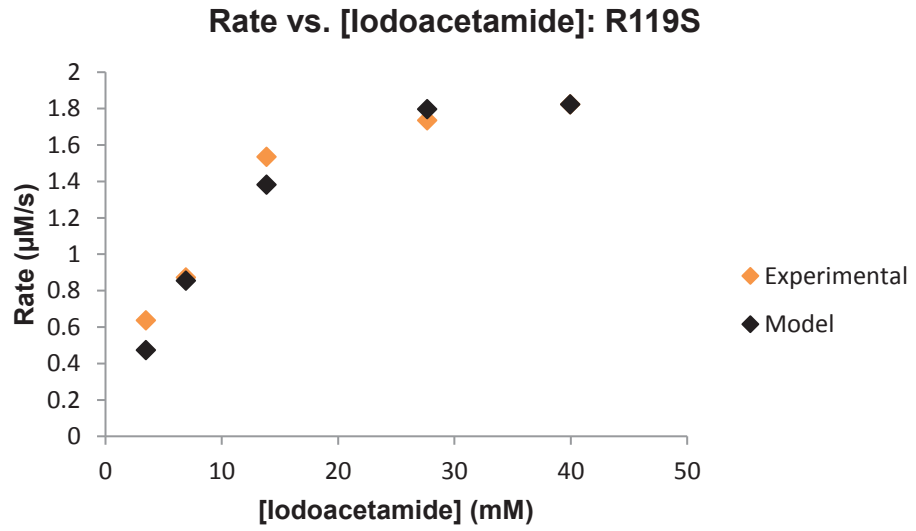

Figure 3-67: A plot of the rate of R119S-catalyzed iodoacetamide-GSH conjugation versus iodoacetamide concentration with experimental rate (orange) and model rate with inhibition (black). [GSH]: 3.6 mM; [R119S]: 1.1 μM; reaction time: 3 min; R^2: 0.994.

Table 3-13: Wild type and mutant GstB kinetic parameters for the iodoacetamide-GSH conjugation reaction with respect to iodoacetamide.

Enzyme	$K_M^{El.}$ (mM)	$K_I^{El.}$ (mM)	$k_{cat}^{El.}$ (s^{-1})	$k_{cat}^{El.}/ K_M^{El.}$ ($mM^{-1}s^{-1}$)
WT GstB	18.4	34.5	4.21	0.229
R119A	28.1	31.5	3.85	0.137
R119H	18.2	24.5	4.72	0.259
R119Q	34.9	36.5	15.2	0.436
R119S	38.0	35.5	5.27	0.139

Varying GSH Concentration

Figures 3-68 through 3-71 include the experimental and model Michaelis-Menten curves for the GSH-iodoacetamide conjugation reaction in which the concentration of GSH was varied. Table 3-14 displays that R119Q, R119S, and R119A had higher affinities for GSH, with K_M values of 2.25, 3.60, and 4.60 mM, respectively, compared to 4.85 mM for the wild type. R119H had the poorest affinity for GSH with a K_M of 10.3 mM.

Wild type GstB experienced inhibition by GSH at high concentrations, with a K_I of 30.5 mM. R119Q and R119A were more susceptible to inhibition than the wild type, with K_I values of 19.5 and 25.3 mM, respectively. Interestingly, R119H and R119S were not inhibited by GSH to any extent over the range of GSH concentrations tested.

Only R119H had a higher turnover number than wild type GstB: 6.46 s^{-1} versus 4.75 s^{-1}. The other mutants suffered a decrease in turnover number, with that of R119S as low as 2.43 s^{-1}. R119Q had a catalytic efficiency of 1.17 $mM^{-1}s^{-1}$, exceeding the 0.979 $mM^{-1}s^{-1}$ value for the wild type enzyme. The catalytic efficiency of R119A was nearly identical to the wild type at 0.933 $mM^{-1}s^{-1}$. The R119H and R119S mutants demonstrated a 30% decrease in catalytic efficiency compared to wild type GstB, with values of 0.627 and 0.675 $mM^{-1}s^{-1}$, respectively.

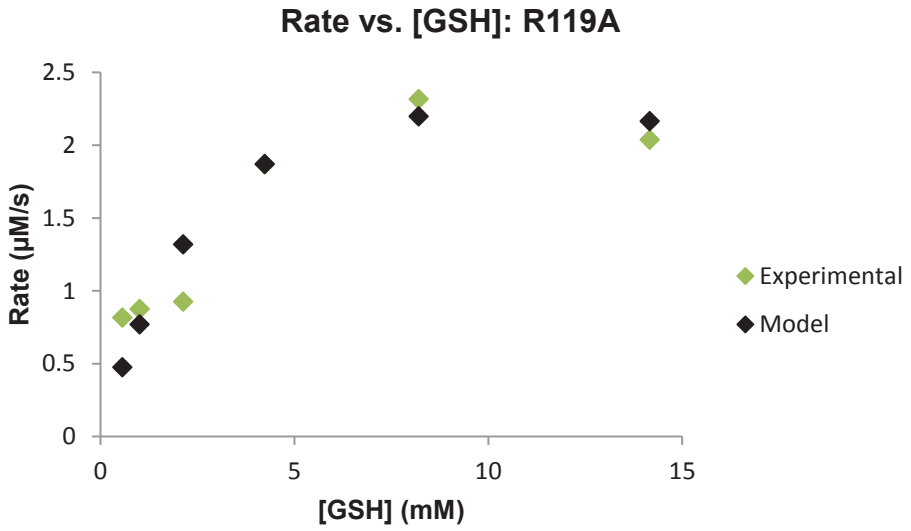

Figure 3-68: A plot of the rate of R119A-catalyzed iodoacetamide-GSH conjugation versus GSH concentration with experimental rate (green) and model rate with inhibition (black). [Iodoacetamide]: 18 mM; [R119A]: 1.1 μM; reaction time: 3 min; R^2: 0.980.

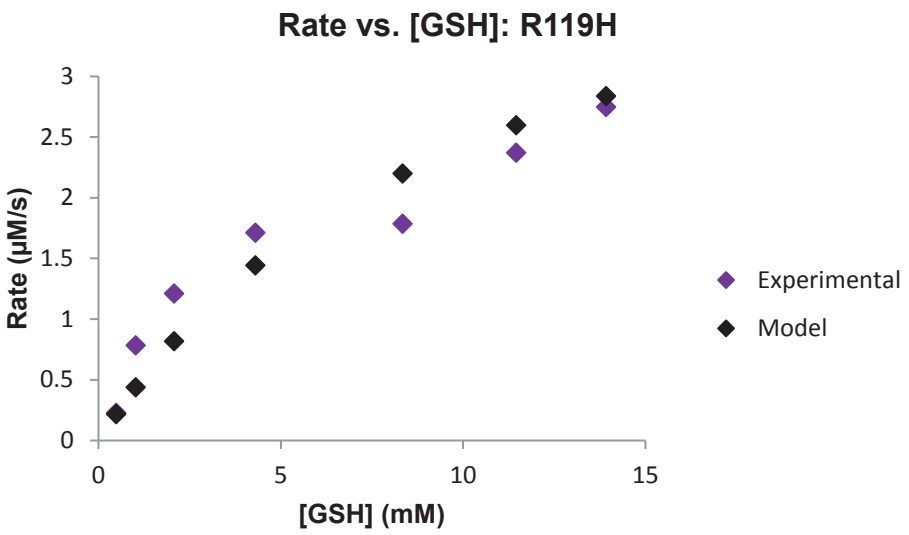

Figure 3-69: A plot of the rate of R119H-catalyzed iodoacetamide-GSH conjugation versus GSH concentration with experimental rate (purple) and model rate without inhibition (black). [Iodoacetamide]: 18 mM; [R119H]: 0.93 μM; reaction time: 3 min; R^2: 0.975.

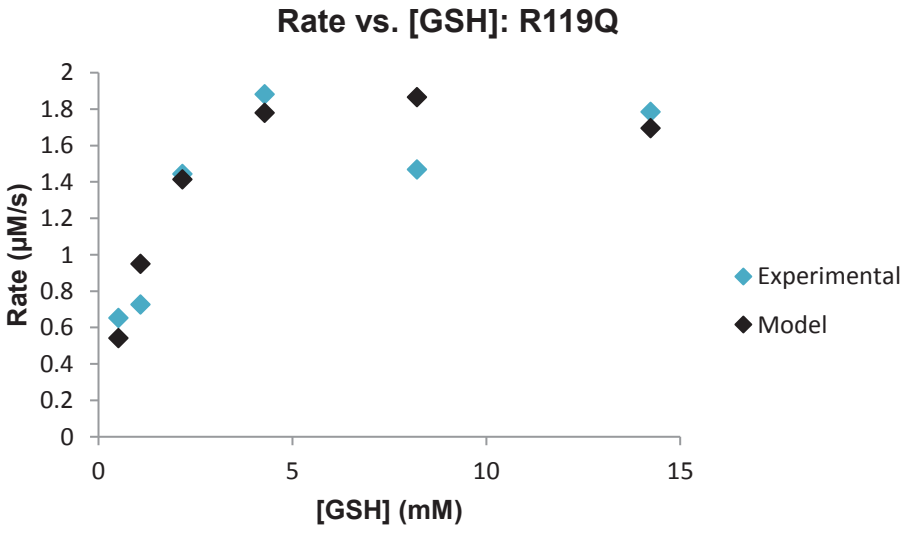

Figure 3-70: A plot of the rate of R119Q-catalyzed iodoacetamide-GSH conjugation versus GSH concentration with experimental rate (blue) and model rate with inhibition (black). [Iodoacetamide]: 18 mM; [R119Q]: 1.0 μM; reaction time: 3 min; R^2: 0.982.

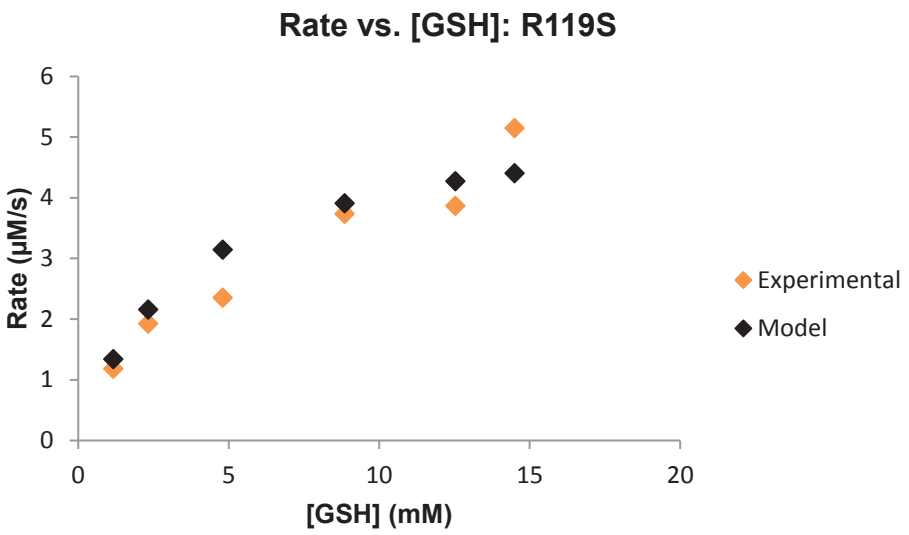

Figure 3-71: A plot of the rate of R119S-catalyzed iodoacetamide-GSH conjugation versus GSH concentration with experimental rate (orange) and model rate without inhibition (black). [Iodoacetamide]: 18 mM; [R119S]: 2.3 μM; reaction time: 3 min; R^2: 0.980.

Table 3-14: Wild type and mutant GstB kinetic parameters for the iodoacetamide-GSH conjugation reaction with respect to GSH.

Enzyme	K_M^{GSH} (mM)	K_I^{GSH} (mM)	k_{cat}^{GSH} (s^{-1})	k_{cat}^{GSH}/K_M^{GSH} ($mM^{-1}s^{-1}$)
WT GstB	4.85	30.5	4.75	0.979
R119A	4.60	25.3	4.29	0.933
R119H	10.3	---	6.46	0.627
R119Q	2.25	19.5	2.64	1.17
R119S	3.60	---	2.43	0.675

Wild Type GstB and R119H Mode of Inhibition Study

A study was performed to assess the mode of inhibition of iodoacetamide, specifically, whether this compound was alkylating vital amino acid residues, inactivating the enzyme, or occupying space in the active site. After incubation with a low concentration of iodoacetamide for varying amounts of time, an aliquot of enzyme solution was added to a bromoacetate reaction mixture, and the GSH-bromoacetate conjugation rate was determined. Figures 3-72 and 3-73 indicate that prolonged exposure of the WT and R119H enzymes to iodoacetamide had no effect on activity.

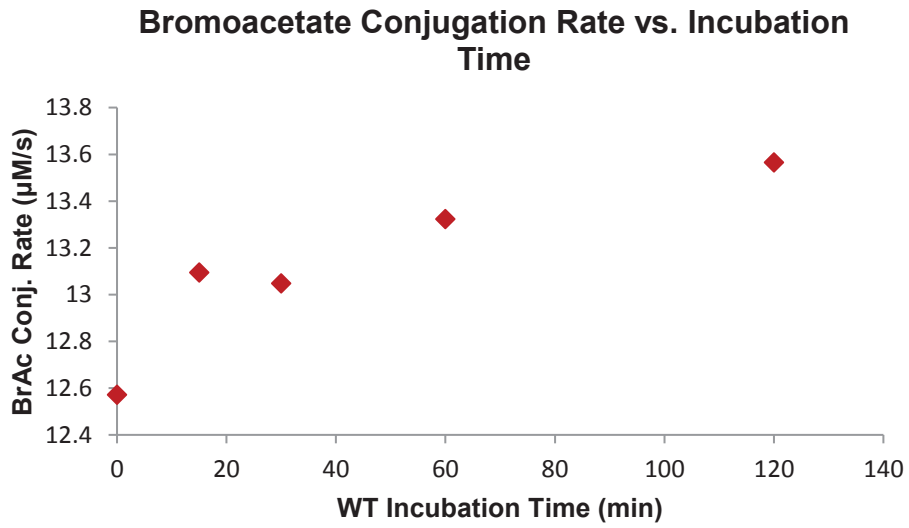

Figure 3-72: A plot of the rate of bromoacetate-GSH conjugation versus incubation time of WT enzyme and 5 mM iodoacetamide. [GSH]: 3.5 mM; [WT]: 0.68 µM; [bromoacetate]: 11 mM; reaction time: 3 min.

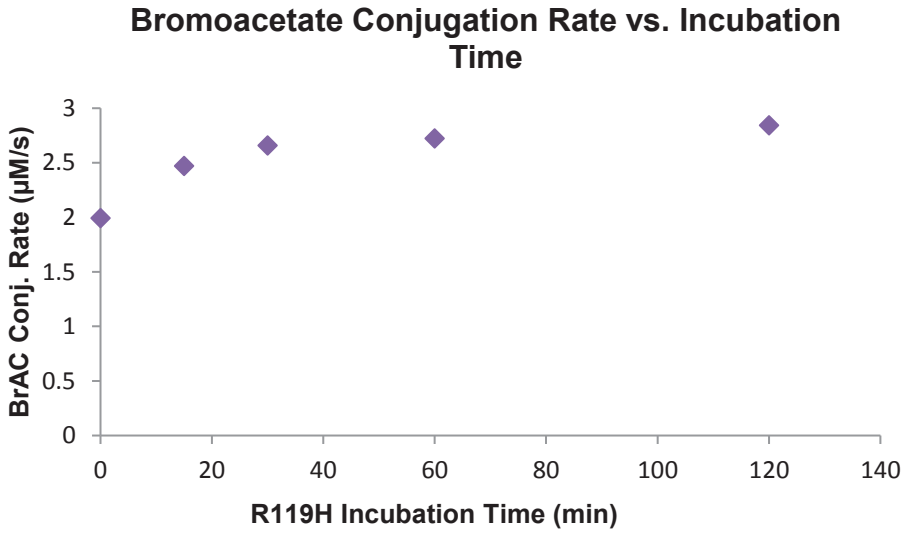

Figure 3-73: A plot of the rate of bromoacetate-GSH conjugation versus incubation time of R119H enzyme and 5 mM iodoacetamide. [GSH]: 3.6 mM; [R119H]: 0.93 µM; [bromoacetate]: 11 mM; reaction time: 3 min.

PART VII. DISK DIFFUSION SENSITIVITY TESTING OF GSTB MUTANTS

Disk diffusion sensitivity tests were conducted with *E. coli* BL21 strains that overexpressed each of the GstB mutants to investigate whether the mutations affected the *in vivo* response of GstB to the electrophiles. A BL21 strain that overexpressed GstB was used as a control. Figure 3-74 and Table 3-15 show that the strains overexpressing the R119A and R119H mutants were significantly more sensitive to iodoacetamide than the other strains; however, these two mutants were significantly more resistant to iodoacetate than the other strains. All four mutants were less sensitive to bromoacetate than the wild type control. Ethyl bromoacetate, 2-bromobutyrate, and chloroacetate did not affect the growth of any of the strains.

Figure 3-75 and Table 3-16 indicate that the same results were obtained for iodoacetamide at a concentration of 150 mM. When the concentration of iodoacetate was

reduced to 100 mM, all four mutants appeared to be more resistant to the compound than the wild type.

As shown in Figure 3-76 and Table 3-17, *E. coli* cells that overexpressed t he R119A and R119H mutants appeared to be resistant to both 1 and 2 M bromoacetate. The R119S mutant was more resistant to both concentrations of bromoacetate than the wild type. While not apparent with 1 M bromoacetate, the R119Q mutant was most sensitive to 2 M bromoacetate.

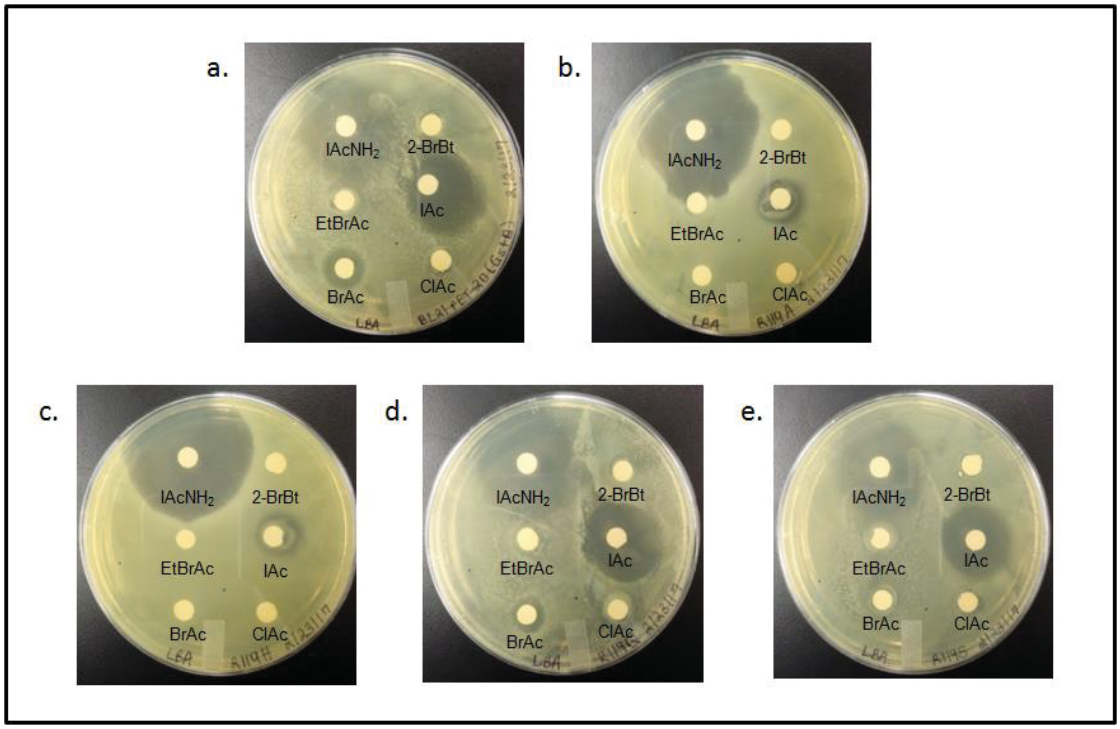

Figure 3-74: Disk diffusion sensitivity screening of *E. coli* BL21 pET-20 **a.** WT; **b.** R119A; **c.** R119H; **d.** R119Q; **e.** R119S with 150 mM iodoacetamide, 100 mM ethyl bromoacetate, 470 mM bromoacetate, 500 mM 2-bromobutyrate, 580 mM iodoacetate, and 500 mM chloroacetate.

Table 3-15: Mutant bacterial growth clearance diameters for disk diffusion sensitivity test.

Electrophile	BL21 pET-20 (*gstB*) (mm)	BL21 pET-20 (*R119A*) (mm)	BL21 pET-20 (*R119H*) (mm)	BL21 pET-20 (*R119Q*) (mm)	BL21 pET-20 (*R11S*) (mm)
300 mM $IAcNH_2$	31.5	39.0	39.0	32.0	31.0
100 mM EtBrAc	None	None	None	11.0	None
470 mM BrAc	13.5	None	None	11.5	None
500 mM 2-BrBt	None	None	None	None	None
500 mM ClAc	None	None	None	None	10.0

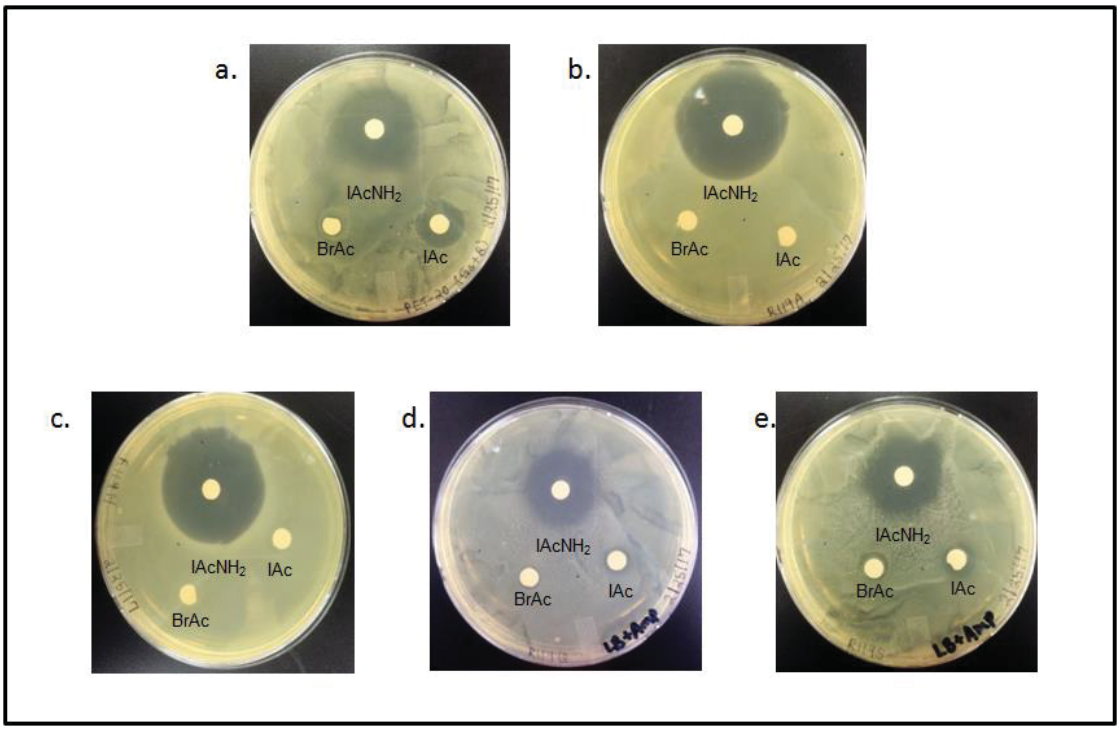

Figure 3-75: Disk diffusion sensitivity screening of *E. coli* BL21 pET-20 **a.** WT; **b.** R119A; **c.** R119H; **d.** R119Q; **e.** R119S with 150 mM iodoacetamide, 230 mM bromoacetate, and 100 mM iodoacetate.

Table 3-16: Mutant bacterial growth clearance diameters for disk diffusion sensitivity test.

Electrophile	BL21 pET-20 (*gstB*) (mm)	BL21 pET-20 (*R119A*) (mm)	BL21 pET-20 (*R119H*) (mm)	BL21 pET-20 (*R119Q*) (mm)	BL21 pET-20 (*R11S*) (mm)
150 mM $IAcNH_2$	27.0	35.0	35.0	25.6	27.5
230 mM BrAc	10.0	None	9.5	8.0	10.0
100 mM IAc	17.5	None	11.0	10.0	11.0

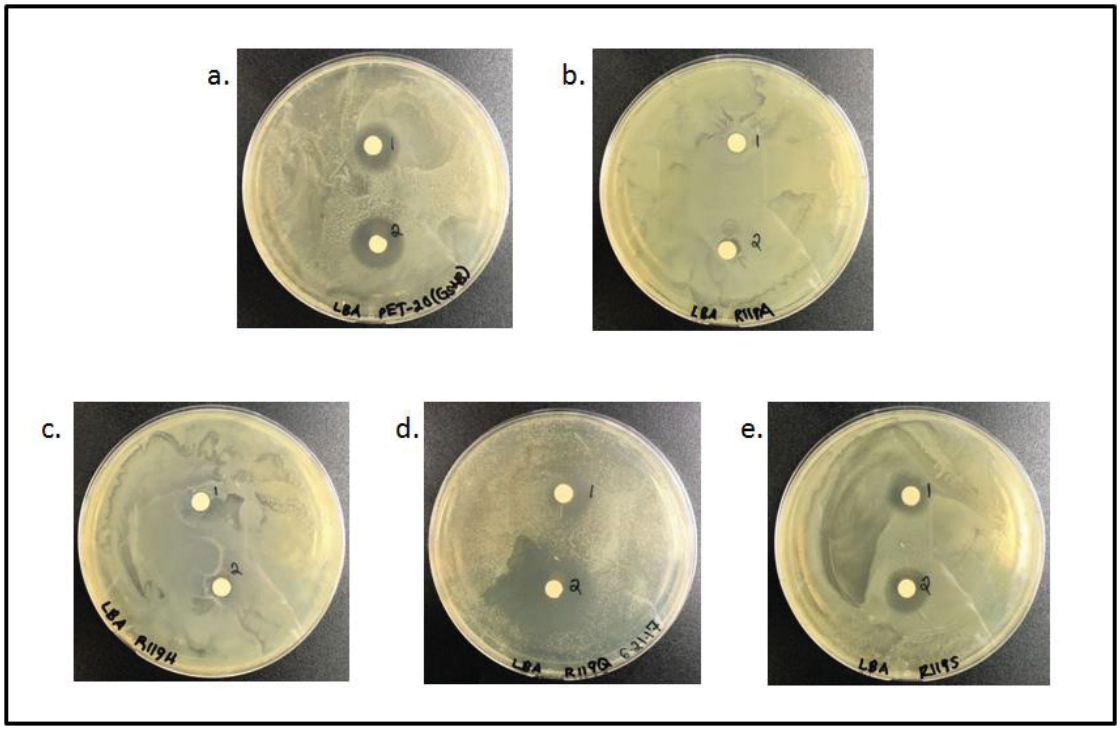

Figure 3-76: Disk diffusion sensitivity screening of *E. coli* BL21 pET-20 **a.** WT; **b.** R119A; **c.** R119H; **d.** R119Q; **e.** R119S with 1 M bromoacetate and 2 M bromoacetate.

Table 3-17: Mutant bacterial growth clearance diameters for disk diffusion sensitivity test.

Electrophile	BL21 pET-20 (*gstB*) (mm)	BL21 pET-20 (*R119A*) (mm)	BL21 pET-20 (*R119H*) (mm)	BL21 pET-20 (*R119Q*) (mm)	BL21 pET-20 (*R11S*) (mm)
1 M BrAc	15.0	None	7.0	13.0	13.5
2 M BrAc	18.5	None	9.0	24.0	15.0

CHAPTER 4. DISCUSSION

OPTIMIZATION OF PROTEIN PURIFICATION PROCEDURES

A previously established procedure for the purification of GstB was optimized to enhance the efficiency of protein precipitation. During this optimization, it was apparent that the bacterial cell sonication step did not adequately release the cellular contents. Therefore, the number of sonication cycles was increased from eight to twelve. Of the three different ammonium sulfate precipitation methods evaluated, the single addition of the salt to 75% saturation proved to be the most efficient. Initial precipitation with 45% ammonium sulfate produced a pellet containing few impurity proteins and a small amount of GstB (Figure 3-1, Lane 6). The separate 25% and 60% precipitation steps were not beneficial, as the 25% and 60% pellets were nearly identical in protein composition (Figure 3-2, Lanes 7 and 9). When one portion of ammonium sulfate was added to 75% saturation, the impurity proteins in the 75% pellet were essentially identical to those found in the 25%, 45%, and 60% pellets. The newly optimized protocol consisted of twelve cycles of sonication and one addition of ammonium sulfate to 75% saturation.

Anion exchange column chromatography further purified the 75% ammonium sulfate pellet. As GstB has a theoretical isoelectric point of 5.05, a pH of 7.4 was consistently maintained for the duration of this purification step. Negatively charged GstB was electrostatically bound to the quaternary amine-substituted matrix and eluted with a 0-400 mM sodium chloride gradient. Figures 3-4 and 3-5 show that many of the eluted fractions contained large amounts of GstB with minimal impurities. Following concentration, SDS-PAGE analysis of a protein sample diluted 100-fold confirmed that sufficiently pure GstB had been obtained (Figure 3-6). All four mutant enzymes were

purified using this same protocol, with the addition of a hydroxylapatite column chromatography purification step for the R119H and R119Q mutants.

WILD TYPE GSTB KINETICS

Desai and Miller reported that GstB possessed activity with bromoacetate and iodoacetate[54]. In this work, several halogenated carboxylate compounds were evaluated to determine if the substrate scope could be broadened. GstB was found to have activity with bromoacetate, 2-bromobutyrate, chloroacetate, and iodoacetate. Table 3-1 indicates that the Michaelis constants of the haloacetates are inversely proportional to the size of the halogen. The catalytic efficiencies increased with increasing leaving group ability. Interestingly, GstB was inhibited at high concentrations of bromoacetate, while similar concentrations of chloroacetate and iodoacetate failed to produce this effect. Whether GstB experiences product inhibition by the GSH-electrophile adduct remains unknown. Product inhibition would likely occur when turnover number is high because a sufficient concentration of product must be available to inhibit the enzyme. Turnover number was highest for bromoacetate conjugation and dropped by ten units for both chloroacetate and iodoacetate. These differences in turnover number could explain whether or not inhibition was observed.

The trends in kinetic parameters with respect to GSH differed from those observed with respect to the electrophiles. Table 3-2 highlights that the Michaelis constant decreased as the halide leaving group ability worsened, with chloride > bromide > iodide for the haloacetates. However, turnover number and catalytic efficiency both increased as leaving group ability increased. While GstB was active with

2-bromobutyrate, catalytic efficiency suffered. This can be attributed to the bromide leaving group's location on a sterically hindered secondary carbon, while all other carboxylates tested were primary halides. Alternatively, 2-bromobutyrate is a chiral molecule, but a racemic mixture of enantiomers was used for this activity assay. Catalytic efficiency may have fallen because GstB is stereospecific, binding only one enantiomer of 2-bromobutyrate in its H-site. Desai and Miller determined that GstB had no activity with bromoacetamide. Iodoacetamide was tested here, and GstB was capable of promoting its conjugation with GSH. While the catalytic efficiency with respect to iodoacetamide was only 0.23 $mM^{-1}s^{-1}$, our data indicate that GstB is not solely limited to carboxylate substrates.

As certain GSTs are known to catalyze Michael additions, the Michael acceptors acrylate and *trans*-cinnamate were tested. It was postulated that GstB may be active with these compounds because they contain carboxylate moieties. GstB possessed a minimal degree of activity with acrylate, but lacked activity with *trans*-cinnamate. Acrylate's small size probably facilitated its acceptance as a substrate, while *trans*-cinnamate was likely too large to be accommodated in the GstB H-site. These findings suggest that GstB can catalyze reactions that proceed via different reaction mechanisms: bimolecular nucleophilic substitution (S_N2) and conjugate addition.

GstB was unable to catalyze the conjugation of GSH and CDNB. Beta class GSTs are characterized by their ability to promote this reaction. It is likely that the relatively conserved beta class H-site amino acid residues are not present in GstB, preventing it from accepting CDNB as a substrate. Therefore, it can be concluded that GstB is not a member of the beta class.

Despite containing the carboxylate functionality, dichloroacetate was not a substrate for GstB. GstB was inactive with the antibiotics fosfomycin and chloramphenicol. The GST FosA is capable of promoting glutathione-mediated epoxide opening, conferring bacterial resistance to the broad-spectrum antibiotic fosfomycin. GstB was incapable of catalyzing the epoxide-opening reaction of this molecule. Though halogenated, the antibiotic chloramphenicol does not contain the carboxylate functionality and may be too large to be accommodated in the GstB H-site. After rigorous screening of substrates representative of GST-promoted reactions, Desai and Miller's hypothesis that the likely physiological substrate for GstB is a small carboxylated molecule was upheld. GstB's activity with iodoacetamide demonstrated for the first time that an amide could be accepted as an electrophilic substrate.

WILD TYPE GSTB DISK DIFFUSION SENSITIVITY SCREENING – ELECTROPHILES

Disk diffusion sensitivity studies were performed in an effort to support GstB kinetic data with the *in vivo* effects of the electrophilic compounds. Two strains of *E. coli* were exposed to the compounds: *E. coli* K-12, the wild type strain, and *E. coli* BW25113Δ*gstB*, a knockout strain lacking the gene encoding GstB. Figure 3-21 and Table 3-3 reveal that the knockout strain was actually more resistant to iodoacetamide than the wild type strain. This appears contradictory as GstB displayed GSH-iodoacetamide conjugation activity. The observed *in vivo* effects may be due to differences in the amount of cells that were distributed on the plates or genetic variations between the two cell types.

Additional tests confirmed that GstB may be implicated in the metabolism of bromoacetate and iodoacetate, as the knockout strain was more sensitive to these compounds than the K-12 strain (Figure 3-22 and Table 3-4). Though GstB displayed activity with 2-bromobutyrate and chloroacetate *in vitro*, the knockout strain did not exhibit increased sensitivity to these two compounds. It is possible that the *E. coli* BW25113Δ*gstB* cells can tolerate these compounds at the concentrations tested, and higher concentrations may need to be assessed in the future. Ethyl bromoacetate, *trans*-cinnamate, and acrylate did not produce differences in sensitivity between the two strains. This is aligned with the fact that these compounds were not GstB substrates *in vitro*.

WILD TYPE GSTB DISK DIFFUSION SENSITIVITY SCREENING – METALS

Glutathione is known to bind and interact with metals, aiding in their intracellular transport and reduction.[13,15] The ability to bind metals has also been demonstrated by certain glutathione transferases isolated from *Ascidia sydneiensis samea* and *Schistoma japonicum*.[63,64] The *E. coli* K-12 wild type and BW25113Δ*gstB* knockout strains were exposed to a variety of toxic metal salts in order to examine the potential role of GstB in metal binding. Additionally, *E. coli* BL21 pET-20(*gstB*) cells that overexpressed GstB and *E. coli* BL21 pET-20 cells that contained only the empty vector were subjected to the same metal species. Of all of the metals tested, only As^{3+}, As^{5+}, Cr^{6+}, and Hg^{2+} produced measurable differences between the cell lines.

Initially, As^{3+} produced differences in sensitivity between the wild type and knockout strains, with the knockout strain being more sensitive to the metal species (Figure 3-23, Table 3-5). When experiments were repeated with varying concentrations

of As^{3+}, there were again differences in sensitivity, with larger clearance zones measured for the knockout strain (Figure 3-24, Table 3-6). Figure 3-28 and Table 3-9 show that the *E. coli* BL21 cells with the empty vector were more sensitive to As^{3+} than BL21 cells that overexpressed GstB. From these results, it is possible that GstB binds As^{3+}, but further studies are required to determine the specific mechanism of this binding. GstB could simply bind As^{3+}, sequestering the toxic species, or it may be involved in the metal's cellular efflux.

E. coli possesses the gene *arsC* encoding an arsenate reductase that reduces pentavalent arsenic to trivalent arsenic, the species that is effluxed from the cell by transport proteins. It was recently discovered that GstB is capable of catalyzing this reduction in the absence of *arsC*, as cells overexpressing GstB were found to be resistant to 5 mM sodium arsenate.[54] *E. coli* BL21 cells containing the empty pET-20 vector were more sensitive to As^{5+} than cells that overexpressed GstB at all concentrations tested. Experiments with the K-12 and *gstB* knockout strains yielded different results. The K-12 strain was actually more sensitive than the knockout strain.

Figure 3-23 displays that the K-12 strain was slightly more sensitive to Cr^{6+} than the knockout strain, but there were no apparent differences between strain sensitivities when additional concentrations of the metal species were tested (Figure 3-24). Experiments with BL21 cells revealed that cells that overexpressed GstB were more sensitive than those that did not (Figure 3-26). It is known that Cr^{3+} is more genotoxic than Cr^{6+}, forming DNA-protein cross-links and that GSH non-enzymatically reduces Cr^{6+} in cultured cells.[65] Also, glutathione reductases are known to reduce Cr^{6+}.[13,16] Since GstB has been found to possess arsenate reductase activity, it is possible that GstB uses

GSH to reduce Cr^{6+} to Cr^{3+}, explaining the increased sensitivity of the K-12 and BL21 pET-20(*gstB*) cell lines. Further study is required to determine the interaction between GstB and chromate.

There was virtually no difference between the sensitivities of the K-12 and knockout cells to Hg^{2+}. However, the BL21 cells containing the empty pET-20 vector were slightly more sensitive to Hg^{2+} at all concentrations tested (Figure 3-28 and Table 3-9). As the results of these two experiments did not agree with one another, an interaction between GstB and Hg^{2+} cannot be conclusively determined.

GSTB SITE-DIRECTED MUTAGENESIS

Chrysostomou and colleagues suspected that the GstB arginine residues at positions 111 and 119 were involved in binding a negatively charged electrophile, such as arsenate.[54] This hypothesis was based on a crystal structure of a GstB homologue isolated from *Salmonella enterica* with 83% sequence identity. The authors indicated that a GstB R111Q/R119Q double mutant failed to demonstrate resistance to arsenate and was unable to catalyze the conjugation reaction between GSH and bromoacetate. Additionally, they reported that a GstB R119Q single mutant was more sensitive to arsenate than an R111Q single mutant. We concluded that R119 was more essential for electrophile binding than R111 due to this difference in sensitivity between the two single mutants. The authors did not indicate whether the R111Q and R119Q single mutants experienced altered activity with bromoacetate. Therefore, we created four GstB mutants with single amino acid substitutions at position 119 and examined their substrate specificities. Site-directed mutagenesis was used to generate GstB enzyme variants in which alanine, histidine,

glutamine, and serine were substituted for arginine at position 119. All four mutants were successfully overexpressed in *E. coli* and demonstrated general stability, as they were active with certain electrophilic substrates. This success indicated that Arg119 is neither essential for the proper folding of GstB into a functional conformation nor for catalysis.

ACTIVITY SCREENING OF GSTB MUTANTS

All four mutants were active with bromoacetate and iodoacetate. However, the mutants' activity levels were lower than that of the wild type enzyme. This reduction in activity can be supported by the fact that the mutant position 119 amino acid residues lack a positive charge at pH 7, the operating activity assay pH. GstB may bind the negatively charged carboxylate substrate via electrostatic interactions with its positively charged guanidino group. Abolishing this positive charge may weaken enzyme-substrate binding interactions. The mutants had no activity with 2-bromobutyrate and chloroacetate, carboxylates with which wild type GstB had some activity. This lack of activity can also be attributed to the perturbed H-site electrostatics.

Homology modeling was performed using Phyre^2 in order to visualize the mutations in the GstB active site. The folding of mutant sequences was modeled using a template structure (PDB 4KH7) from *Salmonella enterica.*[66] Phyre^2 cannot predict any conformational changes in whole protein structure that may result from point mutations because the amino acid residues are incorporated onto a rigid template backbone during modeling. However, the lowest energy rotamer of each amino acid side chain is used in the model, which could provide insight into the potential conformation of position 119 residues. The structure of wild type YliJ from *Salmonella enterica* with bound GSH is

shown in Figure 4-1, in which R119 is situated within the enzyme's active site pocket. X-ray crystal structures of the mutants are required before the impact of the mutations on the enzymatic activities can be understood with any certainty. However, the varying steric and electronic characteristics of the mutant side chains allow for some speculation.

After initial activity screening, all four mutants appeared to be more active with iodoacetamide than wild type GstB. R119A exhibited the largest increase in activity, and this may be due to its small size. The alanine substitution likely provided more room in the H-site to accommodate the substrate, and this extra space was beneficial as iodine is the largest of the halides tested. Histidine, glutamine, and serine could have potentially served as better hydrogen bond acceptors or donors, enhancing their ability to interact with iodoacetamide. Alternatively, these substitutions could have altered the size of the H-site or the projection of other H-site residues, allowing for more facile substrate access. The R119H mutant displayed the highest affinity for iodoacetamide. The planar geometry of histidine's aromatic side chain may provide iodoacetamide with a better fit in the H-site. Alternatively, polar-π interactions between iodoacetamide and the imidazole side chain could afford improved substrate binding. The R119A, R119Q, and R119S mutants had higher affinities for GSH, and this could have resulted from a favorable conformational change in the enzyme's G-site. While wild type GstB was inhibited by high concentrations of GSH, the R119H and R119S mutants were not.

From the Phyre^2 predictions, it is possible that the R119H mutant displayed the greatest affinity for iodoacetamide because H119 was predicted to project into the solvent, as shown in Figure 4-2. This could potentially aid in recruiting iodoacetamide to the active site. Figure 4-3 displays that the R119Q mutant's glutamine residue was also

predicted to project into the solvent. This could provide a rationale for the fact that the catalytic efficiency of the R119Q mutant was the greatest. Alternatively, A119 and S119 were both predicted to project into the hydrophobic core of the protein, and this may explain the decreased catalytic efficiencies of these mutants (Figures 4-4 and 4-5).

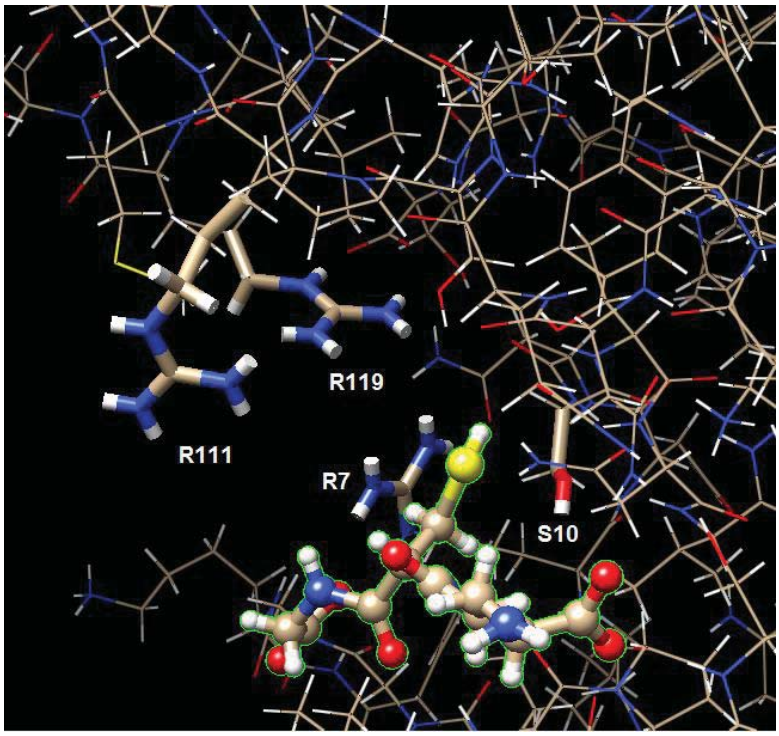

Figure 4-1: X-ray crystal structure of the active site of YliJ from *Salmonella enterica* (PDB: 4kh7) visualized in Chimera. S10 is indicated for reference.

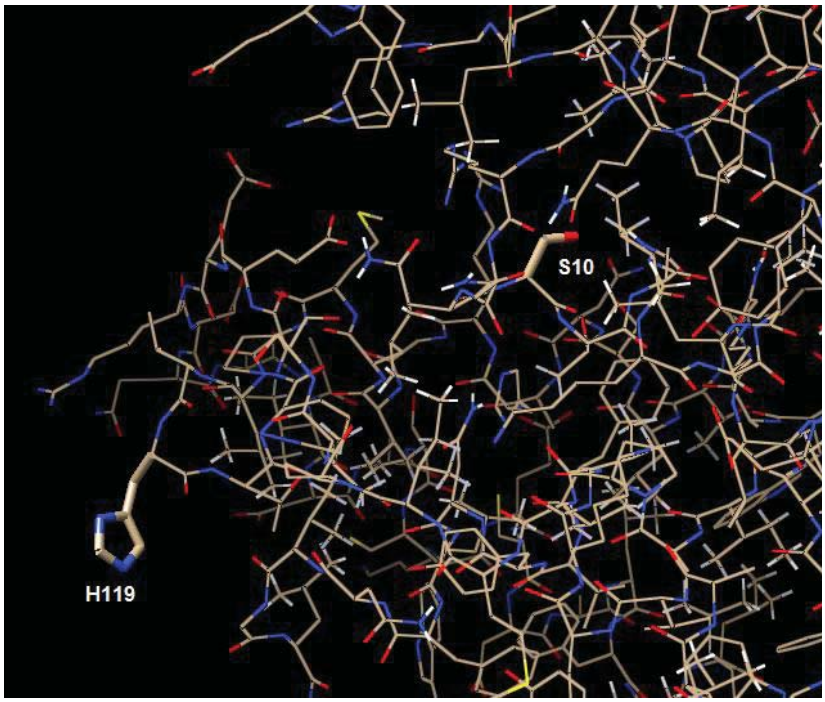

Figure 4-2: Phyre[2]-predicted structure of R119H GstB. S10 is indicated for reference.

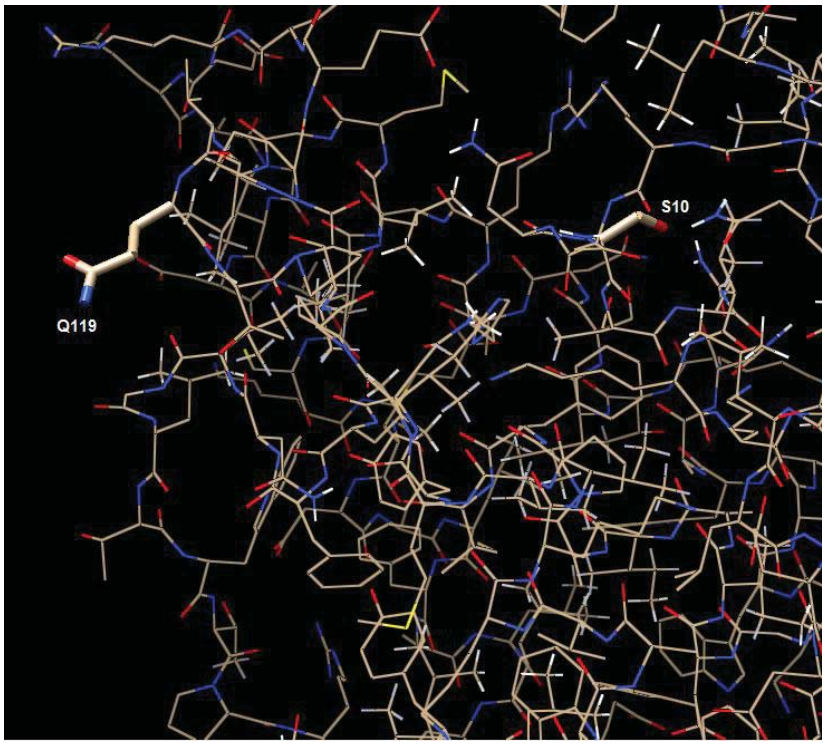

Figure 4-3: Phyre[2]-predicted structure of R119Q GstB. S10 is indicated for reference.

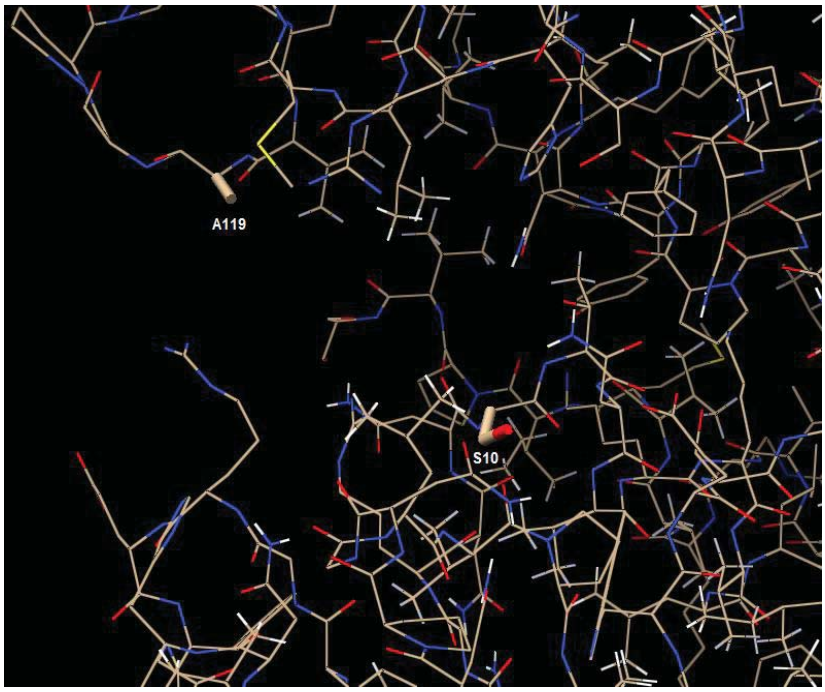

Figure 4-4: Phyre[2]-predicted structure of R119A GstB. S10 is indicated for reference.

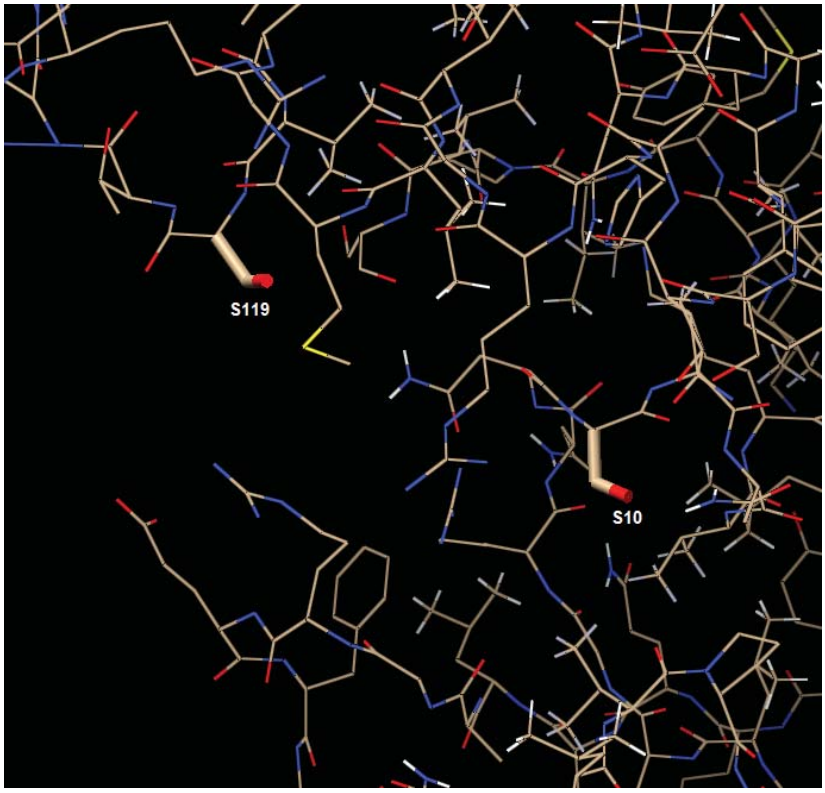

Figure 4-5: Phyre[2]-predicted structure of R119S GstB. S10 is indicated for reference.

DISK DIFFUSION SENSITIVITY TESTING OF GSTB MUTANTS

The mutant diffusion disk experiment trends corroborated certain kinetic results. The R119Q mutant was the mutant most resistant to iodoacetamide, while exhibiting the highest catalytic efficiency with respect to both the GSH and iodoacetamide substrates. R119A and R119H were the most sensitive to iodoacetamide at all concentrations tested. These two mutants were most easily inhibited by iodoacetamide in kinetic experiments. The two mutants had the lowest iodoacetamide inhibition constants out of all of the enzyme variants (R119A K_I: 31.5 mM; R119H K_I: 24.5 mM). It follows that the inhibition of an enzyme responsible for detoxifying a compound would render the cells more sensitive to that compound.

Close examination of Figure 3-75 reveals that the cell density of the BL21 strains overexpressing R119A and R119H is significantly greater than that of the other strains. For this reason, these two strains appeared to be more resistant to iodoacetate than the other strains, when in reality they are likely just as sensitive to the compound. Moreover, the rate data in Figure 3-62 do not uphold this apparent increased resistance, as R119A and R119H are no more active with iodoacetate than the other mutants.

The R119Q mutant was the most sensitive to 2 M bromoacetate. Of the four mutants, R119Q displayed the second lowest activity with the compound *in vitro*. Interestingly, the R119A mutant, which was the least active with bromoacetate *in vitro,* appeared resistant to high concentrations of bromoacetate *in vivo.* The R119H mutant demonstrated consistent results, with the highest activity and a very low degree of sensitivity to bromoacetate.

FUTURE WORK

Future work will involve further characterization of the four GstB mutants. An attempt will be made to crystallize GstB and the mutant enzymes in order to elucidate their structures via X-ray diffraction analysis. This will provide a more complete structural understanding of how the individual mutations impact enzyme function. Additionally, temperature and pH stability profiles will be generated for each mutant. Experiments with R119H will be carried out at a pH that would render this side chain positively charged. All experiments have been performed at pH 7.0, in which histidine's imidazole side chain is deprotonated. The substrate specificity of protonated R119H may differ. Mutant kinetic parameters for the GSH-acrylate conjugation reaction will be acquired with respect to each substrate. Wild type GstB and the mutants will be assayed for peroxide reductase activity. Finally, whether the mutations affect the ability of GstB to interact with metals will be investigated.

CHAPTER 5. CONCLUSION

This work has served to expand the current functional understanding of GstB, a glutathione transferase from *E. coli.* Initially, the protocol for the purification of GstB was successfully optimized, including additional sonication cycles and only one ammonium sulfate precipitation step.

The wild type enzyme's electrophilic substrate scope has been broadened to include 2-bromobutyrate, chloroacetate, and iodoacetamide, in addition to the previously reported compounds bromoacetate and iodoacetate. The observed iodoacetamide activity is of principal importance, as previous work has exclusively identified halogenated carboxylates as active substrates. Kinetic parameters were obtained with respect to both the electrophile and GSH substrates for all five of these conjugation reactions. All substrates with which GstB was inactive *in vitro* failed to produce *in vivo* sensitivity differences between wild type and GstB knockout *E. coli* strains. The bromoacetate and iodoacetate kinetic activities were supported by these *in vivo* sensitivity experiments, but the iodoacetamide activity was not. GSH and certain GSTs are known to bind metals, and experiments supported that GstB may interact with As^{3+}, As^{5+}, Cr^{6+}, and Hg^{2+} species.

Glutathione transferase H-site residues are responsible for binding electrophilic substrates, thus conferring an enzyme's substrate specificity. Four GstB single mutants were generated by substituting the arginine residue at position 119 for alanine, histidine, glutamine, and serine in an effort to modify GstB's substrate specificity. All four mutants were successfully expressed and all demonstrated activity. The mutants exhibited decreased activity with bromoacetate and iodoacetate compared to the wild type, and were completely inactive with 2-bromobutyrate and chloroacetate. Initial activity

screening results indicated that the R119Q and R119S mutants exceeded wild type activity with acrylate. After kinetic studies, it was confirmed that the R119Q mutant outperformed the wild type with regard to iodoacetamide conjugation. The increased mutant activities with these two substrates illustrates that the substrate specificity of a glutathione transferase can indeed be altered by H-site residue substitution.

Mutant disk diffusion sensitivity studies with iodoacetamide loosely aligned with the observed kinetic parameters. The best agreement was that the R119Q mutant had the highest catalytic efficiencies and was most resistant to the compound compared to the other mutants. Further investigation will be required to understand the correlation between the *in vitro* enzymatic activity and the *in vivo* effects of the compounds.

CHAPTER 6. REFERENCES

1. Smirnova, G. V.; Oktyabrsky, Glutathione in Bacteria. *Biochem. (Mosc.)* **2005,** *70* (11)*,* 1199-1211.

2. Kolesnichenko, L. S.; Kulinsky, V. I. The Glutathione System. I. Synthesis, Transport, Glutathione Transferases, Glutathione Peroxidases. *Biochem. (Mosc.) Suppl. Ser. B Biomed. Chem.* **2009,** *3* (2), 129-144.

3. Armstrong, R. N.; Graminski, G. F.; Kubo, Y. Spectroscopic and Kinetic Evidence for the Thiolate Anion of Glutathione at the Active Site of Glutathione *S*-Transferase. *Biochemistry* **1989,** *28*, 3562-3568.

4. Dawson, R. M. C. *Data for Biochemical Research,* 3rd ed.; Oxford University Press: New York, NY, 1987; pp 16-17.

5. Masip, L.; Veeravalli, K.; Georgiou, G. The Many Faces of Glutathione in Bacteria. *Antioxid. Redox Signal*. **2006,** *8*, 753–762.

6. Foreman, H. J.; Rinna, A.; Zhang, H. Glutathione: Overview of its Protective Roles, Measurement, and Synthesis. *Mol. Aspects Med.* **2009,** *30* (1-2), 1-12.

7. Anderson, M. E.; Huang C-S. The Function of the Light Subunit of γ-Glutamylcysteine Synthetase (Rat Kidney). *FASEB J*. **1993,** *7A*, 1102.

8. Huang, C-S.; Chang, L-S.; Anderson, M. E.; Meister, A. Catalytic and Regulatory Properties of the Heavy Subunit of Rat Kidney Glutamylcysteine Synthetase. *J. Biol. Chem*. **1993,** *268,* 19675–19680.

9. Lu, S. C. Glutathione Synthesis. *Biochim. Biophys. Acta* **2013,** *1830* (5), 3143-3153.

10. Jakoby, W. B; Keen, J. H. Glutathione Transferases. Catalysis of Nucleophilic Reactions of Glutathione. *J. Biol. Chem.* **1978,** *253*, 5654-5657.

11. Allocati, N.; Federici, L.; Masulli, M.; Di Illio, C. Glutathione Transferases in Bacteria. *FEBS J.* **2009,** *276,* 58-75.

12. Arner, E. S. J.; Nordberg, J. Reactive Oxygen Species, Antioxidants, and the Mammalian Thioredoxin System. *Free Radic. Biol. Med.* **2001,** *31* (11), 1287-1312.

13. Lushchak, V. I. Glutathione Homeostasis and Functions: Potential Targets for Medical Interventions. *J. Amino Acids* **2012,** *2012,* 1-26.

14. Flanagan, J. U.; Hayes, J. D.; Jowsey, I. R. Glutathione Transferases. *Ann. Rev. Pharmacol. Toxicol.* **2005,** *45,* 51-88.

15. Ballatori, N.; Wang, W. Endogenous Glutathione Conjugates: Occurrence and Biological Functions. *Pharmacol. Rev.* **1998,** *50* (3), 335–355.

16. Cronin, M. T. D.; Morris, H.; Valko, M. Metals, Toxicity and Oxidative stress. *Curr. Med. Chem.* **2005,** *12* (10), 1161–1208.

17. Colombo, G.; Dalle-Donne, I.; Giustarini, D.; Milzani, A.; Rossi, R. Protein *S*-Glutathionylation: A Regulatory Device from Bacteria to humans. *Trends Biochem. Sci.* **2008,** *34* (2), 85-96.

18. Prinarakis, E.; Chantzoura, E.; Thanos, D.; Spyrou, G. *S*-Glutathionylation of IRF3 Regulates IRF3-CBP Interaction and Activation of the IFNβ Pathway. *EMBO J.* **2008,** 27, 865–875.

19. Berk, B. C.; Pan, S. Glutathionylation Regulates Tumor Necrosis Factor-β-induced Caspase-3 Cleavage and Apoptosis: Key Role for Glutaredoxin in the Death Pathway. *Circ. Res.* **2007,** *100*, 213–219.

20. Vlamis-Gardikas, A.; Potamitou, A.; Zarivach, R.; Hochman, A.; Holmgren, A. Characterization of *Escherichia coli* Null Mutants for Glutaredoxin 2. *J. Biol. Chem*. **2002,** *277,* 10861-10868.

21. Booth, J.; Boyland, E.; Sims, P. An Enzyme from Rat Liver Catalysing Conjugations with Glutathione. *Biochem. J.* **1961,** *79*, 516-524.

22. Combes, B.; Stakelum, G. S. A Liver Enzyme that Conjugates Sulfobromophthalein sodium with Glutathione. *J. Clin. Invest.* **1961,** *40* (6), 981-988.

23. Habig, W. H.; Pabst, M. J.; Jakoby, W. B. Glutathione *S*-Transferases: The First Enzymatic Step in Mercapturic Acid Formation. *J. Biol. Chem.* **1974,** *249,* 7130-7139.

24. Allocati, N.; Federici, L.; Masulli, M.; Di Illio, C. Distribution of Glutathione Transferases in Gram-positive Bacteria and Archea. *Biochimie,* **2012***, 94,* 588-596.

25. Mashiyama, S. T.; Malabanan, M. M.; Akiva, E.; Bhosle, R.; Branch, M. C.; Hillerich, B.; Jagessar, K.; Kim, J.; Patskovsky, Y.; Seidel, R. D.; Stead, M.; Toro, R.; Vetting, M. W.; Almo, S. C.; Armstrong, R. N.; Babbitt, P. C. Large-scale Determination of Sequence, Structure, and Function Relationships in Cytosolic Glutathione Transferases across the Biosphere. *PLoS Biol.* **2015,** *12*, 1-19.

26. Kanai, T.; Takahashi, K.; Inoue, H. Three Distinct-type Glutathione *S*-Transferases from *Escherichia coli* Important for Defense against Oxidative Stress. *J. Biochem*. **2006,** *140*, 703–711.

27. Stourman, N. V.; Branch, M. C.; Schaab, M. R.; Harp, J. M.; Ladner, J. E.; Armstrong, R. N. Structure and Function of YghU, a Nu-class Glutathione Transferase Related to YfcG from *Escherichia coli. Biochemistry* **2011,** *50,* 1274-1281.

28. Hayes, J. D.; Pulford, J. D. The Glutathione *S*-Transferase Supergene Family: Regulation of GST and the Contribution of the Isozymes to Cancer Chemoprotection and Drug Resistance. *Crit. Rev. Biochem. Mol. Biol.* **1995,** *30,* 445-600.

29. Dirr, H. W.; Reinemer, P.; Huber, R. X-ray Crystal Structures of Cytosolic Glutathione *S*-Transferases. Implications for Protein Architecture, Substrate Recognition and Catalytic Function. *Eur. J. Biochem.* **1994,** *220*, 645-661.

30. Armstrong, R. N. Structure, Catalytic Mechanism, and Evolution of the Glutathione Transferases. *Chem. Res. Toxicol.* **1997,** *10,* 2-18.

31. Board, P. G.; Baker, R. T.; Chelvanayagam, G.; Jermiin, L. S. Zeta, a Novel Class of Glutathione Transferases in a Range of Species from Plants to Humans. *Biochem. J.* **1997,** *328,* 929-935.

32. Allocati, N.; Cellini, L.; Aceto, A.; Iezzi, T.; Angelucci, S.; Robuffo, I.; Di Ilio, C. Immunogold Localization of Glutathione Transferase B1-1 in *Proteus mirabilis. FEBS Lett.* **1994,** *354*, 191-194.

33. Piccolomini, R.; Di Ilio, C.; Aceto, A.; Allocati, N.; Faraone, A.; Cellini, L.; Ravagnan, G.; Federici, G. Glutathione Transferases in Bacteria: Subunit Composition and Antigenic Character. *J. Gen. Microbiol*. **1989,** *135*, 3119-3125.

34. Perito, B.; Allocati, N.; Casalone, E.; Masulli, M.; Dragani, B.; Polsinelli, M.; Aceto, A.; Di Ilio, C. Molecular Cloning and Expression of a Glutathione Transferase Gene from *Proteus mirabilis*. *Biochem. J.* **1996,** *318,* 157–162.

35. Rossjohn, J.; Polekhina, G.; Feil, S. C.; Allocati, N.; Masulli, M.; Di Ilio, C.; Parker, M. W. A Mixed Disulfide Bond in Bacterial Glutathione Transferase: Functional and Evolutionary Implications. *Structure* **1998,** *15,* 721–734.

36. Allocati, N.; Favaloro, B.; Masulli, M.; Alexeyev, M. F.; Di Ilio, C. *Proteus mirabilis* Glutathione *S*-Transferase B1-1 is involved in the Protective Mechanisms against Oxidative and Chemical Stresses. *Biochem. J.* **2003,** *373*, 305–311.

37. Fortin, P. D.; Horsman, G. P.; Yang, H. M.; Eltis, L. D. A Glutathione *S*-Transferase Catalyzes the Dehalogenation of Inhibitory Metabolites of Polychlorinated Biphenyls. *J. Bacteriol*. **2006,** *188*, 4424–4430.

38. Van Hylckama, V. J. E.; Kingma, J.; van den Wijngaard, A. J.; Janssen, D. B. A Glutathione *S*-Transferase with Activity towards *cis*-1,2-Dichloroepoxyethane is involved in Isoprene Utilization by *Rhodococcus* sp. Strain AD45. *Appl. Environ. Microbiol*. **1989,** *64,* 2800–2805.

39. Van Hylckama, V. J. E.; Kingma, J.; van den Wijngaard, A. J.; Janssen, D. B. Purification of a Glutathione *S*-Transferase and a Glutathione Conjugate-specific Dehydrogenase involved in Isoprene Metabolism in *Rhodococcus* sp. Strain AD45. *J. Bacteriol.* **1999,** *181,* 2094–2101.

40. Anandarajah, K.; Kiefer, P. M. Jr.; Donohoe, B. S.; Copley, S. D. Recruitment of a Double Bond Isomerase to Serve as a Reductive Dehalogenase during Biodegradation of Pentachlorophenol. *Biochemistry* **2000,** *39,* 5303-5311.

41. Masai, E.; Katayama, Y.; Nishikawa, S.; Fukuda, M. Characterization of *Sphingomonas paucimobilis* SYK-6 Genes involved in Degradation of Lignin-related Compounds. *J. Industr. Microbiol. Biotechnol.* **1999,** *23*, 364–373.

42. Masai, E.; Ichimura, A.; Sato, Y.; Miyauchi, K.; Katayama, Y.; Fukuda, M. Roles of the Enantioselective Glutathione *S*-Transferases in Cleavage of β-Aryl Ether. *J. Bacteriol.* **2003,** *185* (6), 1768-1775.

43. Favaloro, B.; Tamburro, A.; Trofino, M. A.; Bologna, L.; Rotilio, D.; Heipieper, H. J. Modulation of the Glutathione *S*-Transferase in *Ochrobactrum anthropi*: Function of Xenobiotic Substrates and Other Forms of Stress. *Biochem. J.* **2000,** *346*, 553–559.

44. Arca, P.; Hardisson, C.; Suárez, J. E. Purification of a Glutathione *S*-Transferase that Mediates Fosfomycin Resistance in Bacteria. *Antimicrob. Agents Chemother.* **1990***, 34*, 844-848.

45. Armstrong, R. N.; Bernat, B. A.; Laughlin, L. T. Fosfomycin Resistance Protein (FosA) is a Manganese Metalloglutathione Transferase related to Glyoxalase I and the Extradiol Dioxygenases. *Biochemistry* **1997,** *36*, 3050–3055.

46. Sheehan, D.; Meade, G.; Foley, V. M.; Dowd, C. A. Structure, Function and Evolution of Glutathione Transferases: Implications for Classification of Non-mammalian Members of an Ancient Enzyme Superfamily. *Biochem. J.* **2001,** *360*, 1-16.

47. Gisi, D.; Leisinger, T.; Vuilleumier, S. Enzyme-mediated Dichloromethane Toxicity and Mutagenicity of Bacterial and Mammalian Dichloromethane-active Glutathione-*S* Transferases. *Arch. Toxicol.* **1999**, *73,* 71-79.

48. Wheeler, J. B.; Stourman, N. V.; Their, R.; Dommermuth, A.; Vuilleumier, S.; Rose, J. A.; Armstrong, R. N.; Guengerich, F. P. Conjugation of Haloalkanes by Bacterial and Mammalian Glutathione Transferases: Mono- and Dihalomethanes. *Chem. Res. Toxicol.* **2001,** *14,* 1118-1127.

49. Stourman, N. V.; Rose, J. H.; Vuilleumier, S.; Armstrong, R. N. Catalytic Mechanism of Dichloromethane Dehalogenase from *Methylophilus* sp. Strain DM11 *Biochemistry* **2003,** *42,* 11048-11056.

50. Wheeler, J. B.; Stourman, N. V.; Armstrong, R. N.; Guengerich, F. P. Conjugation of Haloalkanes by Bacterial and Mammalian Glutathione Transferases: Mono- and Vicinal Dihaloethanes *Chem. Res. Toxicol.* **2001,** *14,* 1107-1117.

51. Gasteiger, E.; Hoogland, C.; Gattiker, A.; Duvaud, S.; Wilkins, M. R.; Appel, R. D.; Bairoch, A. Protein Identification and Analysis Tools on the ExPASy Server. In *The Proteomics Protocols Handbook;* Walker, J. M., Ed.; Humana Press: New York, NY, 2005; pp 571-607.

52. Desai, K. K.; Miller, B. J. Recruitment of Genes and Enzymes Conferring Resistance to the Nonnatural Toxin Bromoacetate. *PNAS* **2010***, 107* (42), 17968-17973.

53. Richardson, S. D.; Plewa, M. J.; Wagner, E. D.; Schoeny, R.; Demarini, D. M. Occurrence, Genotoxicity, and Carcinogenicity of Regulated and Emerging Disinfection By-products in Drinking Water: A Review and a Roadmap for Research. *Mutat. Res.* **2007***, 636,* 178-242.

54. Chrysostomou, C.; Quandt, E. M.; Marshall, N. M.; Stone, E.; Georgiou, G. An Alternate Pathway of Arsenate Resistance in *E. coli* Mediated by the Glutathione *S*-Transferase GstB. *ACS Chem. Biol.* **2015***, 10,* 875-882.

55. T. K. Wood. Molecular Approaches in Bioremediation. *Curr. Opin. Biotechnol.* **2008***, 19,* 572-578.

56. Rui, L.; Kwon, Y. M.; Reardon, K. F.; Wood, T. K. Metabolic Pathway Engineering to Enhance Aerobic Degradation of Chlorinated Ethenes and to Reduce Their Toxicity by Cloning a Novel Glutathione *S*-Transferase, an Evolved Toluene *ortho*-Monooxygenase, and Gamma-glutamylcysteine Synthetase. *Environ. Microbiol.* **2004,** *6,* 491-500.

57. McGuinness, M. C.; Ivory, C.; Gilmartin, N.; Dowling, D. N. Investigation of Substrate Specificity of Wildtype and Mutant $BphK^{LB400}$ (a Glutathione *S*-Transferase) from *Burkholderia* LB400. *Int. Biodeter. Biodegr.* **2006***, 58,* 203-208.

58. McGuinness, M. C.; Mazurkiewicz, V.; Brennan, E.; Dowling, D. N. Dechlorination of Pesticides by a Specific Bacterial Glutathione *S*-Transferase, $BphK^{LB400}$: Potential for Bioremediation. *Eng. Life Sci.* **2007***, 7* (6), 611-615.

59. Brennan, E.; McGuinness, M. C.; Dowling, D. N. Bioinformatic Analysis and *in vitro* Site-directed Mutagenesis of Conserved Amino Acids in $BphK^{LB400}$, a Specific Bacterial Glutathione Transferase. *Int. Biodeter. Biodegr.* **2009***, 63,* 928-932.

60. Federici, L.; Masulli, M.; Di Ilio, C.; Allocati, N. Characterization of the Hydrophobic Substrate-binding Site of the Bacterial Beta Class Glutathione Transferase from *Proteus mirabilis. Protein Eng. Des. Sel.* **2010***, 23* (9), 743-750.

61. Broadhurst, A. V. Hydroxylapatite Chromatography. In *Current Protocols in Protein Science;* Supplement 8, John Wiley & Sons, Inc.: Hoboken, NJ, 1997; pp 8.6.1-8.6.12.

62. Aboagye, C. Biochemical Characterization of Glutathione Transferase YliJ from *Escherichia coli.* M.S. Thesis, Youngstown State University, Youngstown, OH, 2015.

63. Yoshinaga, M.; Ueki, T.; Michibata, H. Metal Binding Ability of Glutathione Transferases Conserved Between Two Animal Species, The Vanadium-rich Ascidian *Ascidia sydneiensis samea* and the Schistome *Schistoma japonicum. Biochim. Biophys. Acta* **2007**, *1770,* 1413-1418.

64. Han, Y.-H.; Seo, H.-A.; Kim, G.-H.; Lee, C.-K.; Kang, Y. K.; Ryu, K. H.; Chung, Y. J. A Histidine Substitution Confers Metal Binding Affinity to a *Schistoma japonicum* Glutathione *S*-Transferase. *Protein Expr. Purif.* **2010**, *73,* 74-77.

65. Zhitkovich, A. et al. Metabolism of Cr (VI) by Ascorbate but not Glutathione is a Low-Oxidant Generating Process. *J. Trace Elem. Med. Biol.* **2012**, *26* (2-3), 192-196.

66. Kelley, L. A. et al. The Phyre2 Web Portal for Protein Modeling, Prediction and Analysis. *Nat. Protoc.* **2015**, *10,* 845-858.